



POLITECNICO DI TORINO

Corso di Laurea Magistrale in Ingegneria  
Energetica e Nucleare

TESI DI LAUREA MAGISTRALE

# **Radiopharmaceuticals diffusion inside human body and problem modelling**

**Candidato**

Mattia Cretoni

**Relatori**

Prof. Gianni Coppa (Dipartimento di Elettronica e  
Telecomunicazioni)

Dott.ssa Faiza Bourhaleb (i-See s.r.l.)

ANNO ACCADEMICO 2018/2019



A mia zia.

## Sommario

Lo scopo del presente lavoro di Tesi è quello di fornire linee guida per il calcolo della dose depositata da un radiofarmaco nei tessuti biologici del corpo umano. Attualmente è possibile conoscere tramite prescrizione medica il quantitativo di dose totale da depositare nei tessuti affetti da neoplasia, ma non si è in grado di definire a priori la dose depositata nei tessuti sani durante il tragitto della sostanza medicinale dal momento dell'iniezione a quello dell'arrivo nell'organo o nel tessuto bersaglio: gli strumenti utilizzati nello svolgimento dello studio permettono di stimare l'ordine di grandezza di tale quantità e quindi di determinare se il trattamento sia conforme ai limiti normativi.

Il primo step è stato quello di modificare il sistema cardiocircolatorio di un paziente virtuale di proprietà della società i-See s.r.l.. Esso presentava un sistema semplificato e perciò è stato necessario effettuare i collegamenti tra i vari vasi e duplicarli in modo da avere sia la componente arteriosa che quella venosa. Questo risulta un punto molto importante perché il sistema circolatorio costituisce il percorso attraverso cui il radiofarmaco viene trasportato all'interno del corpo umano. Il paziente virtuale modificato è stato quindi utilizzato per ottenere, tramite l'utilizzo di un software di grafica 3D (Blender), le immagini della TAC. I dati inerenti la composizione ed i coefficienti di attenuazione ottenuti tramite il processo di sezionamento vengono forniti in input ad un programma basato sul metodo Monte Carlo, tramite cui si è potuto simulare il processo di decadimento, e quindi la conseguente dose rilasciata nei tessuti biologici, di un'innovativa molecola utilizzata per la radiomarcatura (Cuprymina). Si è deciso di focalizzare l'attenzione sugli organi più radiosensibili del corpo che, secondo la Pubblicazione 118 dell'ICRP, sono cuore e occhi.

## **Abstract**

The objective of this Thesis is to provide guidelines to calculate deposited dose by a radiopharmaceutical in biological tissues of the human body. Nowadays it is possible to know the total dose to deposit in tissues affected by neoplasia by means of medical receipt but it is not possible to define a priori the deposited dose in healthy tissues along the path from the injection to the target organ: thanks to the instruments used in this work, one's able to evaluate the order of magnitude of this quantity and so also if the treatment respects the regulatory limits.

The first step followed was the modification of the cardiovascular system of a virtual patient owned by i-See s.r.l.: its own cardiovascular system is schematic and so it has been modified connecting the different vessels and duplicating them in order to get both the arterial and the venous part. This is a very important step because they represent the path through which the radiopharmaceutical is carried inside the human body. Then, the modified virtual patient has been used to generate CT scan images by means of a 3D graphics program (Blender). Data concerning composition and attenuation coefficients obtained through this process constituted the inputs to a Monte Carlo-based program with which it has been simulated the decay process and the consequent deposited dose on biological tissues of an innovative molecule for radiolabelling (Cuprymina). It has been decided to base the analysis on the most radiosensitive organs that are heart and eyes according to ICRP Publication 118.

# Contents

<b>List of Figures</b>	<b>4</b>
<b>Introduction</b>	<b>8</b>
<b>1 Radiation</b>	<b>10</b>
1.1 Introduction . . . . .	10
1.2 Radioactive decays . . . . .	11
1.2.1 Alpha decay . . . . .	15
1.2.2 Beta decay . . . . .	17
1.2.3 Electron capture . . . . .	18
1.2.4 Gamma decay . . . . .	19
1.3 Fundamental quantities . . . . .	19
1.3.1 Activity . . . . .	19
1.3.2 Absorbed dose . . . . .	20
1.3.3 Stopping Power . . . . .	20
1.3.4 Particle Range . . . . .	21
1.3.5 Linear Energy Transfer . . . . .	21
1.4 Interaction of radiation with matter . . . . .	22
1.4.1 Charged particles . . . . .	22
1.4.1.1 Heavy charged particles . . . . .	23
1.4.1.2 Light charged particles . . . . .	24
1.4.2 Neutral particles . . . . .	26
1.4.2.1 Gamma rays . . . . .	26
1.4.2.2 Neutrons . . . . .	29

<b>2</b>	<b>Nuclear Medicine</b>	<b>32</b>
2.1	Radiopharmaceuticals - Cuprymina . . . . .	32
2.2	Radioisotope imaging . . . . .	39
2.3	Radiotherapy . . . . .	44
2.4	Cell surviving fraction . . . . .	48
<b>3</b>	<b>Cardiovascular System</b>	<b>57</b>
3.1	Introduction . . . . .	57
3.2	Blood composition . . . . .	57
3.3	System structure . . . . .	60
3.3.1	Heart structure . . . . .	60
3.3.2	Blood vessels structure . . . . .	65
3.4	Blood flow through cardiovascular system . . . . .	65
<b>4</b>	<b>Software packages used</b>	<b>74</b>
4.1	Blender . . . . .	74
4.2	MATLAB . . . . .	75
4.2.1	Hounsfield Scale . . . . .	75
4.3	Geant4 . . . . .	78
4.3.1	Geant4 structure . . . . .	79
<b>5</b>	<b>Virtual Phantom</b>	<b>82</b>
5.1	General description . . . . .	82
5.2	VPatient3D . . . . .	83
5.3	Vascular system and its implementation . . . . .	85
5.4	CT images generation . . . . .	86
5.4.1	Sectioning . . . . .	86
5.4.2	Compositing . . . . .	87
<b>6</b>	<b>Simulations</b>	<b>96</b>
6.1	Program description . . . . .	96
6.2	Test simulations . . . . .	98
6.3	Eyes simulation . . . . .	102
6.4	Heart Simulation . . . . .	105

<b>7 Conclusions</b>	<b>124</b>
<b>Bibliography</b>	<b>126</b>

# List of Figures

1.1	Absolute value of the binding energy per nucleon (from [16]). . . . .	13
1.2	Nuclide Chart . . . . .	14
1.3	Alpha-decay . . . . .	16
1.4	Beta energy spectrum (from [32]). . . . .	18
1.5	Energy straggling . . . . .	24
1.6	Range straggling . . . . .	25
1.7	Light charged particles range . . . . .	26
1.8	Compton effect (from [15]). . . . .	28
1.9	Compton polar plot . . . . .	29
1.10	Sodium iodine $\frac{\mu}{\rho}$ variation with energy (adapted from [15]). . . . .	30
2.1	$^{64}\text{Cu}$ decay scheme (from [18]). . . . .	37
2.2	$^{18}\text{F}$ -FDG (2- $^{18}\text{F}$ fluoro-2-deoxy-D-glucose) structure (from [22]). . . . .	38
2.3	Radioisotope imaging process using SPECT (from [10]). . . . .	39
2.4	Radioisotope imaging process using PET (from [10]). . . . .	40
2.5	Representation of the human body planes and axes. . . . .	41
2.6	Variation of the attenuation coefficients of the human body tissues with energy (from [4]). . . . .	43
2.7	Collimator characteristics. . . . .	43
2.8	Gamma camera structure (from [15]). . . . .	45
2.9	Guanine structure . . . . .	48
2.10	Cells surviving fraction for high and low LET radiation (adapted from [26]). . . . .	49
2.11	Surviving fraction behaviour with different exposure rates. . . . .	50
2.12	Kerma and absorbed dose behaviour at different depth values (adapted from [26]). . . . .	52

2.13	Principle of therapeutic ratio (from [26]). . . . .	52
2.14	REB variation with LET . . . . .	54
2.15	Cells surviving fraction behaviour for an aerobic cell and for an hypoxic one (from [20]). . . . .	55
2.16	OER behaviour with respect to LET variation (from [26]). . . . .	55
2.17	Re-oxygenation process (from [25]). . . . .	56
3.1	Heart structure . . . . .	61
3.2	Heart valves . . . . .	64
3.3	Cardiovascular system schematisation (from [6]). . . . .	66
3.4	Pressure gradient examples in tubes (from [6]). . . . .	67
3.5	Pressure behaviour along the circulation system . . . . .	68
3.6	Pressure drop dependencies (from [23]). . . . .	69
3.7	Moody chart (from [23]). . . . .	70
3.8	Venturi effect . . . . .	72
3.9	Pressure loss coefficient in case of contraction . . . . .	72
4.1	Geant4 structure flow diagram (from [1]). . . . .	81
5.1	VPatient3D: (a)Body skin; (b)Muscles; (c)Skeleton and main soft tissues; (d)Skeleton. . . . .	91
5.2	Vascular system extrapolated. . . . .	92
5.3	Detail of the vena cava cut: it represents the point where venous blood flows into the right atrium. . . . .	93
5.4	Pulmonary circulation (P.C.) modelisation. . . . .	93
5.5	Final vascular system modelled: (a)Front view; (b)Left view. . . . .	94
5.6	Representation of the sectioning plane. . . . .	95
5.7	Height representation in real world and in Blender world: (a) Front view; (b)Left view. . . . .	95
6.1	Cutting plane and source position for test analysis during simulations: (a)Position of the sectioning plane where the source is located; (b)Source position inside the human phantom. . . . .	108
6.2	Slice that corresponds to the centre of the analysed phantom part for the first analysis: (a)Slice 25 with source located in the centre; (b)Detail of slice 25. . . . .	109

6.3	Slice that corresponds to the centre of the analysed phantom part for the second analysis: (a)Slice 25 with source located in the centre; (b)Detail of slice 25. . . . .	110
6.4	Representation of the slice located below the central slice in the first analysis: (a)Slice 26; (b)Detail of slice 26. . . . .	111
6.5	Representation of the slice located below the central slice in the second analysis: (a)Slice 26; (b)Detail of slice 26. . . . .	112
6.6	Representation of the slice located 3.6 cm below the central slice in the first analysis. . . . .	113
6.7	Representation of the slice located 3.6 cm below the central slice in the second analysis. . . . .	113
6.8	Representation of the slice located 7.2 cm below the central slice in the first analysis. . . . .	114
6.9	Representation of the slice located 7.2 cm below the central slice in the second analysis. . . . .	114
6.10	Cutting plane and source position for eyes analysis during simulations: (a)Position of the sectioning plane where the source is located; (b)Source position inside the human phantom head. . . . .	115
6.11	Slice that corresponds to the centre of the analysed phantom part for the eyes analysis: (a)Slice 11 with source located in temporal zone; (b)Detail of slice 11. . . . .	116
6.12	Representation of the slice located below the central slice in the eyes analysis: (a) Slice 12; (b) Detail of slice 12. . . . .	117
6.13	Representation of the slice located 0.6 cm below the central slice in the eyes analysis. . . . .	118
6.14	Representation of the slice located 2.4 cm below the central slice in the eyes analysis. . . . .	118
6.15	Cutting plane and source position for analysis during heart simulation: (a)Position of the sectioning plane where the source is located; (b)Source position inside the human phantom heart. . . . .	119
6.16	Slice that corresponds to the centre of the analysed phantom part for the heart analysis: (a)Slice 22 with source located in the centre; (b)Particular of slice 22. . . . .	120

6.17	Representation of the slice located below the central slice in the heart analysis: (a)Slice 23; (b)Particular of slice 23. . . . .	121
6.18	Representation of the slice located 0.6 cm below the central slice in the heart analysis. . . . .	122
6.19	Representation of the slice located 5.4 cm below the central slice in the heart analysis. . . . .	122
6.20	Representation of the slice located 8.4 cm below the central slice in the heart analysis. . . . .	123

# Introduction

Nuclear medicine is a branch of medicine that uses natural or artificial radionuclides produced in laboratories for diagnostic and therapy: their decay products are used to detect and/or to destroy tumour cells inside the human body.

The detection or imaging process can be or external or internal. External imaging process is based on an external X-ray source that sends a radiation beam to a human body whose internal composition can be evaluated thanks to the detected radiation which passes through the body itself. Internal imaging process is the most common one today and it is based on the fact that radiation source is located directly inside the patient; the most common technologies are *Positron Emission Tomography* (PET) and *Single Photon Emission Computed Tomography* (SPECT) that differ because of the different used radionuclide decay mode and because of the different detected radiation type.

Radiation is used also in therapeutic field because with modern techniques it is possible to deliver high energy in tumour region. The dose is distributed only in the zone of interest, affecting minimally healthy tissues. It is often used combined to other treatments, like chemotherapy or surgery, according to the type of tumour, its position, its stage and according to the patient conditions. Just like the diagnostic field, also the therapeutic one can be distinguished into an external and an internal one. For what concerns the external radiotherapy, high energy x-rays,  $\gamma$ -rays produced by particular machines or by medical accelerators and heavy ions are the most used radiation types. Internal radiotherapy can be furthermore divided into two more branches. The first one is *Brachytherapy* that consists on the positioning of the radioactive source near the tumour region in order to get a more direct energy release to tumour cells and less energy delivered to healthy tissues. This approach has disappeared in the second half of the last century because of problems linked

to the operators exposure to radiation but in these last years it has been reused thanks to new technological improvements in remote handling field. The second approach to internal radiotherapy is by means of radiopharmaceuticals: they are substances characterised by the presence of one or more radionuclides and that are able to bind to pathological tissues. Radiopharmaceuticals are mostly in liquid form and they are administered to the patient through venous injection. The substance moves inside the human body through blood circulation and, like nutrients, it is sent to the tumour region by means of chemical and metabolic affinity.

Generally, in therapy case, all the tumour characteristics are known and so also the radionuclide quantity and the related dose delivered to the tumour are known. Using radiopharmaceutical, the effective dose delivered to healthy tissues along the path covered by the drug from the injection point to the target is not known. The aim of this work is to simulate the path covered by a radiopharmaceutical to determine the dose that each tissue absorbs.

# Chapter 1

## Radiation

### 1.1 Introduction

Radiation nature has been a discussion topic for scientists since the beginning of times.

In Ancient Greece, Democritus (V-IV sec. B.C.) stated that the atom was the base of all the reality, and so also of the light, but invisible in the real world and appreciable only with an intellectual process. In XI century, the Arabic scientist Hasan Ibn al-Haytham confirmed the corpuscular nature of light, describing for the first time refraction and reflection effects. In 1650, the French scientist Descartes proposed for the first time the description of light as a disturbance having a wave nature. After that, Isaac Newton went back to the corpuscular theory that became dominant in XVII century. In XIX century, Thomas Young with his experiment of the *double slit* demonstrated that light behaves exactly like waves in a river and for this reason the wave nature of light became dominant with respect to the corpuscular one. Afterwards, James Clerk Maxwell noticed that his equations for electromagnetic waves could be applied to describe the behaviour of light. In 1905 there was a further modification in the way of understanding light or, more in general, radiation. Albert Einstein gave the right explanation to the *photoelectric effect*, hypothesising that the electrons emission from a metallic plate depends on the energy transfer from colliding radiation and matter electrons: he proposed that, in order to have energy exchange, light should have corpuscular nature. In 1924, de

Broglie stated that: "*Matter can behaves like a wave: a certain plane wave with a particular wavelength can be associated to each particle that moves with a certain momentum.*".

Today Quantum mechanics is the physic branch that puts in symbiosis the wave and the corpuscular way of view radiation.

Radiation can be defined as *emission or transport of energy in form of waves or particles through the space or through a material medium*. As a wave, radiation is characterised by two main quantities that are *frequency* and *wavelength*: the first one is defined as the number of occurrence of an event per unit of time, while the second one represents the spacial length between two successive wave peaks or throughs. These two quantities are correlated one to each other according to

$$\nu = \frac{c}{\lambda} \quad (1.1)$$

where  $\nu$  is the frequency expressed in hertz (Hz),  $c$  is the speed of light in vacuum that is about  $3 \times 10^8 \frac{m}{s}$  and  $\lambda$  is the wavelength expressed in meters (m). Talking about radiation, the most important quantity in medical field is the energy that it carries: it is evaluated according to the following formula

$$E = h\nu \quad (1.2)$$

that becomes, applying equation (1.1),

$$E = \frac{hc}{\lambda} \quad (1.3)$$

In (1.2),  $E$  is the energy expressed in Joule (J),  $h$  is the *Plank's constant* that is equal to  $6,626 \times 10^{-34}$  Js and  $\nu$  is the frequency expressed in hertz (Hz).

## 1.2 Radioactive decays

Atoms are the fundamental structural unit that forms the matter. They are composed by a nucleus, in turn composed by protons ( $p$ ) and neutrons ( $n$ ) which are also called *nucleons*, and by electrons ( $e$ ) that orbit around it.

Each atom is characterised by two numbers that are the *atomic number*, indicated with the letter  $Z$ , that represents the number of protons inside the nucleus and that, in case of electrical stability, is equal to the number of electrons that orbits around it, and the *mass number*, indicated with the letter  $A$ , that represents the number of nucleons: if two atoms have the same atomic number, so they are of the same element, but they have different mass numbers, they are called *isotopes*. The electron mass is considered negligible with respect to the proton and neutron one because it is much smaller than these last two: the electron rest mass is equal to  $0.511 \frac{MeV}{c^2}$  while the rest masses of protons and neutrons are respectively equal to  $938.232 \frac{MeV}{c^2}$  and  $939.565 \frac{MeV}{c^2}$ .

Looking at the mass of the nucleus, it can be noticed that its value, calculated experimentally, is lower than the one of the unbound system, so than the sum of the single nucleons: this mass defect is called *mass change* ( $\Delta m$ ) and is expressed, neglecting the electrons mass contribution, as follow:

$$\Delta m = m(N, Z) - \left( \sum_{i=1}^Z m_p + \sum_{i=1}^{A-Z} m_n \right) < 0. \quad (1.4)$$

In the previous equation,  $m(N, Z)$  represents the mass of the atom with  $N$  neutrons and  $Z$  protons,  $m_p$  is the mass of the proton and  $m_n$  is the mass of the neutrons. According to the relation  $E = mc^2$ , the mass defect is converted into energy according to

$$B.E. = \Delta mc^2 \quad (1.5)$$

where  $\Delta m$  represents the *mass change* and  $c$  is the speed of light.  $B.E.$  represents the *Binding Energy*, whose behaviour is shown in Figure 1.1: it is the energy thanks to which nucleons hold on inside the nucleus and it's value is lower than zero because of its attractive nature.

Electrically stable atoms are neutral and so their total charge is equal to zero because the number of protons, that have a positive charge of  $1,602 \times 10^{-27}$  C, is equal to the number of electrons that have a negative charge equal to the opposite of the protons one, so of  $-1,602 \times 10^{-27}$  C, while neutrons have zero charge; being the nucleus positively charged, neutrons act like reducers of charge repulsion and so they are fundamental for the equilibrium.

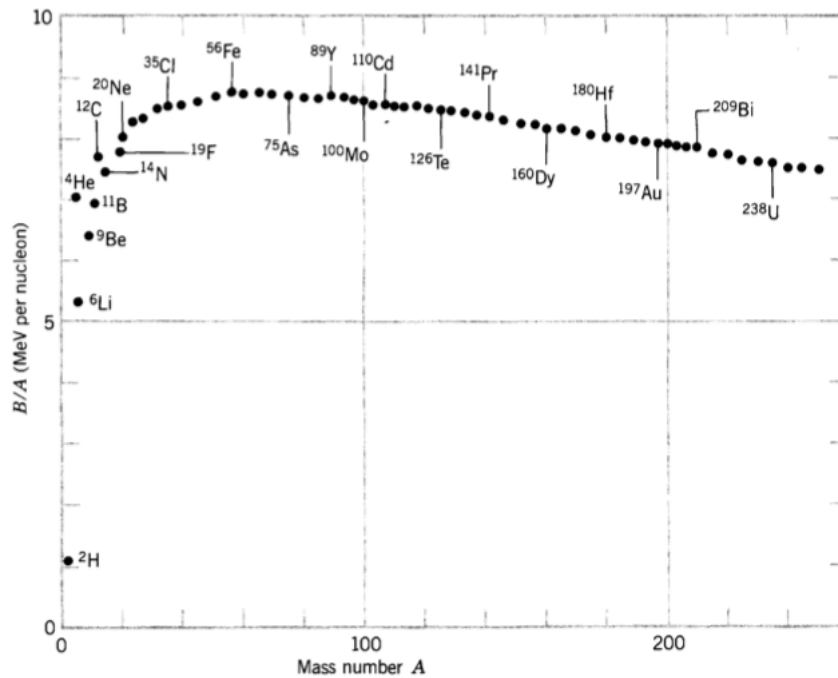


Figure 1.1: Absolute value of the binding energy per nucleon (from [16]).

All the elements present in nature can be represented in a special graph, called *Nuclide Chart* and that is showed in Figure 1.2: on the x-axis the number of neutron is represented while on the y-axis the number of protons.

An atom can be defined stable if, in absence of external input, it continues to stay in that condition and the number of protons and neutrons remains constant in time. In the Nuclide Chart, the most stable region is the one on the bottom left part of the bisector, where the value of the neutrons to protons ratio is included in a range between 1 and 1.5; with the atom becoming larger and larger, this last thing becomes no more true, more neutrons are needed to give stability to the atom itself and the value of the neutrons to protons ratio becomes larger than 1.5: an atom that falls outside this neutrons to protons ratio boundaries (1-1.5) is called unstable.

There are three different cases in which an atom can be defined unstable:

1. too big atom,
2. too many neutrons,

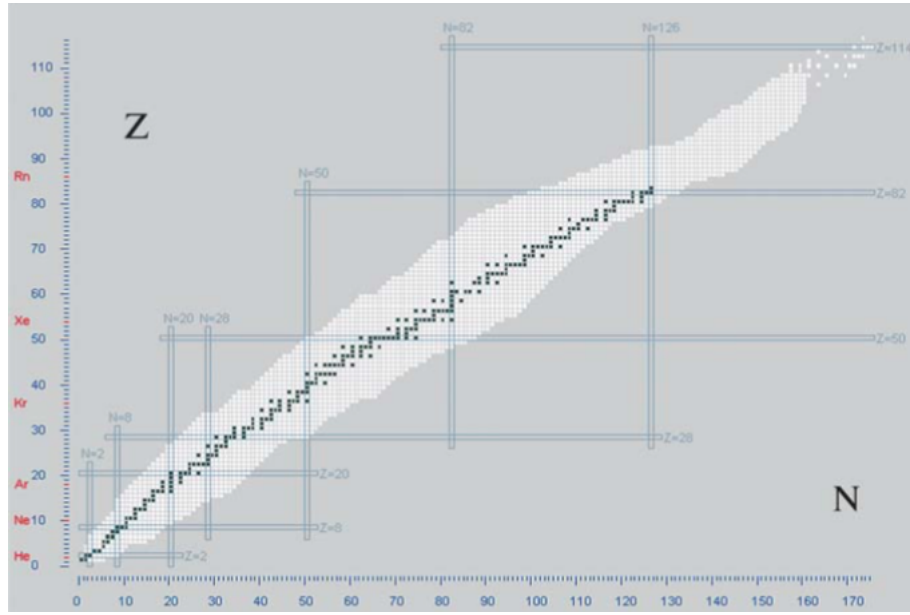


Figure 1.2: Nuclide chart. The black line represents the stability region, where the neutrons to protons ratio is about included between 1 and 1.5; the white region is characterised by a neutrons to protons ratio larger than 1.5 or lower than 1 (from [19]).

3. too few neutrons.

*Instability* is defined as a condition according to which the Binding Energy is not maximised and, for this reason, unstable atoms try to reach this condition through what is called *radioactive decay*.

These are spontaneous processes and it is due to the value of the *Reaction Energy* that, being larger than zero, indicates that the reaction is exothermal. The value of the Reaction Energy, indicated as  $Q$ , is evaluated as

$$Q = (M_i - M_f)c^2 = K_f - K_i. \quad (1.6)$$

$M_i c^2$  and  $M_f c^2$  are respectively the rest mass energies before and after the reaction and  $K_i$  and  $K_f$  are the kinetic energies in the initial and in the final state.

If  $n_0$  is the number of unstable atoms at  $t = t_0$ ,  $n(t)$ , that is the number of unstable atom at  $t > t_0$ , will be smaller than the initial quantity because part of the atoms

will modify their structure in order to reach the stability condition. The average probability for an atom to decay in a time  $dt$  between  $t$  and  $t + dt$  is given by the quantity  $\lambda dt$ :  $\lambda$ , expressed in  $[\frac{1}{s}]$ , is the probability per unit time for an atom to decay, it is constant in time and it changes according to the different types of elements. The variation of the number of radioactive atoms in time  $dt$  is described by the law

$$-dn(t) = n(t)\lambda dt. \quad (1.7)$$

Integrating equation (1.7) with respect to time, given the initial condition  $n(t = 0) = n_0$ , the result obtained is

$$n(t) = n_0 e^{-\lambda t}. \quad (1.8)$$

As it can be seen in the previous equation, because of its negative exponential behaviour in time, the quantity of radioactive atoms tends to zero for  $t \rightarrow \infty$ .

According to type of atom and to the nucleus composition, there are three different decay modes:

1.  $\alpha$  decay,
2.  $\beta$  decay,
3.  $\gamma$  decay.

### 1.2.1 Alpha decay

This decay mode is peculiar of too big atoms that tries to reduce their dimensions by the emission of this an  $\alpha$  particle: it is a nucleus of  ${}^4_2\text{He}$ , characterised by two protons and two neutrons. Applying the equation for the Reaction Energy, equation (1.6) becomes

$$\begin{aligned} Q_\alpha &= (M(A, Z) - (M(A - 4, Z - 2) + m(4, 2)))c^2 = \\ &= T_{M(A-4, Z-2)} + T_\alpha(+E_i) > 0 \end{aligned} \quad (1.9)$$

where  $M(A, Z)c^2$  is the rest mass energy of the atom before the decay,  $M(A - 4, Z - 2)c^2$  and  $m(4, 2)c^2$  are respectively the rest mass energies of the daughter atom and of

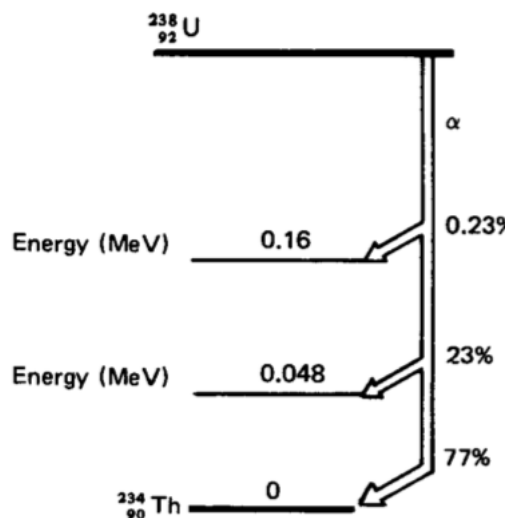


Figure 1.3: Alpha decay of  $^{238}\text{U}$ . On the right of the figure there are the probabilities to decay to the corresponding energy level (from [32]).

the  $\alpha$  particle after the decay and  $T_{M(A-4,Z-2)}$  and  $T_{(\alpha)}$  are the kinetic energies of the daughter atom and of the  $\alpha$  particle after the radioactive decay. The values of the kinetic energies can be evaluated applying the Conservation of Momentum law and, from it, it comes out that the two values are

$$T_{\alpha} \approx \frac{A-4}{A}(Q_{\alpha} - E_i) \quad (1.10)$$

$$T(M) \approx \frac{4}{A}(Q_{\alpha} - E_i). \quad (1.11)$$

Moreover, in (1.9), (1.10) and (1.11),  $E_i$  is the *Excitation Energy*: there could be the possibility that the daughter atom is emitted in an excited state and so, in order to go back to the energy ground state, the nucleus emits a photon ( $\gamma$ -ray), whose energy is equal to the energy difference between the two energy levels. Being a two body decay, the  $\alpha$  decay is characterised by a discrete energy spectrum, as it can be seen in Figure 1.3.

Examples of this type of decay are  $^{226}\text{Ra}$ ,  $^{222}\text{Rn}$  and  $^{238}\text{U}$ .

## 1.2.2 Beta decay

The  $\beta$  decay mode is characterised by the emission of a light charged particle. It is characteristic of those atoms endowed with too many neutrons or with too many protons: in the first case, a neutron turns into a proton and an electron ( $\beta^-$  particle) is expelled outside the nucleus

$$n \rightarrow p + \beta^-, \quad (1.12)$$

while, in the second case, a proton turns into a neutron and a positron ( $\beta^+$  particle, indicated with the symbol  $e^+$ ) that is the electron antiparticle, endowed with the same electron mass and the opposite electric charge, is expelled from the nucleus

$$n \rightarrow p + \beta^+. \quad (1.13)$$

As in the case of  $\alpha$  decay, the  $\beta$  decay mode is spontaneous and the equation (1.6) becomes for  $\beta^-$  decays

$$\begin{aligned} Q_{\beta^-} &= (M(A, Z) - (M(A, Z + 1) + m(\beta^-)))c^2 \\ &= T_{M(A, Z+1)} + T_{\beta^-} + T_{\bar{\nu}_e} (+E_i) > 0, \end{aligned} \quad (1.14)$$

and for  $\beta^+$  decays

$$\begin{aligned} Q_{\beta^+} &= (M(A, Z) - (M(A, Z - 1) + m(\beta^+)))c^2 \\ &= T_{M(A, Z-1)} + T_{\beta^+} + T_{\nu_e} (+E_i) > 0. \end{aligned} \quad (1.15)$$

In equations (1.14) and (1.15), there are two additional terms with respect to (1.9) that are, respectively, the *antineutrino* and *neutrino* kinetic energies: these two particles are elemental subatomic particles having no charge and a mass one billion times smaller than the one of the electron; they have been discovered in order to justify the results obtained applying the *momentum preservation law*. For this reason,  $\beta$  decay is a *three-body decay* and, unlike  $\alpha$  decay, it is characterised by a continuous energy spectrum because there are different possible combination in which the particles can share energy after decay. This behaviour can be seen in

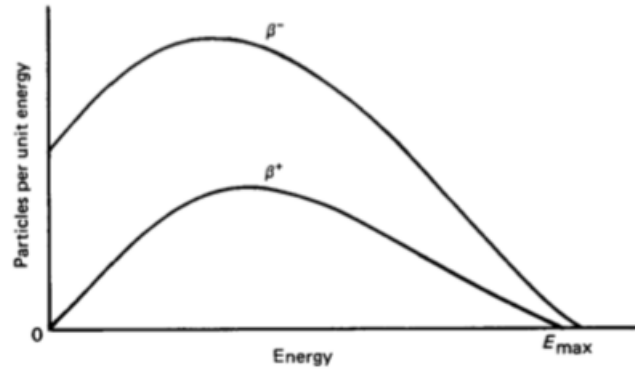


Figure 1.4: Beta energy spectrum (from [32]).

Figure 1.4 where the value of  $E_{max}$  represents the maximum value of the energy gained by the  $\beta$  particle after the decay and it is linked to the fact that or the  $e^-$  or the  $e^+$  takes all the available energy.

### 1.2.3 Electron capture

Electron capture is a process similar to the decay because it has almost the same effects. It consists on the capture by the nucleus of an electron from the atoms electronic shell. As in the  $\beta^+$  decay, there is the transmutation of a nucleus proton into a neutron with a neutrino that is expelled in order to preserve the conservation laws.

In this kind of transmutation mode, it happens that

$$p + e^- \rightarrow n, \quad (1.16)$$

and for this reason

$$X(A, Z) \rightarrow X(A, Z - 1). \quad (1.17)$$

## 1.2.4 Gamma decay

This last decay mode is characterised by the emission of a photon ( $\gamma$ -ray)\*. It happens when the nucleus of an atom is not in its ground energy level and the photon is the result of its de-excitation process: in fact, this kind of decay usually follows  $\alpha$  or  $\beta$  decays .

$^{99m}\text{Tc}$  is an example of this type of decay.

## 1.3 Fundamental quantities

### 1.3.1 Activity

*Activity* is a measure of the decay rate that represents the number of disintegrations per unit time. In the *International System of Unit (S.I.)*, it is measured in *becquerel* (Bq) where  $1\text{Bq}=1\frac{\text{disintegration}}{\text{s}}$ . Another old activity unit of measure is the *curie* (Ci) that is defined as about  $3,7 \times 10^{10}$  disintegration per seconds: so  $1\text{Ci} \simeq 3,7 \times 10^{10}\text{ Bq}$ .

In nuclear medicine field, *specific activity* is more used than activity. It is defined as the ratio between total radioactivity and the reference radioactive quantity according to the following equation

$$a = \frac{A}{m}. \quad (1.18)$$

If the the activity is expressed with  $A = \lambda m = \lambda N_A n$  and the mass with  $m = n A_0$ , where  $N_A$  is the Avogadro number equal to  $6.022e^{23}\text{ mol}^{-1}$ ,  $n$  is the moles number and  $A_0$  is the mass number, equation (1.18) becomes

$$a = \frac{\lambda N_A}{A_0} \quad (1.19)$$

with the specific activity measured in  $\frac{\text{Bq}}{\text{g}}$ .

---

\**Xrays* are very similar to *γrays* but they nature: in fact, while the former ones come from energetic transitions in the electronic shell, the latter ones come from nuclear energetic transitions and for this reason *xrays* are not considered talking about decays.

### 1.3.2 Absorbed dose

The *absorbed dose* is defined as the quantity of energy deposited by radiation per unit mass and in a finite volume. It is indicated with

$$D = \frac{E}{m}. \quad (1.20)$$

$E$  is representative of the whole energy that enters the control volume under study, and so it considers both the direct and the indirect radiation, while  $m$  is the mass of the volume itself. It's a quantity whose unit is the *grey* (Gy) and so  $1 \text{ Gy} = 1 \frac{\text{J}}{\text{kg}}$ .

### 1.3.3 Stopping Power

The *stopping power* or *linear stopping power* is a characteristic quantity of charged particles that interacts, as it is better explained in 1.4.1, mainly with the external electronic shell electrons. It is defined as the differential energy lost by a particle divided by the differential distance covered:

$$S = -\frac{dE}{dx}, \quad (1.21)$$

where  $-\frac{dE}{dx}$  is also called *energy loss rate*. The value of  $S$  can be evaluated thanks to the *Bethe Formula*:

$$S = -\frac{dE}{dx} = \frac{4\pi e^4 z^2}{m_0 v^2} NB, \quad (1.22)$$

with

$$B = Z \left[ \ln\left(\frac{2m_0 v^2}{I}\right) - \ln\left(1 - \frac{v^2}{c^2}\right) - \frac{v^2}{c^2} \right]. \quad (1.23)$$

In equations (1.22) and (1.23),  $ze$  represents the charge of the incident particle,  $m_0$  is the rest mass of the electron,  $N$  is the atomic density of the medium,  $I$  is the average excitation and ionisation potential,  $c$  is the speed of light and  $B$  is a quantity that takes into account the relativistic effects and so its last two terms become significant only with  $v \ll c$ . As it can be seen from (1.22), the value of the stopping power is strongly influenced by the charge of the incident particle, it is inversely proportional to the incident particle energy because of the dependency to the term  $\frac{1}{v^2}$  and it is directly proportional to the density of the incident medium.

### 1.3.4 Particle Range

The *range* is defined as the maximum penetration distance of a particle. This quantity depends on the definition of *stopping power* because it is defined as

$$R = - \int_0^{E_0} \frac{dx}{dE} dE = \int_0^{E_0} \frac{1}{S(x)} dE. \quad (1.24)$$

In equation (1.24), the quantity  $\frac{dx}{dE}$  represents the path covered by a particle per unit energy lost and the two extremes of integration represent the initial and the final particle energy.

### 1.3.5 Linear Energy Transfer

The *Linear Energy Transfer (LET)* is a quantity that is very similar to the stopping power: it is the variation of energy per unit path covered by the radiation.

$$LET = \frac{dE}{dl} \quad (1.25)$$

The difference between equation (1.21) and (1.25) is the minus sign. In fact these two concepts differ because they represent the same quantity but with different points of view: *stopping power* represents the quantity of energy released by the radiation while *LET* is referred to the quantity of energy deposited in a medium. This difference comes from the fact that not all the energy released by the radiation is deposited in a certain  $dx$  because during the ionisation process there could be the generation of some secondary  $e^-$  that deposit their energy somewhere else.

The unit of LET are  $\frac{eV}{\mu m}$ .

There can be the possibility to exclude the interactions that produce secondary electrons with an energy larger than a certain quantity  $\Delta$ , called *limiting energy*. This kind of LET is defined *restricted* and is indicated with

$$LET_{\Delta} = \left( \frac{dE}{dl} \right)_{\Delta}. \quad (1.26)$$

In equation (1.26),  $\Delta$  excludes all secondary electrons produced having an energy larger than its value. Taking the limit for  $\Delta$  that tends to infinity,  $LET$  becomes *unrestricted* and it equal to the the stopping power

$$|LET|_{\infty} = S. \quad (1.27)$$

$\gamma$  rays, X rays and  $\beta$  radiation under a certain energy level are considered *low LET radiation*;  $\alpha$  particles, protons, neutrons, heavily charged particles and  $\beta$  radiation above a certain energy lever are considered *low LET radiation*. The energy threshold to distinguish low LET radiation from high LET radiation is about  $10 \frac{keV}{\mu m}$ .

## 1.4 Interaction of radiation with matter

Radiation can be divided into two big families depending on the fact that its electric charge is different from or equal to zero.

According to the characteristic distance of penetration, charged radiation can be furthermore divided into:

- *Heavy charged particles*: radiation whose characteristic penetration distance is  $10^{-5}$  m and they include *protons* and  *$\alpha$  particles*;
- *Light charged particles*: radiation whose characteristic penetration distance is  $10^{-3}$  m and include category includes *electrons* and *positrons*.

Radiation no electrically charged can also be divided into

- *Neutrons*,
- *X-rays and gamma rays*.

### 1.4.1 Charged particles

Charged particles interact with the electrons of the atoms electronic shells. These last ones generate an electric field whose interaction range is infinite but whose intensity decreases for values of the distance that tends to infinity because those interactions are of the Coulomb types (the force intensity is proportional to

the inverse of the square of the distance). For this reason, there is a continuous interaction between the  $e^-$  and charged particles that continuously lose their energy along their path according to (1.28)

$$\Delta E_{max} = E \frac{m_e}{m_{colliding}} \quad (1.28)$$

where it can be seen that the value of the energy lost is proportional to the initial energy but inversely proportional to the mass of the colliding particle.

#### 1.4.1.1 Heavy charged particles

There are two different ways in which heavy charged particles interact with matter, that is *excitation* and *ionization*. In the first case, the outermost electrons of the electronic shell are excited to the upper levels and they emit radiation going back to the state of minimal energy configuration (ground state); in the second case, the energy of the colliding particle is larger than the ionisation potential of the atom so causing the release of a *secondary electron* that then behaves like a new charged particle: this last phenomenon is known as  *$\delta$ -ray effect*.

For heavy charged particles, equation (1.28) becomes

$$\Delta E_{MAX} \simeq E \frac{m_{e^-}}{m_{HCP}}. \quad (1.29)$$

It can be seen that the energy lost during the path by heavy charged particles is negligible because their mass is much bigger than the electrons one: this big difference causes also small deflections of the particles trajectory with respect to the straight one and a continuous energy and velocity reduction according to (1.22). Heavy charged particles continue losing energy and velocity until they reach the equilibrium condition with electrons of the electronic shells and, at the end, they disappear in terms of radiation because their energy is lower than the atoms ionisation potential: for this reason, they have a finite range inside matter. For example, considering  $\alpha$  particles, reference ranges are

$$\alpha|_{air} \rightarrow R \sim \text{few cm},$$

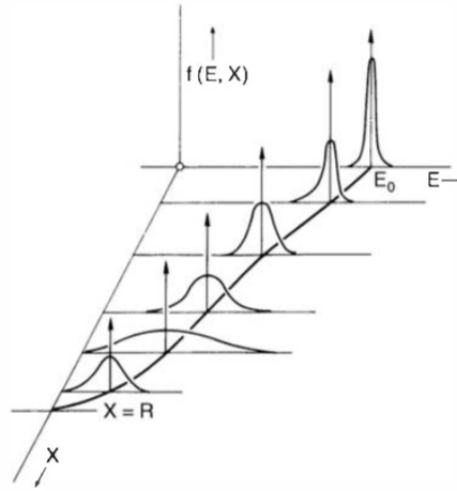


Figure 1.5: Energy distribution of a monoenergetic particles beam at different depths.  $E_0$  is the mean initial energy value and  $X$  is the depth (from [30]).

$$\alpha|_{human\ tissues} \rightarrow R \sim few\ mm.$$

All that has been said is referred to a single heavy charged particle but, in real cases, particles beams are characterised by a distribution of energy whose mean value is the quantity  $E_0$  and, because of the stochasticity of the process, they do not lose energy all in the same way: this is what is called *energy straggling* (look at Figure 1.5). Due to this phenomenon, particles experience also *range straggling* with some of them that are able to propagate after and others that disappear before the range mean value (Figure 1.6).

#### 1.4.1.2 Light charged particles

As the previous case, they interact with the electrons of the electronic shell of the medium but they suffer larger deflections: according to (1.28), the two interacting masses are comparable and so light charged particles experiences larger energy exchanges than heavy charged particles ones. Another difference with the previous case is that the relativistic effects become relevant, being  $e^-$  speed closer to the speed of light than the heavy charged particles one.

Light charged particles have also a finite range inside matter but the expression

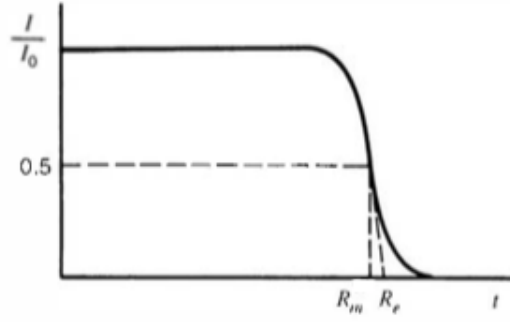


Figure 1.6: Range straggling:  $I_0$  and  $I$  represent respectively the initial and the detected intensity of the particle beam,  $t$  is the thickness of the propagation mean,  $R_m$  is the mean range and  $R_e$  is the extrapolated range (from [15]).

of the stopping power is different than the one expressed with (1.22) and (1.23), valid for heavy charged particles. The stopping power in this case is defined as

$$S = \left(-\frac{dE}{dx}\right)_c + \left(-\frac{dE}{dx}\right)_r, \quad (1.30)$$

with

$$\left(-\frac{dE}{dx}\right)_c \propto Z \log E \quad (1.31)$$

and

$$\left(-\frac{dE}{dx}\right)_r \propto EZ^2. \quad (1.32)$$

Equation (1.31) is the collisional contribution of equation (1.30) that takes into account the particles electromagnetic interactions with other electrons and it is relevant for particles whose energy is above the MeV, being proportional to the logarithm of the particle energy and to the medium density. Equation (1.32) is the radiation contribution of equation (1.30) that becomes relevant in "heavy" mediums, being proportional to the square of the medium density and to the particle energy: during the deflection, energy lost by particles is emitted in in form of radiation as a consequence of the Momentum Conservation law. This phenomenon is called *bremstrahlung* and it is negligible for heavy charged particles because they suffer a negligible deflection.

In Figure 1.7 is represented the behaviour of a light charged particles beam inside matter.

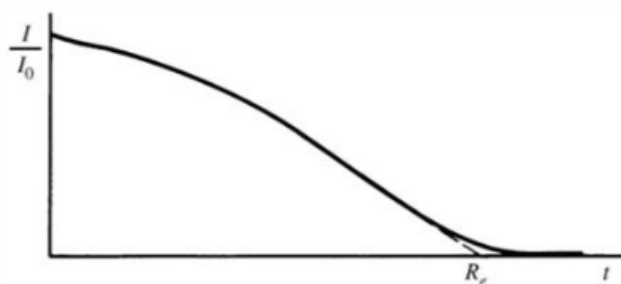


Figure 1.7: Monoenergetic electrons beam transmission curve inside matter.  $R_e$  is the extrapolated range for electrons (from [15]).

## 1.4.2 Neutral particles

The interaction physics is completely different with respect to charged particles one because they do not interact electromagnetically with electrons of the electronic shell but mainly with nuclei. During the interaction process, neutral particles can interact with atoms, exchanging energy and direction, or they can disappear because of absorption processes.

Interaction processes are characterised by stochasticity and so they are studied in terms of probability.

In this chapter X-rays are not discussed because, as it has been said, they have a completely different nature with respect to gamma rays.

### 1.4.2.1 Gamma rays

The *intensity* of a photons beam is defined as the number of photons that collide on a surface per unit area and per unit time and it is indicated with  $I$ . Supposing to have a wall whose thickness is  $dx$ ;  $I_0$  and  $I$  are the beam intensities measured respectively in  $x = 0$  and  $x = dx$ . Being  $-dI$  the differential beam intensity (negative quantity: the beam intensity decreases along the path due to absorption phenomena), it has been shown experimentally that, if the experiment is performed

in a *good geometry*<sup>†</sup>,  $\frac{-dI}{I}$  is proportional to the path itself as it follows:

$$-\frac{dI}{I} = \mu dx. \quad (1.33)$$

The symbol  $\mu$  is the proportionality constant and it is called *attenuation coefficient*: it represents the probability per unit path for a photon to collide. It is measured in  $\frac{1}{cm}$  and it is proportional to  $\frac{Z^4}{E^3}$ ; its value is different for each material.

Integrating (1.33) and considering constant the attenuation coefficient value, the result obtained is

$$I(x) = I_0 e^{-\mu x}. \quad (1.34)$$

As it can be seen in the previous equation, the intensity of the beam is equal to zero only for  $x \rightarrow \infty$ : for this reason the range of photons can be considered infinite.

According to the value of the beam energy, there could be three different ways in which gamma rays can interact with the surrounding matter.

The first kind of interaction is the *Photoelectric Effect*. It happens for low energies that are of the order of 50-150 keV. Gamma rays interact directly with the outer electrons of the electronic shells of atoms that are the less bounded: the photon is absorbed and so it disappears, its energy is sufficient to cause ionisation and so an electron, called *photoelectron*, is emitted with energy

$$E_{e^-} = E_\gamma - \Phi. \quad (1.35)$$

In equation (1.35),  $E_\gamma$  is the energy of the incident photon and  $\Phi$  is the binding energy of the electron. The photoelectron released behaves like the electron of  $\delta$ -ray effect, so it is able to generate further ionisations in the surrounding matter.

The second kind of interaction is the *Compton Effect*. It happens for energies values between 100 keV and about 1 MeV. In this case, the photon does not disappear: the electron with which the photon interacts, called *recoil electron*, is at rest at the

---

†

- all photons collimated at the beginning,
- after  $dx$  only photons still collimated are measured.

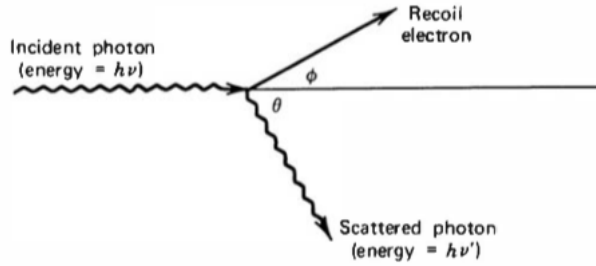


Figure 1.8: Compton effect (from [15]).

beginning but after interaction it can gain a quantity of energy that varies from zero to a fraction of the incident photon energy because gamma ray is slowed-down and deflected after collision (Figure 1.8). Using equation (1.2) to express gamma ray energy, applying the Momentum and Energy Conservation and laws and before and after the collision, the resulting photon energy is given by

$$h\nu' = \frac{h\nu}{1 + \frac{h\nu}{m_0c^2}(1 - \cos\theta)}. \quad (1.36)$$

In equation (1.36),  $h$  is the Plank's constant,  $\nu$  and  $\nu'$  are respectively the incident photon frequency before and after collision,  $m_0$  is the mass of the target particle that in this case is an electron,  $c$  is the speed of light and  $\theta$  is the deflection angle of the scattered photon. This last value is strongly influenced by the incident photon energy because the bigger is the colliding energy and the smaller is the deflection and forward scattering is preferred, as it can be seen in Figure 1.9

The last kind of interaction is the *pair production* whose probability of happening becomes relevant for gamma ray energies larger than 1.022 MeV, that corresponds to the rest mass energy of the couple electron+positron. In this situation, the photon disappears and it is replaced by an electron and a positron: being this last one the antiparticle of the electron, they undergo by annihilation process, producing two photons having an energy equal to 0.511 MeV and moving in opposite direction as result of momentum and energy conservation.

The value of the attenuation coefficient is given by the sum of these three contribution:

$$\mu = \mu_{P.E.} + \mu_{C.E.} + \mu_{P.P.}. \quad (1.37)$$

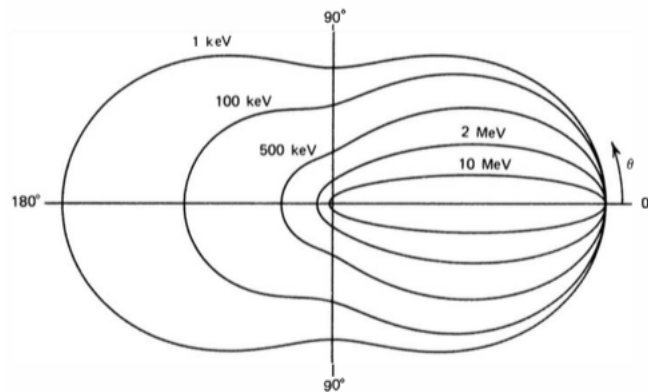


Figure 1.9: Compton effect polar plot: once chosen the energy value, intersecting the horizontal axis with a vertical line corresponding to a certain value of deflection angle, the distance from the center gives the entity of the corresponding deflection probability (from [15]).

An example of the resulting behaviour of the attenuation coefficient can be shown in Figure 1.10

#### 1.4.2.2 Neutrons

As the gamma rays, neutrons does not have electric charge and so they do not are influenced by Coulomb interaction but, unlike them, neutron interaction could bring to the formation of heavy charged particles. The way in which neutrons interact with the surrounding matter depends on the particle energy, according to which they are divided into

- slow neutrons,
- fast neutrons.

The way in which they interact are very different.

The first kind of interaction is *scattering* that can be either *elastic* and *inelastic*. In the first case, energy and momentum of the system " $n + target$ " is preserved and so there is kinetic energy transfer from the incident particle to the target; this kind of interaction is peculiar of slow neutrons that, interacting with atoms of comparable size, are slowed-down or thermalised. In the case of inelastic scattering, the neutron energy is so high that, during the collision, there is energy exchange between the



The previous reactions need the availability of free neutrons and here it comes the last way of interaction between neutron and the surrounding matter: *nuclear fission*. During the absorption process, if the atom is too big, it becomes unstable and it falls in the nuclide chart into the instability region characterised by too many neutrons: in order to become more stable, the heavy father atom splits into two or more light fission products with the emission of one or more fast neutrons. The total interaction probability per unit path is indicated with  $\Sigma$  and it is called *macroscopic cross section*: it is equal to

$$\Sigma = N\sigma \quad (1.39)$$

with  $N$  that is the number of nuclei per unit volume, measured in  $\frac{1}{m^3}$ , and  $\sigma$  that is the *microscopic cross section*, whose unit measure is the barn (1 barn =  $10^{-28}m^2$ ). The value of the total interaction probability per unit path is given by the sum of all the cross section of all the possible interaction processes explained until now and for this reason

$$\Sigma_{tot} = \Sigma_{elastic\ sc.} + \Sigma_{inelastic\ sc.} + \Sigma_{capture} + \Sigma_{fission}. \quad (1.40)$$

The way in which neutrons interact with matter is very similar to the photons one and so the structure of equation that controls their behaviour is similar to equation (1.34), considering that the  $\Sigma_{tot}$  meaning for neutrons is the same as the one of  $\mu$  for photons:

$$I(x) = I_0 e^{-\Sigma_{tot}x}. \quad (1.41)$$

As in can be seen from equation (1.41), the neutron intensity falls down exponentially with thickness.

# Chapter 2

## Nuclear Medicine

### 2.1 Radiopharmaceuticals - Cuprymina

Radiopharmaceuticals are widely used in nuclear medicine, especially in these last years when this field has become more and more important. They are drugs that can be used both *in vitro* and *in vivo* and they are distinguished in two different categories:

- *tracers*: they are made of chemical compounds that are used to follow the path of a particular substance allowing the study of the metabolic and functional processes of a certain target; the "trace" in nuclear medicine is constituted by the radioactive decay products of an unstable atom with which tracers are chemically bounded.
- *indicators*: they define position and dimensions of an anatomical structure.

Both these types of radiopharmaceuticals can be furthermore classified into *positive* or *negative*: the former accumulate in regions where there is the abnormal functioning while the latter are the opposite because they accumulate more in regions characterised by normal functioning and so their concentration defect indicates some malfunction. In general, this type of division depends on the radiopharmaceutical used and on what the target to be measured or controlled is, so there could be cases in which a single radiopharmaceutical can be either positive and negative.

Other important factors that characterises the radiopharmaceuticals classification are:

- physical characteristics like mass number and half-life,
- radioactivity level at a certain time instant,
- specific activity,
- radioactive concentration in the injected solution,
- type of radiation emitted.

In the *in vivo* uses, they are administered venously directly inside the vascular system or, rarely, orally (for example the radioiodine  $^{131}\text{I}$ , that is used to treat thyroid cancers because of its affinity with the thyroid glands). The quantities injected are very small and, in fact, at least some milligrams are administered in order to avoid problem to the organism, but although that the risks are not null.

In order to define the most used radionuclides in nuclear medicine today, *diagnostic* must be distinguished from *therapy*.

Great part of the diagnostic radiopharmaceuticals today are  $\gamma$ -emitters or  $\beta^+$ -emitters: they are used in SPECT (*Single Photon Emission Computed Tomography*), if they decay emitting a single gamma ray, or in PET (*Positron Emission Tomography*), if they decay emitting a positron that annihilates almost instantaneously with the matter electrons emitting two gamma rays, as it has been explained at the end of Chapter 1.4.2.1. Thanks to some instrumentations that are able to detect the single ray emitted in SPECT or the two rays in PET and taking advantage of the infinite range of  $\gamma$  rays, one is able to determine with a very high precision the emitting position and so the radiopharmaceutical distribution inside the body. In Table 2.1 the main chemical elements used in SPECT with their own characteristics are shown while in Table 2.2 main positron emitters used in PET with their own characteristics are shown. The half-lives of the different isotopes listed in Table 2.1 and Table 2.2 are very short and for this reason they must be produced where they are needed, thus avoiding problems linked to the isotope disappearance during transportation. The half-life of these isotopes has not to be too short because it is not known a priori the exact location and time instant in which the radioisotope

Table 2.1: Elements used in SPECT with their main characteristics (Data from [2]).

Nuclide	$T_{\frac{1}{2}}$	Decay mode	$\gamma$ emission [keV] (% abundance)
$^{67}\text{Ga}$	3.26 d	EC	93 (36%); 185 (20%); 300 (16%); 394 (4.5%)
$^{99\text{m}}\text{Tc}$	6.0 h	$\gamma$ -em.	141 (87%)
$^{123}\text{I}$	13.1 h	EC	159 (83%); 528 (1.4%)

Table 2.2: Elements used in PET with their main characteristics (Data from [2]).

Nuclide	$T_{\frac{1}{2}}$	$\beta^+$ energy [MeV]	$\gamma$ energy (keV)
$^{11}\text{C}$	20.4 min	0.385 (99.8%)	[-]
$^{13}\text{N}$	9.97 min	0.492 (99.8%)	[-]
$^{15}\text{O}$	112 s	0.735 (99.9%)	[-]
$^{18}\text{F}$	110 min	0.250 (100%)	[-]
$^{82}\text{Rb}$	75 s	1.532 (83.3%) 1.157 (10.2%)	0.776 (13.4%) [-]

must be placed; then, the half-life has to be upper-bounded in order to guarantee that the residual activity inside the patient when he moves is negligible so that its peak is reached during the exam.

For what concerns therapy, it must be distinguished into two different branches: internal and external radiotherapy. Both approaches use *gamma* rays characterised by higher energies than the diagnostic case, as it can be seen in Table 2.3, because their purpose is to kill the tumour cell. In case of therapy purpose,  $\gamma$  rays are also used for diagnostic. The internal radiotherapy uses also  $\beta^-$  emitters and, rarely,  $\alpha$  emitters because of their finite range: the radiation source is directly implanted near the tumour region and it is possible to reduce in this way the problem to a short range one.

Radiopharmaceuticals production can be divided into two successive steps: the first one is the radioisotope production and then the second one is the process that brings to the complete radiopharmaceutical production.

Radioactive isotopes are produced in different ways:

Table 2.3: Isotopes characteristics used for internal and external radiotherapy (Data from [2]).

Decay mode	Nuclide	$T_{\frac{1}{2}}$	$E_{MAX}$ [MeV]	Associated $\gamma$ energy [keV]
$\gamma$	$^{60}\text{Co}$	5.3 y	1.17 and 1.33	[-]
	$^{137}\text{Cs}$	30 y	0.622	[-]
	$^{152}\text{Eu}$	13.4 y	0.6	[-]
$\beta^-$	$^{89}\text{Sr}$	50.5 d	1.5	[-]
	$^{90}\text{Y}$	2.7 d	2.3	[-]
	$^{131}\text{I}$	8 d	0.6	354(81%), 637(7%)
$\alpha$	$^{211}\text{At}$	7.2 h d	5.9	[-]
	$^{212}\text{Bi}$	1 h	7.8	727(12%)
	$^{225}\text{Ac}$	10 h	5.8	[-]

- *n-capture*: it can happen that a stable nucleus becomes unstable after the capture of an incident neutron and so it starts to decay in order to reach a more stable condition; this process needs a nuclear reactor.
- *nuclear fission*: almost all the fission products coming from a nuclear reactor are unstable and some of them can be used in medical field if produced in research reactor.
- *bombardment*: this process is characteristic of accelerators, where targets are bombarded with stable projectiles.
- *radionuclide generators*: radioactive elements are directly produced inside these particular machines.

After the radioactive isotope production, the radiopharmaceutical is produced following different methodologies. The first one is the direct substitution of an atom of the original molecule with its radioactive isotope: this is the case, for example, of the  $^{127}\text{I}$  that is substituted by the radioactive isotope  $^{131}\text{I}$  in the L-Tiroxina that is made of four iodine atoms. Adopting this method, the resulting molecule is practically identical to the starting one and for this reason the metabolic processes that it undergoes are the same of the original molecule. If there is no possibility to get an identical molecule after substitution, there is a second option that consists in

Table 2.4:  $^{64}\text{Cu}$  decay modes (Data from [11]).

Decay mode	Prob.	En. rel. [keV]	Decay prod. (condition)
$\beta^-$	39%	579	$^{64}\text{Zn}$ (stable)
$\beta^+$	18%	653	$^{64}\text{Ni}$ (stable)
$e^-$ conversion	43%	1675	$^{64}\text{Zn}$ (stable)

substituting a functional group ( $-\text{H}^+$ ,  $-\text{OH}^-$ ,  $-\text{CH}_3$ ) with the radioactive element, paying attention to the fact that the resulting dimensions and electric charge of the produced compound must be similar to the starting one in order to do not change too much the metabolic processes that the molecule follows. This last process is commonly used with big molecules, like proteins.

After being produced, radiopharmaceuticals distribute inside the human body thanks to the blood circulation and they reach the target thanks to chemical processes and to metabolic affinity.

The study is focused on a particular substance called *Cuprymina*.

Cuprymina is a radiopharmaceutical precursor produced by  $ACOM_{srl}$  (Advanced Center Oncology - Macerata). This product can not be administered to human beings because it has not passed the clinical phase 3 yet: the third phase is based on one or more clinical tests where a new drug is compared to a standard-of-care drug efficacy, effectiveness and safety; it is checked if they are better in the new case than in the old one. Phase 3 is the last but one phase that is then followed by the FDA (Food and Drug Administration) approval.

Cuprymina is made of  $^{64}\text{Cu}$ -Copper Chloride.

$^{64}\text{Cu}$  is an unstable isotope of the stable element  $^{63}\text{Cu}$  that is solid for nuclear medicine purposes, and so at ambient temperature, because its boiling point is at  $T_{boil}=2840$  K. The unstable isotope  $^{64}\text{Cu}$  is characterised by an half-life equal to 12.7 h and, being a relatively light atom and according to what is said in Chapter 1.2.2, it decays through the emission of light particles and so emitting electrons or positrons (see Table 2.4 and Figure 2.1). Copper-64 is a radioactive isotope used in nuclear medicine that has both diagnostic and therapeutic function: it is used as an imaging radionuclide in PET thanks to the possible positron emission during the

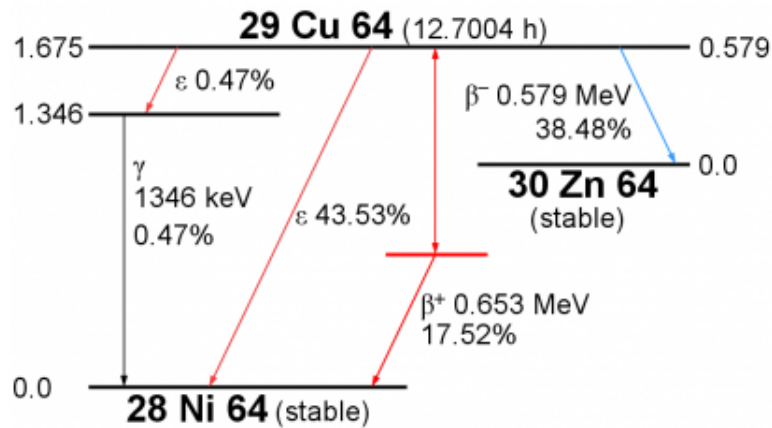


Figure 2.1:  $^{64}\text{Cu}$  decay scheme (from [18]).

decay process; it is also a therapeutic agent because of the possible electron emitted during the decay and the two *Auger electrons*\* released that can kill directly the tumour cells if the source is placed near the ill region. This radioactive isotope can be obtained irradiating a nickel target with a proton beam of 10-12 MeV causing the reaction  $[^{64}\text{Ni}(p,n)^{64}\text{Cu}]$ . Another way to produce it is to use a deuterons beam activated by special cyclotrons bombarding a nickel or a zinc target. In this last case, the most important reactions are  $[^{64}\text{Ni}(d,2n)^{64}\text{Cu}]$  at 15-18 MeV,  $[^{64}\text{Zn}(d,2p)^{64}\text{Cu}]$  at about 19.5 MeV and  $[^{64}\text{Zn}(d,\alpha)^{64}\text{Cu}]$  at about 40 MeV.

$^{64}\text{Cu}$  are contained in bottles in which the activity varies from a maximum value of 925 MBq to a minimum value of 2.779 MBq (the equivalent copper quantity is included in the range 0.25-0.75  $\mu\text{g}$ ).

In the entire world there are a few centres that are able to produce  $^{64}\text{Cu}$  targets: they are about 35 but only one of them, own by  $ACOM_{srl}$ , has obtained the qualification as GMP (*Good Manufacture Practice*: it is a recognition given to drugs assuring the respect of quality standards regarding their production and control); after approval, it will be used to develop  $^{64}\text{Cu}$ -labeled molecules. Although the

---

\*It is a physical phenomenon that characterises atoms with a vacancy left by a core electron removal. This vacancy is filled by an electron of the outer electronic shell levels, thus causing the emission of an energy quantity equal to the energy difference between the two energy levels. Energy is usually released in form of a photon but there could also be situations in which part of it is used to release an electron that is then ejected out of the electronic shell if it is larger than the ionisation potential of the atom: the released electron is called *Auger electron*.

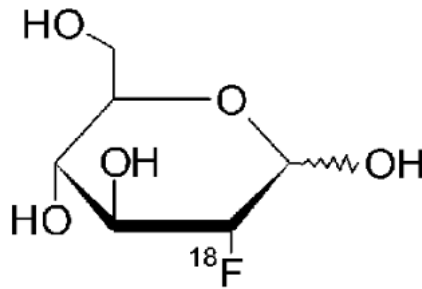


Figure 2.2:  $^{18}\text{F}$ -FDG (2- $^{18}\text{F}$ ]fluoro-2-deoxy-D-glucose) structure (from [22]).

$^{64}\text{Cu}$  production is easy and inexpensive, its irradiation facilities need particular shielded rooms. This last point constitutes the real problem to the construction of a  $^{64}\text{Cu}$  producing network because the great part of the existing one is equipped with  $^{18}\text{F}$  production targets.

$^{18}\text{F}$  today is the most common radionuclide used for PET.  $^{18}\text{F}$  is a positron-emitter radionuclide that is connected to a glucose molecule (see Figure 2.2). It is produced thanks to specific cyclotrons situated near where it is needed because of its short half-life ( $T_{\frac{1}{2}}=110$  min): the production cycle is based on the bombardment of heavy water enriched in the  $^{18}\text{O}$  isotope by protons, thus causing the reaction  $[^{18}\text{O}(\text{p},\text{n})^{18}\text{F}]$ ; the resulting  $^{18}\text{F}$  is then attached chemically to a deoxyglucose molecule, producing the so called Fludeoxyglucose molecule. It is used to evaluate the glucose metabolism but also to individuate tumour centres during PET because of the so called *Warburg effect*: tumour cells activity is higher than the normal ones and so they are characterised by a larger glycolytic activity that can be individuated with concentrations that exceed normal values.

The action mechanism of  $^{64}\text{Cu}$  is similar to the one described for  $^{18}\text{F}$  because copper is one of the main cell constituent and in particular it is active in the DNA structure: once injected inside the human body, it accumulates in the nucleus of cells having a larger metabolic activity (tumour cells) and for this reason the effects of particles coming from its decay become more direct although their low penetration range. As  $^{18}\text{F}$ , it is not used only for tumours but also to study genetic diseases concerning copper metabolism, like *Wilson* and *Menke diseases*.

In conclusion, it has been proved that Cuprymina, and so  $^{64}\text{Cu}$ , gives better image quality during PET exams but there are still problems linked to its use:

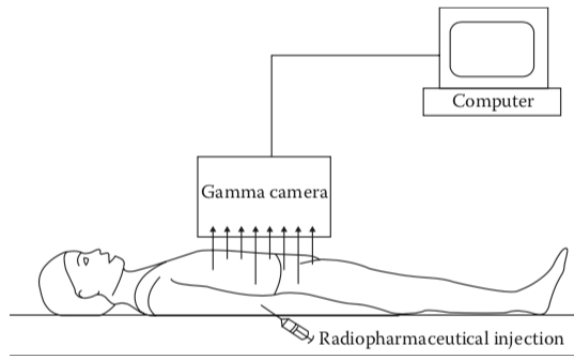


Figure 2.3: Radioisotope imaging process using SPECT (from [10]).

- a producing  $^{64}\text{Cu}$  network does not exist today,
- no  $^{64}\text{Cu}$  labeled molecule has passed the clinical phase III;
- $^{89}\text{Zr}$  seems to be better for PET use, especially because its production network exists,
- to obtain pure  $^{64}\text{Cu}$  without contamination is very difficult under the chemical point of view.

## 2.2 Radioisotope imaging

Nuclear medicine imaging is a process thanks to which one is able to get information on what there is inside an object whose composition is unknown, that is the human body.

General radioisotope imaging processes underwent by a division into two different branches in 1980s: as already said in Chapter 2.1, SPECT (Figure 2.3), in which a single gamma ray emitted by the radionuclide is detected, and PET (Figure 2.4), in which two gamma rays coming from the annihilation of a positron from a positron-decaying radionuclide with an electron of the surrounding matter are detected. The main objective of radioisotope imaging is the detection of the radiation emitted by a source, that in this case is a radiopharmaceutical or a radioisotope emitter situated inside the body. It is known how each single isotope or the different macromolecules distribute inside the human body according to

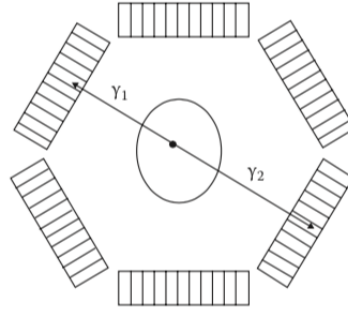


Figure 2.4: Radioisotope imaging process using PET (from [10]).

chemistry and to cells metabolism: starting from this information and using the detected data, particular machines are able to reconstruct a 3D picture of the human body.

As it has been said, photons are the detected radiation. They are emitted inside the human body but, before detection, they experience

1. *No interaction* if their free-flight is larger than the body thickness.
2. *Absorption* if their free-flight is smaller than the body thickness and, after interaction with the surrounding matter atoms, they are lost.
3. *Scattering* if, after collision, they do not disappear but they get out with different direction and velocity than the ones before the interaction.

Point 1 and point 3 are the most important concerning imaging. In fact, all the uncollided photons and the scattered ones give information about what there is in between the radiation source and the detection method system.

The uncollided photons are also called *primary photons* while the photons that reach the target after scattering are called *secondary photons*: the total detected radiation is made of both the contributions and it can be written as

$$I_{tot} = I_{primary} + I_{secondary} = I_{primary} \left( 1 + \frac{I_{secondary}}{I_{primary}} \right) = I_{primary} (1 + R), \quad (2.1)$$

where  $R$  is defined *disturbance ratio* or *scatter-to-primary ratio* and it represents the weight of the secondary photons compared with the primary ones.

The physical law that regulates the photons diffusion phenomenon is the same

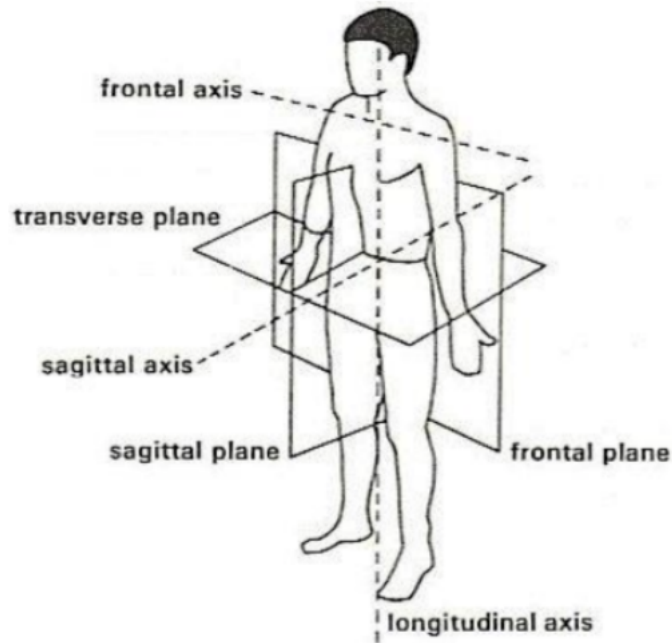


Figure 2.5: Representation of the human body planes and axes: the frontal axis corresponds to the x-axis, the sagittal one to the y-axis and the longitudinal one to the z-axis (from [24]).

expressed in equation (1.33) but in this last case there is a crucial difference because the result of the integration is different than the one obtained in equation (1.34): referring to Figure 2.5 and considering that both PET and SPECT analyse the body taking slices on the transversal plane at different  $z$  values, the attenuation coefficient varies inside the different points of the slices and so it is no more a constant value but a function of the  $x$  and  $y$  coordinates as it follows:

$$\mu = \mu(x, y). \quad (2.2)$$

This is due to the fact that the machine is sectioning a non-homogeneous material and so different points are characterised by different compositions, density values,...For this reason, integrating equation (1.33) on the analysed surface and neglecting the scattering contribution, the result obtained is

$$I(\vec{r}) = I_0(\vec{r}_0)e^{-\int_R \mu(s)ds}. \quad (2.3)$$

In (2.3),  $I(\vec{r})$  and  $I_0(\vec{r}_0)$  are respectively the measured and the starting beam intensities and  $\mu(s)$  represents the attenuation coefficient that varies along the photon path, indicated by  $\Gamma$ .

Substituting equation (2.3) into (2.1), the equation for the total beam intensity detected, and so considering also the scattering contribution, is

$$I(\vec{r}) = I_0(\vec{r}_0)e^{-\int_{\Gamma}\mu(s)ds}(1 + R). \quad (2.4)$$

The general problem becomes an inverse problem because, in the last expression, being the detected photons beam intensity known as well as the one of the source, the only unknown is represented by the value of the attenuation coefficient that is not constant but it varies according to the position.

The scattering term, represented by the disturbance ratio, must be avoided or reduced in order to simplify the problem. The influence of the scattering term is strongly influenced by the thickness of the matter that radiation crosses: the value of  $R$  increases monotonically because the probability to interact increases and the rate of scattering becomes more and more important. For this reason, a first solution to decrease the scattering influence is to reduce the dimensions of the body to be analysed but it is not possible because it is fixed in a given patient. It could be thought to increase the value of the photons energy thus increasing the forward peaked scattering probability, according to Figure 1.9. This last point is characterised by a problem: looking at Figure 2.6, it can be seen how the different attenuation coefficients of the different tissues become undistinguishable one from each other with increasing values of photon energy and for this reason energies values used in nuclear medicine field are included in range 50-150 keV. The scattering influence can be also reduced mechanically using filters: they are composed by lamellae parallel to the direction of the uncollided photons made of material able to absorb radiation like lead. In this way, all those rays that are not aligned with the desired direction are absorbed by the shielding material. This device is called *collimator*. The two parameters that characterise collimators are the depth of the shielding material, indicated with the letter  $h$ , and the distance between two consecutive lamellae, indicated with the letter  $D$  (see Figure 2.7): the

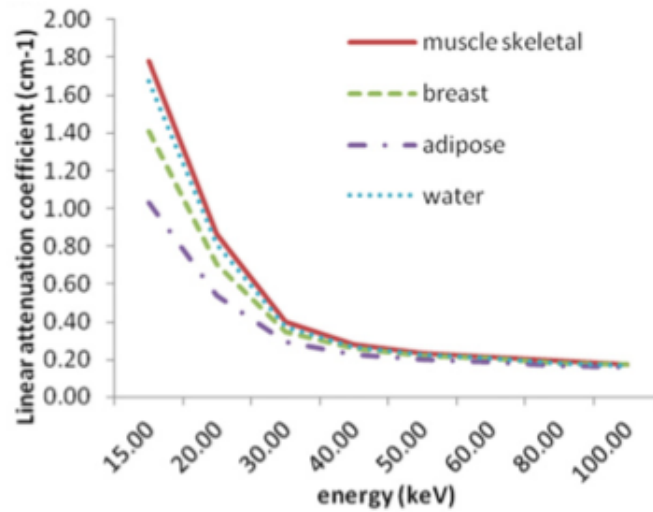


Figure 2.6: Variation of the attenuation coefficients of the human body tissues with energy (from [4]).

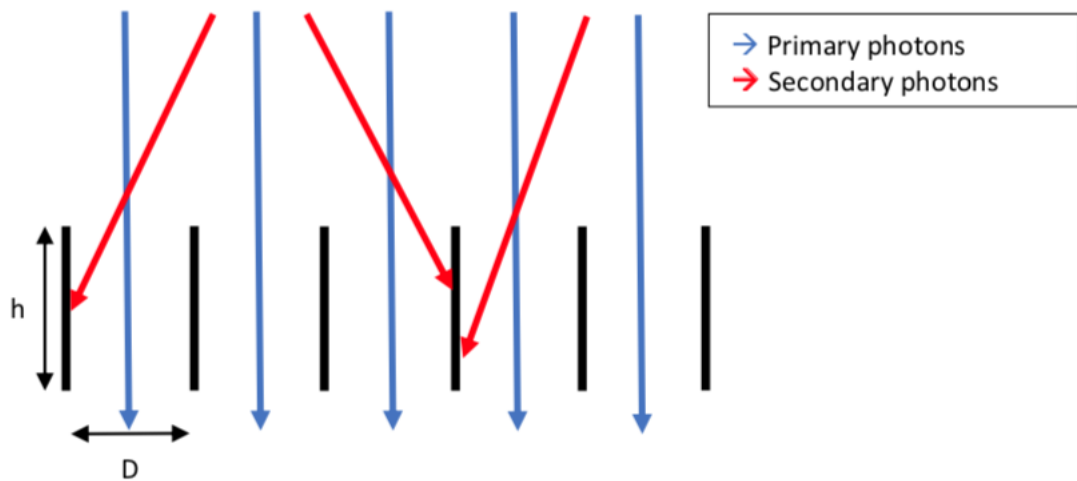


Figure 2.7: Collimator characteristics.

ratio between these two parameters is called *grid ratio*

$$R_G = \frac{h}{D} \quad (2.5)$$

In general,  $D \sim 10 \mu\text{m}$  and  $R_G$  value is included in the range 5-10.

The detection system in both PET and SPECT performs a very important

function: it receives photons emitted by the source inside the patient and, thanks to it and to the systems related, it possible to identify univocally the of the source position and to get a functional image of the body interior. In order to get the information, the detector type used in nuclear medicine imaging is the *scintillator*. These kinds of detectors are able to convert the absorbed ionising radiation into visible light thanks to the fluorescence mechanism. Fluorescent materials are able to absorb radiation that excites an electronic shell electron to an higher energy level. The electron de-excites almost immediately into intermediate states, emitting energy at each passage. The last de-excitation process is characterised by the emission of visible light: the energy emitted in the last step is lower than the one absorbed by the medium and so it is characterised by a smaller wavelength characteristic of the visible range. Scintillators can be dividend into two different categories that are

1. Organic scintillators (anthracene, stilbene, naphthalene),
2. Inorganic scintillators (NaI(Tl), BGO).

Scintillators are used today in *gamma cameras*: they are composed by (see Figure 2.8)

- *Collimator*: it selects only radiation oriented to the right direction.
- *Scintillation crystal*: it detects the colliding radiation and it re-emits radiation of a different nature (visible light).
- *Photomultiplier*: it increases the signal emitted by the previous component.
- *Electronics and computers*: these components convert the incoming signal into the desired result.

## 2.3 Radiotherapy

Radiotherapy is a medical practice that consists on the use of ionising radiation to treat some kinds of tumour.

The birth and the development of the tumour cells is a very complicated mechanism.

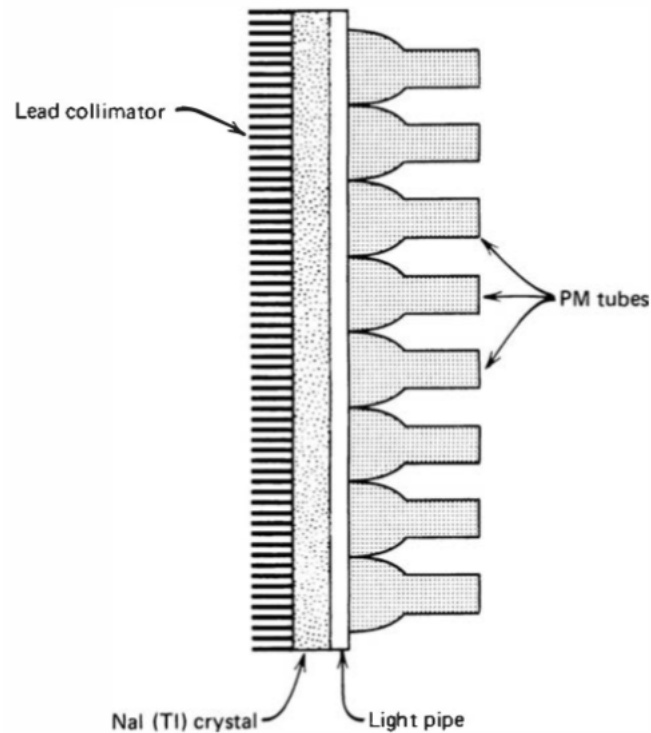


Figure 2.8: Gamma camera structure (from [15]).

These kinds of cells are characterised by mutations and the first one regards the reproductive mechanism. At the beginning, each healthy cell is able to reproduce thanks to the cellular division process: in this way, starting from a parent cell and after the DNA duplication process, two daughter cells are generated, one of them contains the parent cell DNA and the other one contains its copy. This process can be repeated many times but at the end the cell dies. Tumour cell has a faster reproductive capability, condition that is called *hyperplasia*, and it is also equipped with certain enzymes, called *telomerase*, that are able to inhibit the cell ageing, thus increasing the cell life. Moreover, they can avoid the *apoptosis* process that is a sort of self-destruction mechanism that healthy cells use if they are damaged in order to prevent the generation of other damaged cells. In addition to the variation of the proliferation process speed, there could be other mutations that can arise concerning the cell behaviour or its shape and orientation (*dysplasia*). Just like healthy cells, tumour cells need nutrients to live and for this reason there is a net

of capillaries that develops all around and then there could be two different ways in which the tumour can evolve:

- The tumour dimensions do not change in time because the inner cells are not fed by the blood circulation and so they die; the death rate is equal to the generation rate so the tumour is in a stable condition. This situation is called *in situ tumour* and it is surrounded by a convective tissue membrane.
- The tumour cells can produce a particular substance that cause the division of the vascular cells in order to produce new blood vessels towards the tumour in a process called *angiogenesis*. At the beginning also this kind of tumour is covered by a convective tissue membrane but the continuing growing cells can go out of it, diffusing in tissues and other organs thanks to the blood or lymphatic system or they can diffuse and settle in body cavities.

The targets of radiotherapy are the cancer cells and in particular their DNA that is responsible of the cell duplication: if radiation destroys it, the cell reproductive capability is lost and for this reason it can be considered death. Moreover, it has been shown experimentally that the cells radiosensitivity is directly proportional to the reproduction velocity and for this reason tumour cells are the most sensitive, being their reproduction rate higher than the healthy cells one.

Radiation could have both *direct* and *indirect* effects.

Direct effects are characteristic of radiation that directly interacts with the nucleus of the tumour cell: this kind of radiation is able to break the DNA chain, thus causing the cell death. Direct effects are characteristic of heavily ionising radiation having a high LET (see Chapter 1.3.5), like  $\alpha$  particles, protons, neutrons and electrons over a certain energy level.

Indirect effects are linked to  $\gamma$ -rays, X-rays and electrons characterised by energy below a certain treshold. This kind of radiation hits the cells generating high energy electrons that then interact with water stored inside the body (about 60% of the human body is composed by water): the interaction with water generates free radicals. They are chemical compounds characterised by an high level of reactivity because they have an unpaired valence electron and for this reason they try to reach their stable condition. Free radicals can diffuse inside the cells and they can

cause modifications to the cell components, especially to the DNA. The different free radicals generation phases are the following:

1.  $\text{H}_2\text{O} \xrightarrow{\text{radiation}} \text{H}_2\text{O}^+ + e^-$ ,  
 $e^- + \text{H}_2\text{O} \rightarrow \text{H}_2\text{O}^-$ ;
2.  $\text{H}_2\text{O}^+ \rightarrow \text{H}^+ + \text{OH}^0$ ,  
 $\text{H}_2\text{O}^- \rightarrow \text{H}^0 + \text{OH}^-$ ;
3.  $\text{RH} + \text{OH}^0 \rightarrow \text{R}^0 + \text{H}_2\text{O}$ ,  
 $\text{RH} + \text{H}^0 \rightarrow \text{R}^0 + \text{H}_2$ .

Free radicals are the compounds that appear in phase 2:  $\text{OH}^0$  and  $\text{H}^0$ . Generally they react with volatile organic compounds (VOCs). In this specific situation, as it can be seen in phase 3, the reaction takes place with an *alkane*, indicated with  $\text{RH}$ , producing water, hydrogen and a molecule that is different with respect to the starting one, called *alkyl radical*: it is a reactive compound made by an alkane missing an hydrogen atom. Thanks to another chemical agent called *alkylating antineoplastic agent*, alkyl radical reacts with DNA cells and in particular with nitrogen atom in position seven in the purine ring of the guanine base (see Figure 2.9). This DNA structure modification could bring to errors during the cell reproductive phase. As it has previously said, tumour cells reproduce faster than the other cells and they are not completely able to repair damages; for this reason alkyl radicals are used to destroy them.

The use of radiation to treat tumours could bring to a no consequences condition but there could be cases in which radiation use could have positive and negative effects.

Positive effects of radiation are

- *Division delay.*
- *Apoptosis*: it is a sort of controlled cellular death; the first step is the DNA fragmentation that is followed by a cellular one. The resulting organic structures are incorporated by the surrounding cells or by the macrophages.
- *Reproductive failure.*

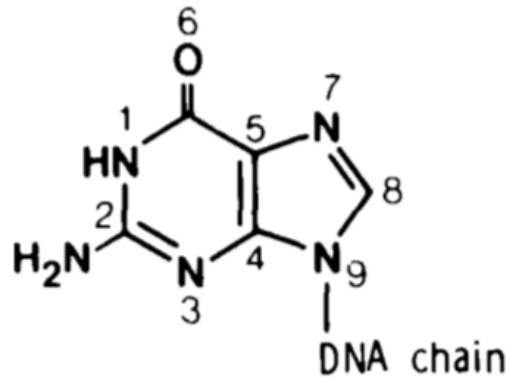


Figure 2.9: Guanine structure: the nitrogen atom indicated by number 7 is the one that is substituted by the alkyl radical (from [9]).

- *Genomic instability*: it can cause problems to the cell reproductive process.

Negative consequences of radiation exposure imply that the tumour cell survives after the treatment or that the exposure itself could have some consequences on the surrounding healthy cells. Examples of negative effects are

- *Mutation*: also healthy tissues are crossed by radiation and so there is always the probability to generate mutation in them.
- *Transformation*: it is a consequence of the previous point because the cell mutation could cause the variation of the specialisation type of the cell.
- *Bystander effect*: it consists on the fact that the cells surrounding an irradiated one begin to behave as they were irradiated because of the effect of some signals sent by the target one.
- *Adaptive response*: after irradiation, cells can become more resistant to radiation exposure.

## 2.4 Cell surviving fraction

The *Cell surviving fraction* is an important parameter that characterises radiotherapy: it represents the fraction between the cells that survive after radiation treatment and the whole initial population. It depends on many parameters.

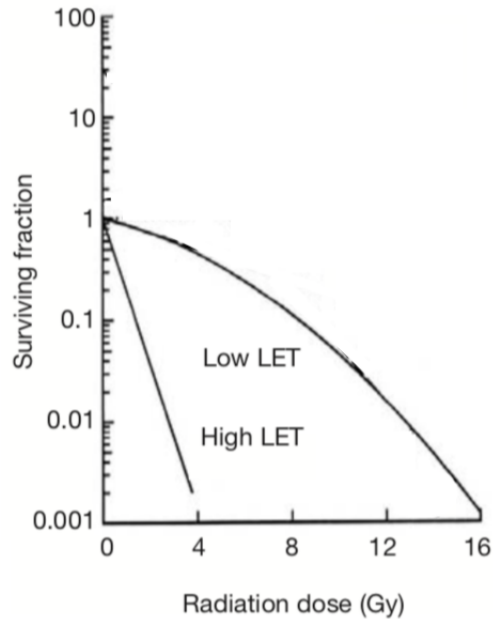


Figure 2.10: Cells surviving fraction for high and low LET radiation (adapted from [26]).

LET is one of the influencing parameter. In fact, high and low LET radiation behaves differently with respect to biological tissues as it can be seen in Figure 2.10: high LET radiation is more effective in destroying tumour cells than the low LET one. In order to get the same cell surviving fraction, a high LET radiation needs a lower dose distributed to the patient with respect to low LET radiation. For both kinds of radiation, time of exposure is another important parameter that influences the cell surviving fraction. As it can be seen in Figure 2.11, considering incident radiation at constant energy, the more the exposure time increases, the less effective is the radiation and so the higher is the cell surviving fraction: this is due to the fact that cells have time in order to recover themselves.

In nuclear medicine there is a quantity that is very similar to LET that is *Kerma*. It is the defined as

$$K = \frac{dE_{tr}}{dm}, \quad (2.6)$$

where  $dE_{tr}$  represents the differential amount of energy that the radiation deposits on matter, while  $dm$  is the reference material differential mass. For a photon beam,

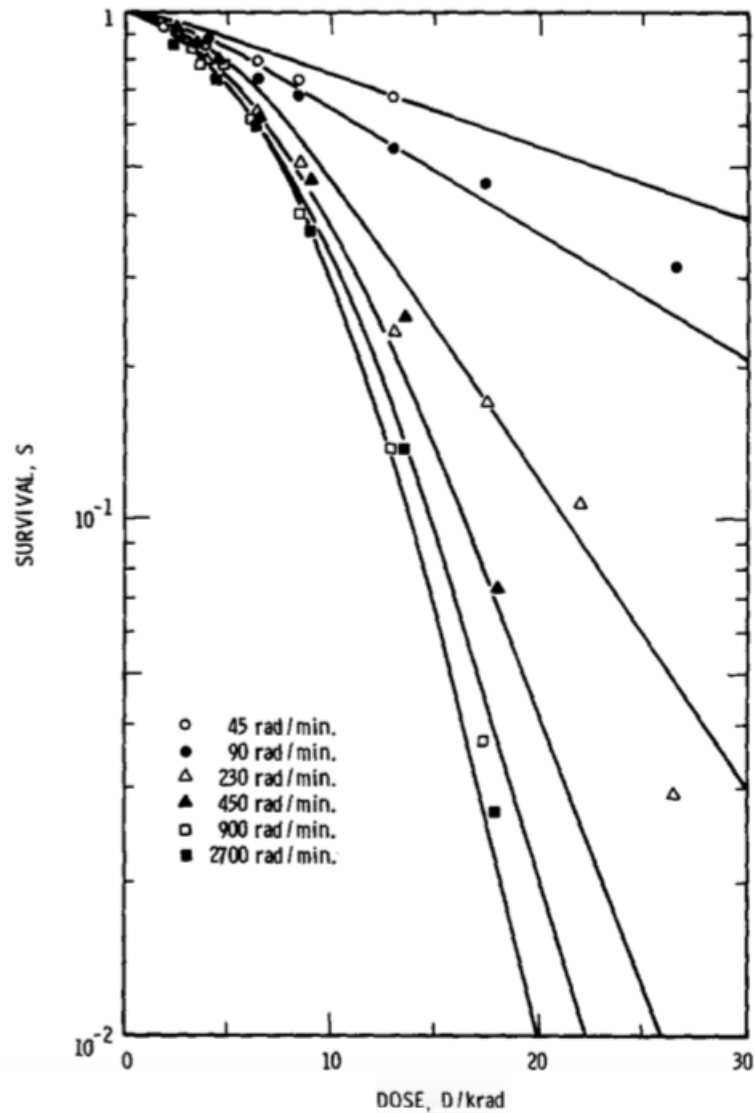


Figure 2.11: Surviving fraction behaviour with different exposure rates: the curves represent the effect of different exposure rates on a specific eukaryote alga population. The exposure time diminishes with increasing values of the exposure rate and with constant distributed dose values (from [31]).

Kerma is defined as

$$K = \Psi \left( \frac{\bar{\mu}_{tr}}{\rho} \right). \quad (2.7)$$

In equation (2.7),  $\Psi$  is the *photon energy fluence*, defined as the integral of the beam intensity with respect to time, and  $\frac{\bar{\mu}_{tr}}{\rho}$  is the *mass energy transfer coefficient*

that represents the probability per unit mass for a photon to be transferred. According to their definitions, kerma and absorbed dose represent the same quantity but on different points of view: in fact kerma represents the energy released on the radiation point on view while absorbed dose is the equivalent concept but on the matter point of view. In Figure 2.12 it can be seen how kerma reaches its maximum at the entrance of the medium, where the corresponding absorbed dose value is close to zero; according to the negative exponential behaviour of radiation inside matter previously described, kerma value decreases with increasing depth values while the dose increases until a maximum value beyond which it starts decreasing: the region in which kerma and absorbed dose values becomes comparable is called TCPE region (*Transient Charged Particle Equilibrium*). The initial difference between the two quantities is due to the *skin sparing effect*<sup>†</sup>; the reason why the absorbed dose value remains above the kerma one after its maximum point is linked to photons attenuation and scattering phenomena.

Radiotherapy purpose is to destroy tumour cells without delivering an excessive dose quantity to healthy cells in order to avoid all the negative consequences that have been listed in the previous lines. In general, the delivered dose is selected taking into consideration the two curves in Figure 2.13 that represent the principle of *therapeutic ratio*: *Curve A* represents the *TCP* (Tumour Control Probability), while *Curve B* represents the *NTCP* (Normal Tissue Complication). In order to avoid complications, in radiotherapy the dose is included in the interval  $TCP \geq 0.5$  and  $NTCP \leq 0.05$ .

*Equivalent dose* is another important parameter. It is a quantity similar to the absorbed dose (see chapter 1.3.2) but it takes into account the effect of radiation on biological tissues. It is indicated with the letter *H* and it is measured in sievert

---

<sup>†</sup>The skin sparing effect is a phenomenon that is characteristic of the first skin layers and it consists on the difference between the energy released by radiation and the effective one absorbed by matter. The penetrating radiation energy is sufficient to generate ionisations and so to create free electrons that will deposit their energy somewhere else; after that, when the radiation energy becomes comparable with the ionisation potential, the behaviour of the two quantities are almost the same.

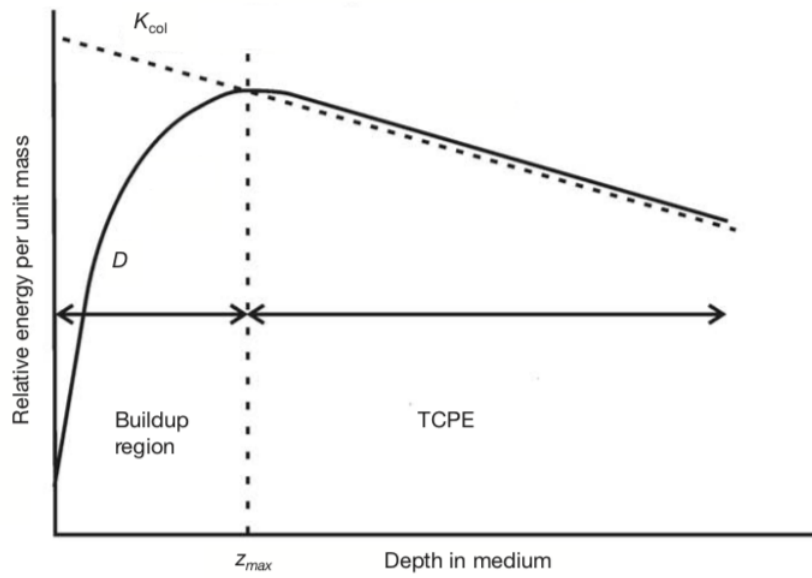


Figure 2.12: Kerma and absorbed dose behaviour at different depth values (adapted from [26]).

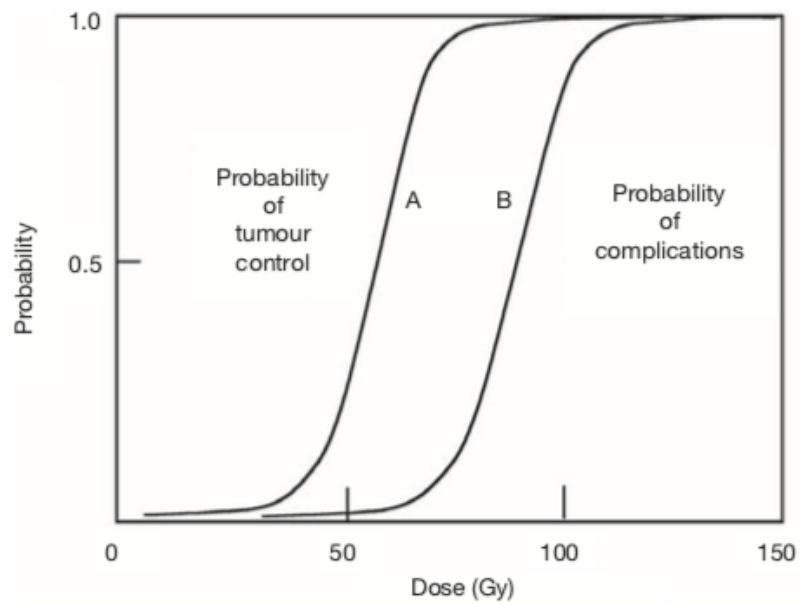


Figure 2.13: Principle of therapeutic ratio (from [26]).

( $Sv$ ). The equivalent dose is defined as

$$H = w_R D, \tag{2.8}$$

Table 2.5: Radiation weighting factors (data from *European Nuclear society*).

Radiation type [-]	Energy [MeV]	Radiation weighting factor ( $w_R$ ) [-]
Photons	all energies	1
Electrons, Mhyons	all energies	1
Protons	>2 MeV	5
$\alpha$ particles Fission fragments Heavy nuclei	all energies	20
Neutrons	<1 MeV	$2.5+18.2e^{-\frac{[\ln(E_n)]^2}{6}}$
	$1 \text{ MeV} \leq E_n \leq 50 \text{ MeV}$	$5.0+17.0e^{-\frac{[\ln(2E_n)]^2}{6}}$
	$E_n > 50 \text{ MeV}$	$2.5+3.25e^{-\frac{[\ln(0.04E_n)]^2}{6}}$

where  $D$  is the absorbed dose expressed in grey and  $w_R$  is the *weighting factor*. This last term indicates the radiation effectiveness on biological tissues and it depends directly on radiation type and on its energy according to Table 2.5. Starting from the equivalent dose definition, it can be defined another quantity that is the *radiation biological effectiveness* (RBE). It is defined as

$$RBE = \frac{\text{Dose from a sample radiation to produce a certain biological effect}}{\text{Dose from actual radiation to produce the same biological effect}}. \quad (2.9)$$

The sample radiation in the previous equation is currently produced by  $\gamma$  rays beam from a  $^{60}\text{Co}$  source, while in the past it was constituted by a 250 kVp X rays beam. Unlike the weighting factor, RBE depends also on the kind of biological tissue and on the dose rate value. RBE is strongly influenced by LET value as it can be seen in Figure 2.14: from a REB value equal to one in the low LET region, in the high LET one its value increases with increasing LET values.

Oxygen presence is also a parameter that affects the cells surviving fraction during irradiation. The alkyl radical explained before in this chapter can react with oxygen, making the cell damage permanent according to the following reaction and

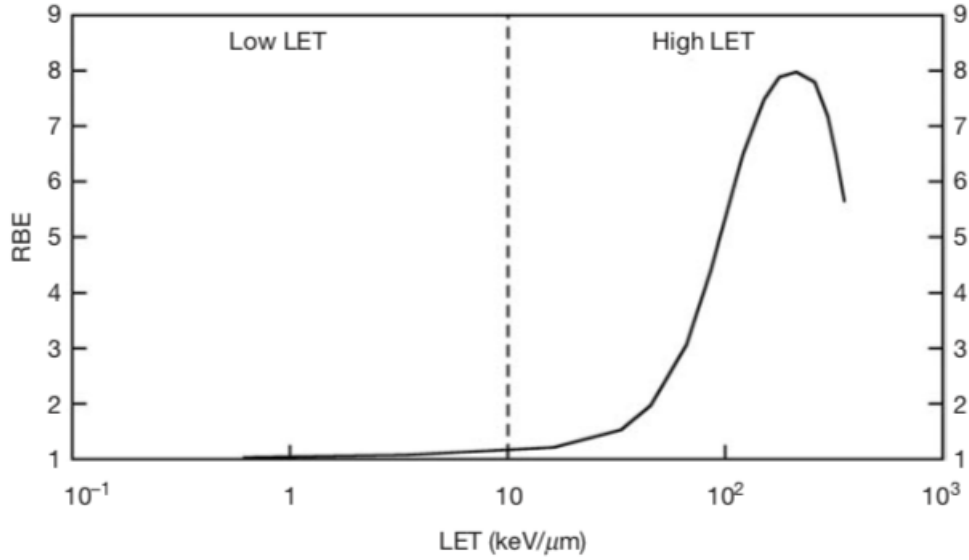
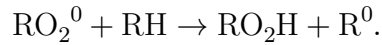
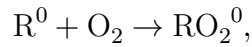


Figure 2.14: RBE variation with LET: the dashed line represents the limit value that divides the high LET from low LET region (from [26]).

inducing the reproductive process that will bring eventually to the cell death:



The oxygen effectiveness can be evaluated with the OER (*Oxygen Enhancement Ratio*), defined as follows

$$OER = \frac{\text{dose required to obtain a certain effect without oxygen}}{\text{dose required to obtain the same effect with oxygen}}. \quad (2.10)$$

In Figure 2.15, it can be seen the variation of the cells surviving fraction for an aerobic cell and for an hypoxic one: in order to guarantee the same value, an aerobic cell needs a lower dose with respect to an hypoxic one.

LET influences also OER and the dependence is shown in Figure 2.16. The OER value is larger in low LET region and it decreases with increasing LET values. It is not actually clear the reason of this behaviour but it could be due to the oxygen

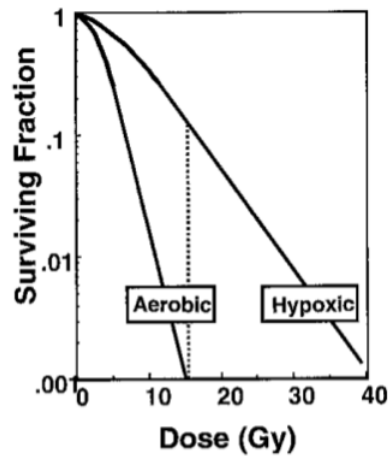


Figure 2.15: Cells surviving fraction behaviour for an aerobic cell and for an hypoxic one (from [20]).

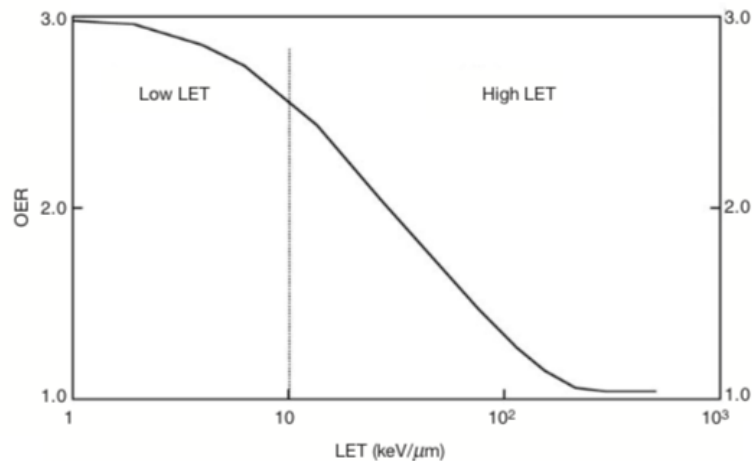


Figure 2.16: OER behaviour with respect to LET variation (from [26]).

role that is linked to radiation indirect effect and so to low LET values.

Oxygen influence on radiation effectiveness can be furthermore exploited thanks to the re-oxygenation process. In fact, tumour cells are characterised by high density: the inner cells are surrounded by less blood vessels than the outer ones and so the oxygen quantity stored is lower. In this way, the effect of radiation is more efficient on the external part with respect to the inner one that is hypoxic. After irradiation, this last part can be exposed to an oxygen flux in order to increase its concentration and to make the irradiation more effective. This procedure, called

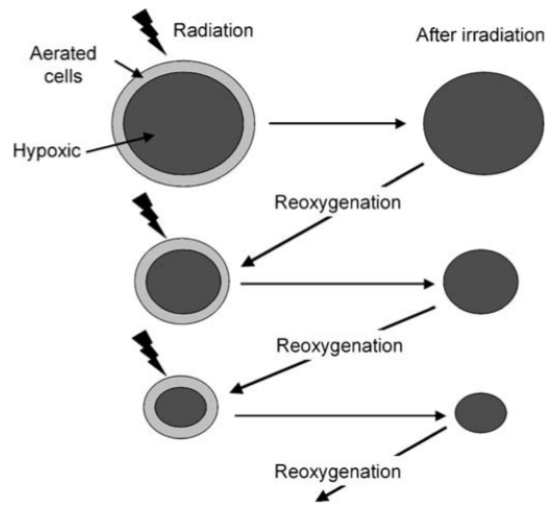


Figure 2.17: Re-oxygenation process (from [25]).

*re-oxygenation* is repeated, alternating irradiation phases to oxygenation phases until the tumour mass is destroyed (see Figure 2.17).

# Chapter 3

## Cardiovascular System

### 3.1 Introduction

The cardiovascular system is composed by a series of tubes in which blood flows driven by a sort of pump, that is the heart: it generates pressure that makes the blood flow through the various vessels. The blood delivers oxygen, taken in the lungs, and nutrients, taken in the intestine zone, to the cells that yield heat and wastes to be removed by the human body. Another important blood function is the interconnection among cells and their protection against foreign bodies.

So the main functions of the cardiovascular system can be resumed with:

- transport of nutrients, water and gases from the external environment,
- exchange of material among cells,
- transport of the cells wastes.

### 3.2 Blood composition

Blood is the fluid that flows in the cardiovascular system. In an average person the total amount of blood in his body is about 7.7% of his weight: it is composed for 55% by a liquid part, called *plasma*, and for the remaining 45% by a corpuscular part: for this reason, inside vessels it is considered a non-Newtonian fluid.

Plasma is the fluid part of the blood. It is a yellow-coloured liquid characterised by the presence of suspended elements transported by the flow. Its composition is similar to the one of the interstitial fluid: it is composed for the great part by water, by some chemical elements like sodium, potassium, chloride and other kind of ions, by some organic compounds like lipids and glucose and also by dissolved gasses. The difference with respect to interstitial fluid is that plasma has a larger hydrostatic pressure due to the presence of plasma proteins that are produced by the liver.

The corpuscular portion of the blood is composed by *red blood cells* (RBCs), also called *erythrocytes*, *white blood cells* (WBCs), also called *leukocytes* and *platelets*. All these kinds of cells are produced starting from the same precursor, called *pluripotent hematopoietic stem cell*, that can be found inside the bone marrow located in the bones center.

RBCs constitute the great majority of the corpuscular blood part because they are about 99% of the total.

With the cell differentiation starting from the precursor inside the bone marrow, the RBC loses its nucleus and other cellular organelles; for this reason, they lose their reproductive capability and they die after four months with part of them that is recycled by the liver. RBC are red-coloured and they are characterised by a biconcave shape that is due to a protein called *spectrin*.

Their main function is the transport of oxygen collected in lungs to the body cells and of the carbon dioxide discharged to the lungs. In general, blood can carry oxygen dissolved in plasma or thanks to a particular protein that constitutes red blood cells, called *haemoglobin*. This kind of macrobiological molecule is a protein composed by four chains of globin, each one linked to an iron-containing chemical structure, where the ion  $Fe^{2+}$  links directly with the oxygen molecule.

The RBCs quantity inside blood is indicated with a ratio called *hematocrit* that represents the ratio of the volume occupied by erythrocytes over the whole volume occupied by blood. Its value must be included in the range 37-47% for women and 42-52% for men: values lower than the intervals minima bring to a condition called *anaemia* while values larger than the intervals maxima bring to a condition called *polycythemia*; both these conditions are dangerous for human life.

WBCs are another constituent of the corpuscular blood part. They are less

numerous than RBCs and in fact they represent about 1 % of the total corpuscular blood volume.

This kind of cells differs from the other ones composing the blood corpuscular part because they do not eject their nucleus during the differentiation process of the cell precursor and for this reason they are bigger than RBCs and platelets. They can be found inside the blood circulation but they have also the capability to go out from it and to move inside the lymphatic system in order to perform their function where it is necessary. Their main function is to protect the human organism from external attack of pathogenic agents like parasites, virus, bacteria and fungi. They can be classified according to many parameters but the most diffused classification today is the one that divides them according to the presence or not of granules inside the cell cytoplasm. If leukocytes has granules inside their cytoplasm, they are called *granulocytes* and there is another classification according to the granules properties:

- *Neutrophil* granulocytes: they act against bacteria and fungi, encasing them through the phagocytosis mechanism.
- *Eosinophil* granulocytes: they act against worms infestations and allergic disorders, releasing the toxic content of their granules once the extraneous organism has been incorporated.
- *Basophils* granulocytes: they act releasing particular substances, like *histamine*, to fight against inflammatory reactions.

The entire previous list is referred to WBCs characterised by a nucleus with a non well defined form and made of "lobes".

Another class of leukocytes is composed by *Mononuclear leukocytes*. They are characterised by a well defined form of the nucleus and by the granules absence inside the cell cytoplasm. They can be furthermore subdivided into two different groups:

- *Monocytes*: they are the precursors of the *macrophages* that act against every type of pathogenic organism, once differentiated along the path from the bone marrow to the blood circulation. Each external body is phagocytized

and then, inside the cell cytoplasm, it is digested by the macrophage Golgi apparatus and its various vesicles.

- *Lymphocytes*: they can be found in the lymphatic system and, according to the kind of response to the pathogenic organism, they can be subdivided into *T cells* (thymus cells), *B cells* (bone-marrow cells) and *NK cells* (natural killer cells).

Platelets are the last components of the corpuscular blood part. They are smaller than WBCs and RBCs and, like these last one, they do not have a nucleus. Their main function is linked to the haemostasis and to the blood coagulation: in fact they are active parts when a blood vessel breaks and there is blood leak. In case of vessel rupture, vasoconstriction is the first thing to happen in order to reduce blood flow and pressure to reduce loss of blood. Then, platelets start to interact with the exposed vessel collagen thus releasing inside the blood a protein called *cytokine*: it attracts other platelets that aggregates to form a plug. At the same time, in order to start the coagulation process, from the collagen the damaged vessel part emits into the blood some factors that, thanks to a series of chemical reactions, creates the *fibrin*, that is a protein thanks to which the previous platelets plug is stabilised and reinforced: the new structure is called *clot*. The clot is then stabilised and the new epithelium is formed above it. At the end, thanks the some enzymes action, the clot is degraded and the initial situation is restored.

### 3.3 System structure

The cardiovascular system is composed by *heart* and *blood vessels*.

#### 3.3.1 Heart structure

Blood moves through the cardiovascular system thanks to the heart that is a muscle that provides the required prevalence in order to guarantee blood circulation inside the body. It is situated inside the thoracic cavity, in the middle-right side of the chest, between the two lungs and protected by the rib cage.

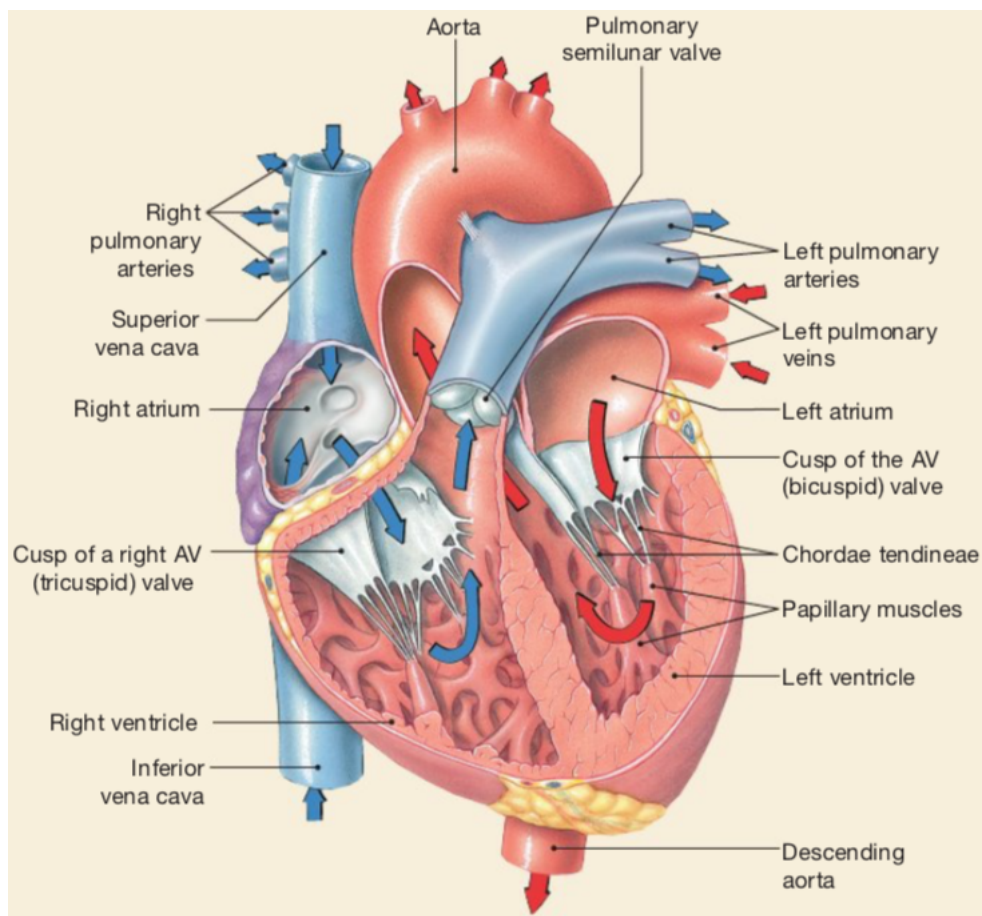


Figure 3.1: Heart structure: following the arrows, it can be noticed the one-way flow through it (from [6]).

The heart is divided into two halves by a central wall called *septum*. Both left and right halves are subdivided into two different cavities, *atria* and *ventricles*, that are respectively the upper cavities and the lower ones (see Figure 3.1): atria receive blood coming from the body circulation while ventricles pump it towards the vascular system. The righthand heart half receives blood coming from body cells; via the right ventricle contraction, it is pumped to the lungs where it is re-oxygenated and then it goes back to the heart. The lefthand heart half receives blood coming from the lungs: it is full of oxygen and so it is ready to be pumped towards the body tissues by mean of the left ventricle contraction phase.

The one way flow is ensured by two sets of valves: the first ones are the *atrioventricular valves* (AV) that are located between atria and ventricles and the second ones are the *semilunar valves* (SL) that are located between the ventricles and the rest of the vascular system.

As it can be seen from Figure 3.1, each atrium is connected to the corresponding ventricle thanks to the AV that are made of thin flaps of tissue connected to tendons called *chordae tendineae*: they prevent that the valves flaps are pushed inside atria during the ventricular contraction phase thus generating a condition named *prolapse*. There are two AV valves: the first one connects the right atrium with the corresponding ventricle and it is called *tricuspid valve* because it has three flaps; the second one connects the left atrium with the left ventricle and it is called *mitral* or *bicuspid valve* because it has two flaps.

The semilunar valves connect ventricles with the vascular system. They are the *aortic valve*, located at the exit of the left ventricle, and the *pulmonary valve*, located at the exit of the right one. They are open during the ventricle contraction phase, called *diastole*, and they are closed during the ventricle relaxation phase, called *systole*. As a matter of fact, valves condition during the heart cycle varies according to the phases that are simultaneous for both left and right heart half :

1. *atrial and ventricular diastole* (0.4 s): both atria and ventricles muscles are relaxed, blood comes from the vascular system and it flows inside them; AV valves open when the atrial pressure is larger than the ventricular one and blood flows because of gravity; SL valves are closed because the pressure in the arteries is larger than the ventricular chamber one after the ventricular contraction phase.
2. *atrial systole* (0.1 s): atria contract and they pump all the remaining blood towards ventricles that are still in diastolic condition; during this phase, some blood is sent backwards to the venous circuit because of the absence at the atria entrance of one-way flow-valves; AV and SL valves position does not change during this phase with respect to the previous one.
3. *ventricular systole* (0.3 s): ventricles muscles start contracting so the fluid pressure inside them increases; AV valves close because the ventricle chamber

pressure becomes larger than the one of the veins system, SL valves open because a positive pressure gradient is generated between ventricles chambers and the arterial circulation environment and so blood is sent to the vascular system; during this phase, atria are in diastolic condition so blood starts to fill them.

After ventricles systole phase, a new heart cycle begins: ventricles relax and, when the arterial pressure becomes larger than the one in the ventricles chambers, blood back-flow starts, thus causing the SL valves closure. A new cycle starts, repeating phases from 1 to 3 just mentioned.

In Figure 3.2 the behaviour of the different valves can be seen during the heart cycle.

The heart is covered by a thin membrane, called *pericardium*, inside which there is a pericardial fluid that provides lubrication to the external muscles surface during the systole and the diastole phases.

The heart in turn is made of *myocardium* that is a cardiac muscle different from the other ones inside the human body because they work without any innervation. In fact, there is about 1% of the myocardial cells, called *auto-rhythmic cells*, that is specialised in generating action potential spontaneously, so it means that they generate electric signals without any external input.

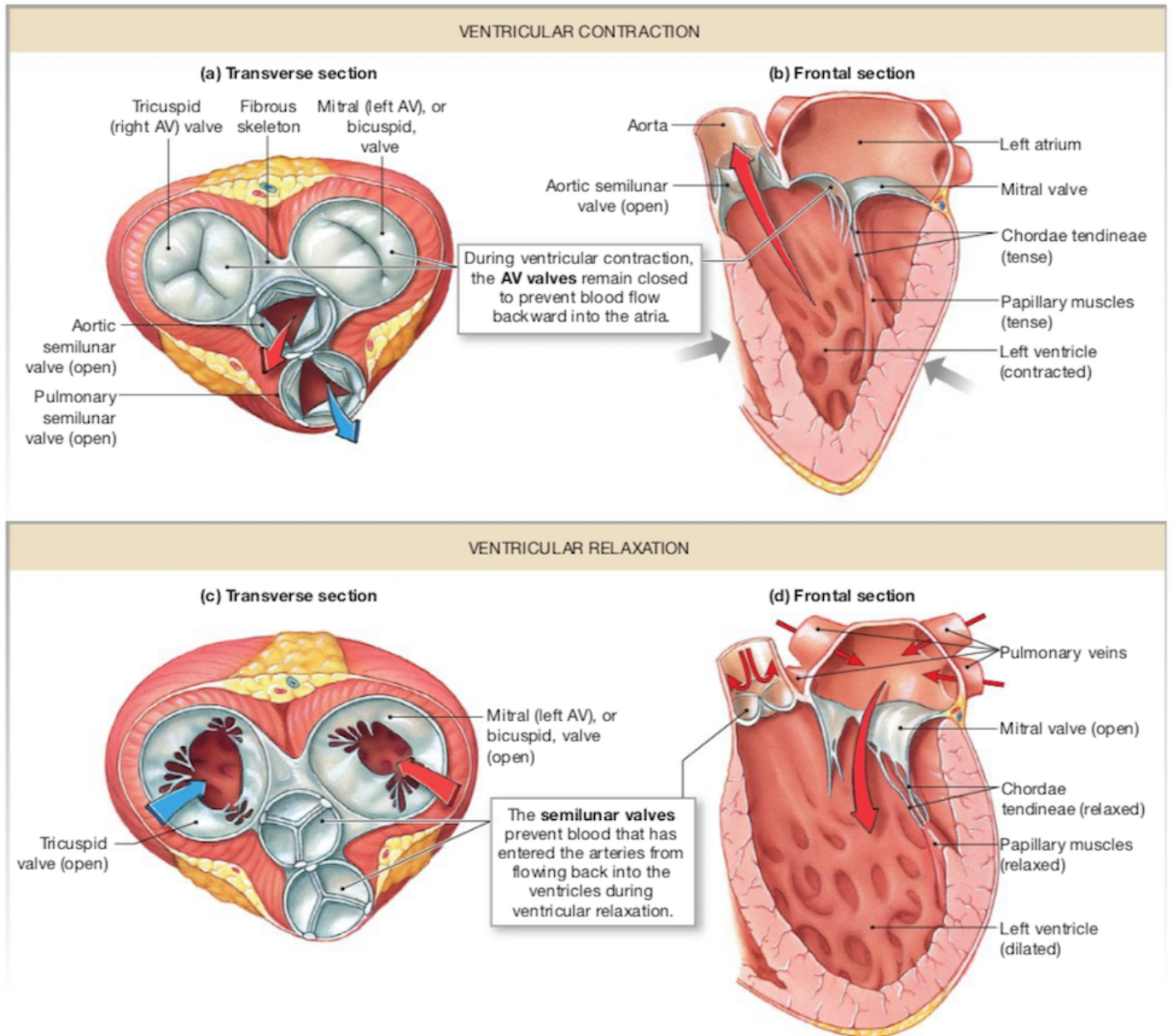


Figure 3.2: Heart valves during ventricular systolic and diastolic phases (from [6]).

### 3.3.2 Blood vessels structure

The vascular system function is blood transport. It is composed by two different types of elastic conduits: *arteries*, that carry blood away from heart, and *veins*, that return the blood to it. Full oxygenated blood has a lighter colour than the venous one that is full of cells wastes: for this reason, conventionally, the former is graphically represented with red colour while the latter with the blue colour.

There are two different types of circulation that repeats cyclically: *pulmonary circulation* and *systemic circulation*.

Pulmonary circulation starts in the right atrium, the blood flows to the right ventricle and, with the ventricular systole, it is pumped towards the lungs by mean of the *pulmonary artery*; in the lungs, blood gives wastes gasses and it gets oxygen. After that, blood goes back to the heart through the *pulmonary veins*.

Blood circulation continues with the systemic circulation that starts in the left atrium, where the blood is after the pulmonary circulation is ended. It passes in the left ventricle and then it is pumped out in the most important artery of the whole body: the *aorta*. Starting from it, the different arteries branches, reducing their size more and more until the small network of *capillaries* : here, arterial blood exchanges nutrients, water and gasses with cells wastes. The circulation becomes venous and it goes back to the heart right atrium with the veins diameter that becomes larger and larger: they join in the upper part of the body to form the *superior vena cava* and in the lower part the *inferior vena cava* that flow into the right atrium.

In Figure 5.2 a simplified cardiovascular system is represented.

## 3.4 Blood flow through cardiovascular system

Blood flows through the cardiovascular system and its movement can be considered similar to the one of a fluid inside a pipes system. Blood flow is indicated with the letter  $Q$  and it is measured in  $\frac{l}{min}$ . It is proportional to the pressure gradient along the vessels system:

$$Q \propto \Delta p \tag{3.1}$$

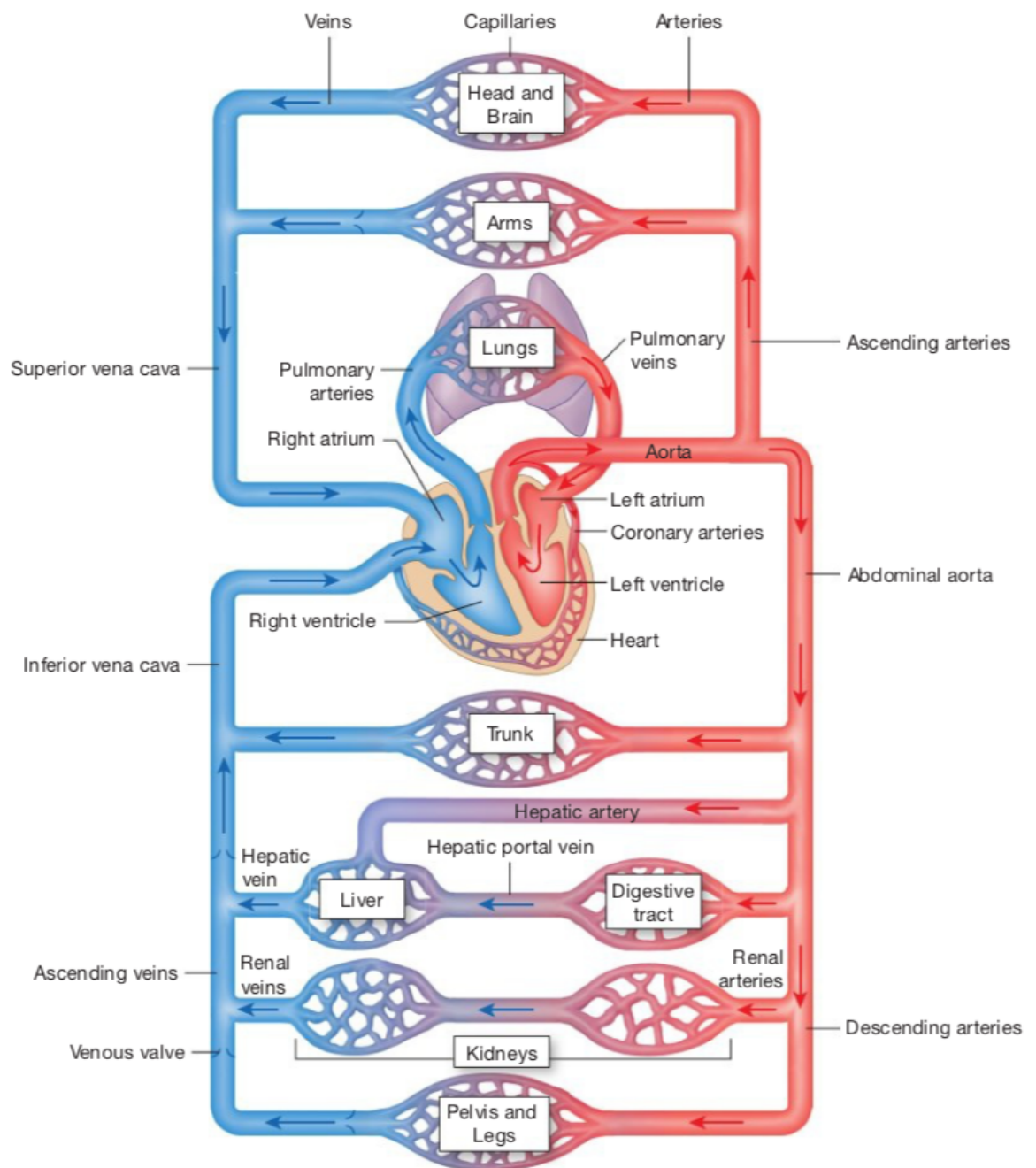


Figure 3.3: Cardiovascular system schematisation (from [6]).

where  $\Delta p$  represents the pressure drop between two different vessel section, with pressure expressed in medicine field in millimetres of mercury (mm of Hg). As it can be seen in Figure 3.4a, fluid flow develops from region characterised by high pressure

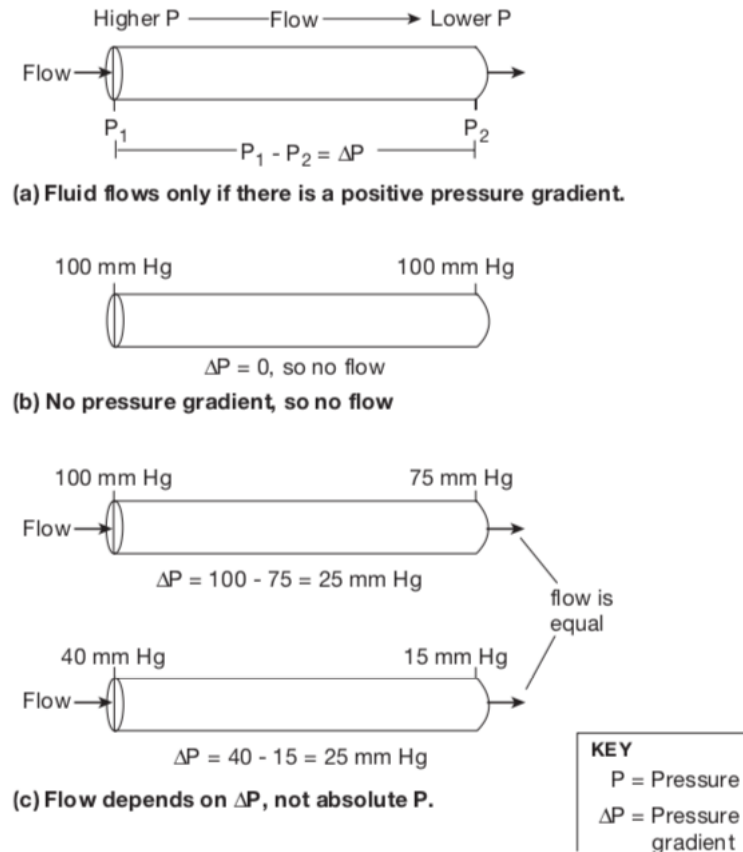


Figure 3.4: Pressure gradient examples in tubes (from [6]).

to regions characterised by low pressure region. According to proportionality expressed in (3.1), blood flows only with a pressure drop between two sections different from zero, that is Figure 3.4b case, and it does not depend on the absolute pressure value: in Figure 3.4c, it can be seen how different absolute pressure values bring to the same pressure drop. In the cardiovascular system, the higher pressure value is given by the heart prevalence during the ventricular systole phase and it decreases along the path because of friction losses according to dynamic laws, reaching its minimum value in the venae cavae and so at the entrance of the right atrium; during the systole phase, the pressure inside the whole vessels circuit is maintained by the arteries that act like pressure reservoirs thanks to the resistance that they oppose to the fluid flow. In Figure 3.5 pressure behaviour along the circulator system is shown.

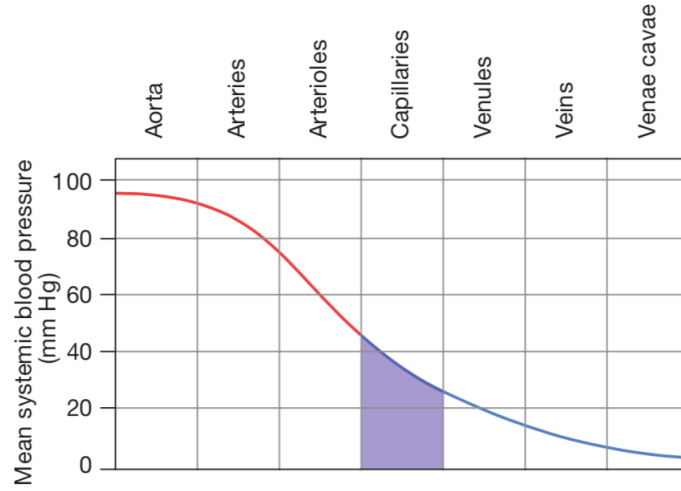


Figure 3.5: Pressure behaviour along the circulation system: maximum pressure value of about  $93\text{ mm of Hg}$  is reached in the first aorta sections and then it drops to about  $2\text{ mm of Hg}$  inside the venae cavae (from [6]).

The overall pressure drop along a pipe is due to two different contributions:

$$\Delta p = \Delta p_{major} + \Delta p_{minor} \quad (3.2)$$

whit  $\Delta p_{major}$  represents the *major losses* while  $\Delta p_{minor}$  represents the minor losses.

Major losses in a pipe are due to friction and they depend on a series of parameters as it is shown in the following functional form

$$\Delta p_{major} = \Phi(v, D, l, \epsilon, \mu, \rho). \quad (3.3)$$

The pressure drop value along a pipe depends on parameters characteristic of the pipe itself and of the general flow and on fluid properties: in fact, in (3.3),  $v$  is the average fluid velocity on the pipe section,  $D$  is the pipe diameter,  $l$  is the pipe length or the length,  $\epsilon$  is the roughness of the pipe walls and  $\mu$  and  $\rho$  are respectively the fluid dynamic viscosity and density. Referring to the blood, these last two parameters are affected by the hematocrit but in general they can be considered constant along the whole vessels circuit. Parameters  $D$ ,  $l$  and  $\epsilon$  depend on the anatomy of the body; in particular  $D$  is maximum in the aorta, it becomes

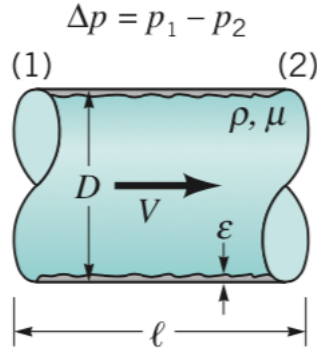


Figure 3.6: Pressure drop dependencies (from [23]).

smaller and smaller till the capillaries where it reaches its minimum value and it then starts to grow up again: in fact, in the aorta it is equal to about 3 cm, in capillaries it varies from a few dozen of  $\mu m$  to some  $\mu m$  and in the two venae cavae it assumes values of about 2 cm. The value of the blood velocity is strongly influenced by the vessel diameter because it is expressed as

$$v = \frac{Q}{A} \quad (3.4)$$

where  $A$  is the vessel cross section that depends on the diameter according to

$$A = \pi \frac{D^2}{4}. \quad (3.5)$$

Substituting (3.5) into (3.4), the velocity expression becomes

$$v = \frac{4Q}{\pi d^2}. \quad (3.6)$$

In equation (3.6), considering the blood volumetric flow rate constant in time along a blood vessel part, it can be seen how the velocity changes with diameter variations: fluid speed decreases with larger values of cross section and vice versa. The functional form (3.3) can be evaluated as follow:

$$\Delta p = f \frac{l}{D} \frac{\rho v^2}{2}. \quad (3.7)$$

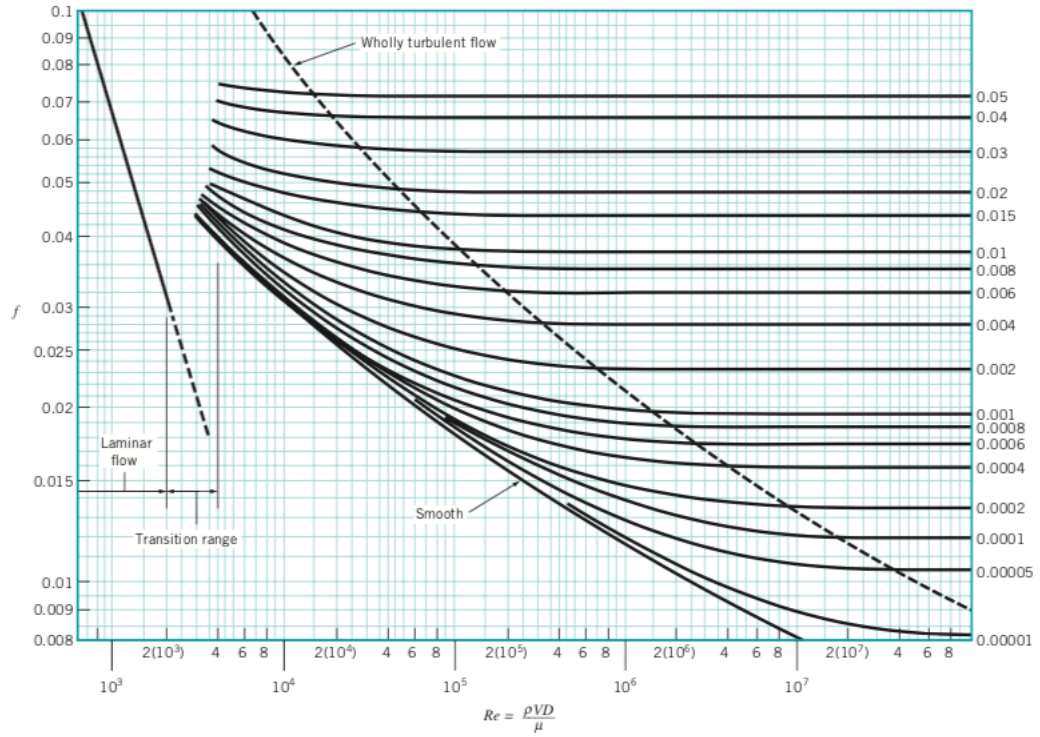


Figure 3.7: Moody chart (from [23]).

In equation (3.7),  $f$  is the *friction factor* that is a function of the Reynolds number ( $Re = \frac{\rho v d}{\mu}$ , where  $\rho$  is the fluid density in ( $\frac{kg}{m^3}$ ),  $v$  is the fluid speed in ( $\frac{m}{s}$ ),  $d$  is the characteristic length of the observed phenomenon in ( $m$ ) and  $\mu$  is the fluid dynamic viscosity in ( $Pa \cdot s$ )) and of the ratio of  $\frac{\epsilon}{D}$  and whose value depends on the kind of flow regime:

- laminar flow ( $Re < 2300$ ):  $f = \frac{64}{Re}$
- turbulent flow ( $Re > 4000$ ): the values of the friction factors can be evaluated thanks to the *Colebrook formula*

$$\frac{1}{\sqrt{f}} = -2.0 \log\left(\frac{\epsilon}{3.7D} + \frac{2.51}{Re\sqrt{f}}\right) \quad (3.8)$$

that is graphically represented in the *Moody chart* (Figure 3.7).

In normal conditions, the blood flow regime is laminar and it is turbulent only in the regions of the cardiac valves. Turbulent flow regime could rise downstream of

the stenosis in case of stenotic vessel, in case of hematocrit value reduction due to a haemoglobin reduction (Re increase is due to a reduction of the fluid viscosity) and in case of increase of blood pumped by heart due to an excessive nutrients consumption by cells (for example, in case of physical activity).

Minor losses in pipes are due to the presence of valves or changes in geometry. In the blood vessels case, the only contribution to the minor losses is given by the change of the flow passage geometry.

The expression of the minor losses is similar to the major ones:

$$\Delta p_{minor} = K_L \frac{1}{2} \rho v^2, \quad (3.9)$$

where  $K_L$  represents the *loss coefficient* that is a function of the Reynolds number and of the geometry.

There could be two different cases of geometry variation in vascular physics:

- aneurysm: it is a condition of button of the blood vessel that is usually due to atherosclerotic phenomena; according to the *Venturi effect* (Figure 3.8), the fluid slows down and its pressure increases, generating a force on the vessel walls that could bring to rupture, internal bleeding and death. The value of the loss coefficient is expressed as

$$K_L = \left(1 - \frac{A_1}{A_2}\right)^2 \quad (3.10)$$

and it depends on the flow passage area before ( $A_1$ ) and after ( $A_2$ ) the expansion.

- stenosis: it is the condition in which there is a reduction of the vessel flow passage area that is usually due, as the previous case, to atherosclerotic phenomena; according to the *Venturi effect*, the fluid velocity increases causing a reduction of the pressure that could worsen the situation. The value of the loss coefficient in this case depends on the type of junction as in can be seen in Figure 3.9.

Another parameter that influences the blood flow inside the cardiovascular

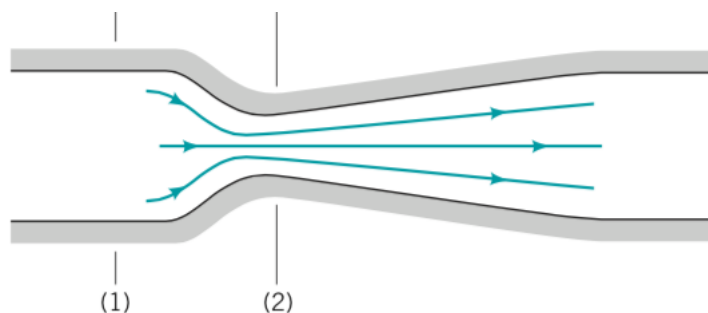


Figure 3.8: Venturi effect. The Venturi tube is a duct characterised by a reduction of the flow passage area (from 1 to 2). Applying the Bernoulli equation to an horizontal Venturi tube, it becomes  $p + \frac{1}{2}\rho v^2 = const.$  and it can be seen how a velocity reduction causes a pressure increase and vice versa ( $A_1 > A_2 \rightarrow v_1 < v_2 \rightarrow p_1 > p_2$ ) (from [23]).

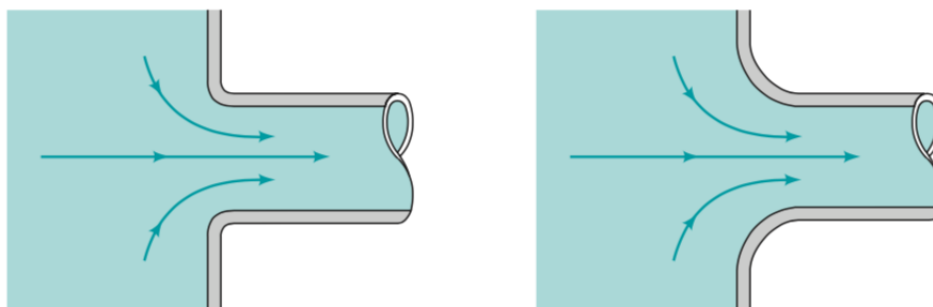


Figure 3.9: Pressure loss coefficient in case of contraction: slightly rounded case (lefthand-side figure)  $K_L = 0.2$ , well-rounded case (righthand-side figure)  $K_L = 0.04$  (from [23]).

system is the system resistance to the flow indicated with  $R$ . The dependency between the flow and the resistance is given by

$$Q \propto \frac{1}{R}. \quad (3.11)$$

As it can be seen from (3.11), the bigger is the resistance value and the lower is the blood flow and vice versa.

The flow resistance depends on other parameters and it is expressed thanks to the

*Poiseuille's law*

$$R = 8 \frac{l\mu}{\pi r^4} \quad (3.12)$$

In (3.12),  $l$  is the vessel length,  $\mu$  is the dynamic viscosity and  $r$  is the vessel radius. As previously said, blood properties can be considered constant inside the whole circulation and the length of the vessels depends only on the anatomy of the body: for this reason the resistance value can be considered affected only by the vessel radius.

To sum up, putting together (3.4) and (3.12), it comes to

$$Q \propto \frac{\Delta p}{R} \quad (3.13)$$

that means that the blood flow is directly proportional to the pressure drop along the system and inversely proportional to the resistance opposed by the system.

# Chapter 4

## Software packages used

### 4.1 Blender

Blender is a professional open-source 3D computer graphic software. It is possible to do a great variety of things thanks to its features that include simulations of every type, from the fluid and smoke ones to the particles ones, the possibility to generate animations of 3D models, images rendering, video editing, video games projects,... Among Blender characteristics there is the possibility to interact directly with the program thanks to an integrated Python console where the user can write the code that corresponds to the desired instruction that he wants to be solved. Blender is a software easy to learn, especially thanks to the various shortcuts given by keyboard inputs, though the mouse use still remains more intuitive.

Blender version used is 2.79b. The two main objects management methods, that are also the only two used during the work, are *Object Mode* and *Edit Mode* (after selected an object, it is possible to pass from the first to the second thanks to the *tab* button): the former is used to manipulate objects, while the latter is used to manipulate the objects data and structures, like *faces*, *edges* and *vertices*. The software let the user to use more than one scene and to work on different layers up to a maximum of twenty .

Blender has been used to develop the first part of the work. The first thing used is the integrated modifier "*Boolean Union*" thanks to which it

has been possible to join different parts of the required system.

Virtual phantom sectioning has been another operation made in Blender. It has been performed thanks to a particular integrated tool called *Dynamic Paint*. It is a modifier that transforms the objects in the analysed scene into *brushes* and *canvas* thanks to which it is possible to generate coloured images. It has been used to generate the CT images of the used virtual phantom. This tool is linked to a restriction: it is possible to dissect one object at a time. For this reason it has been used a Python script developed by a former student, M. Mezzano, that automates the whole procedure. The CT images relative to each organ are saved in a folder named `<organ_name.vol>` and each image is saved as `<organ_progressive_number.png>`.

## 4.2 MATLAB

The output of the sectioning process becomes the input of the following step, the composition of the whole CT image. As well as the previous one, this procedure is also automatised thanks to a MATLAB script written by the same previous student: the script receives as input the set of images generated in the previous step, it converts them into greyscale and they are sorted from the larger to the smaller one; this way of sorting is useful because, after that, CT images can be superposed to obtain the global sections in greyscale. The MATLAB script gives also two more outputs that are two binaries 3D matrices containing the information about the organs Hounsfield numbers (see Chapter 4.2.1) and their own IDs. These last outputs are the inputs for the real simulation on *Geant4*.

### 4.2.1 Hounsfield Scale

In order to get the dose distribution in the body tissues, CT images are needed. They are generated by particular types of machineries able to elaborate the radiation signals detected. Equation (2.3) is the physical law that describes the photons behaviour inside the human body and, as it has been said, it depends on the energy and on position ( $\mu = \mu(E, s)$ ). Considering a single spatial location point, the

attenuation coefficient value is defined as

$$\mu(E) = \rho N_A \sum_{i=1}^n \left( \frac{\omega_i}{A_i} \sigma_i(E) \right) \quad (4.1)$$

where  $\rho$  ( $\frac{g}{cm^3}$ ) is the mass density,  $N_A$  ( $\frac{1}{mol^{-1}}$ ) is the Avogadro Number,  $\omega_i$  ([–]),  $A_i$  ( $\frac{g}{mol}$ ) and  $\sigma_i$  (*barn*) are respectively the weight, the total cross section and the atomic mass of the  $i^{th}$  element. In order to remove the energy dependence of the parameter, the attenuation coefficient can be evaluated as a mean value with respect to a spectral function  $f(E)$  as follow

$$\bar{\mu}(s) = \frac{\int f(E) \mu(E, s) dE}{\int f(E) dE}. \quad (4.2)$$

Different kinds of scanners could give different results also with the same input: in order to get rid of this problem and to get comparable outputs, the result has been converted into a new scale called *Hounsfield scale*, indicated with the letter  $H$

$$H = \left( \frac{\bar{\mu}(s)}{\mu(H_2O)} - 1 \right) * 10^3. \quad (4.3)$$

In (4.3),  $\bar{\mu}(s)$  is the parameter evaluated in (4.2) and  $\mu_{H_2O}$  is the reference value of the attenuation coefficient that has been chosen equal to the water one: the water value of  $H$  is equal to 0 and the air one is equal to  $-1000$ .

In general, it can be said that the  $f(E)$  distribution is not known a priori and for this reason it is difficult to calculate  $H$  value. Although that, considering an energy distribution inside the characteristic range of nuclear diagnostic field, it is possible to parametrise the cross section:

$$\sigma_i(E) = Z_i (K(E))^{KN} + Z_i^{2.86} (K(E))^{sca} + Z_i^{4.62} (K(E))^{ph}. \quad (4.4)$$

In (4.4),  $K^{KN}$  represents the *Klein-Nishima coefficient*,  $K^{sca}$  takes into consideration the coherent scattering and the binding correction due to the incoherent scattering and  $K^{ph}$  takes into account the photoelectric absorption.

Substituting (4.4) into (4.1), the result obtained is

$$\mu(E) = \rho N_A \sum_{i=1}^n \left( \frac{\omega_i}{A_i} (Z_i \bar{K}^{KN}(E) + Z_i^{2.86} \bar{K}^{sca}(E) + Z_i^{4.62} \bar{K}^{ph}(E)) \right). \quad (4.5)$$

In (4.5),  $\bar{K}^{KN}$ ,  $\bar{K}^{sca}$  and  $\bar{K}^{ph}$  are averaged with respect to the spectral function. Considering the attenuation in water, the attenuation coefficient value is given by

$$\frac{\bar{\mu}(S)}{\mu_{H_2O}} = \frac{\rho}{\rho_{H_2O}} \frac{\sum_{i=1}^n \left( \frac{\omega_i}{A_i} \right) (Z_i + Z_i^{2.86} k_1 + Z_i^{4.62} k_2)}{\frac{\omega_H}{A_H} (1 + k_1 + k_2) + \frac{\omega_O}{A_O} (8 + 8^{2.86} k_1 + 8^{4.62} k_2)}, \quad (4.6)$$

where

$$k_1 = \frac{\bar{K}^{sca}}{\bar{K}^{KN}} \qquad k_2 = \frac{\bar{K}^{ph}}{\bar{K}^{KN}}.$$

It is possible to obtain the value of the attenuation coefficient expressed in Hounsfield units substituting (4.6) in (4.3).

If the analysed system is composed by only two subsystems, it can be defined a direct relation between the CT numbers of the two tissues and their physical parameters. The two subsystems are characterised by different densities, weights and H values: the first subsystem is described by  $\rho_1$ ,  $\omega_{1,i}$  and  $H_1$  while the second one by  $\rho_2$ ,  $\omega_{2,i}$  and  $H_2$ , hypothesising that  $H_1 < H_2$ ; the total system is described by its own parameters ( $\rho$ ,  $\omega_i$  and  $H$ ). Indicating with the symbol  $W_1$  the first subsystem quantity, consequently  $W_2$ , that represents the second subsystem quantity, is equal to the complement to unity of  $W_1$  ( $W_2 = 1 - W_1$ ). So for the total system:

$$\omega_i = W_1 \omega_{1,i} + W_2 \omega_{2,i} = W_1 (\omega_{1,i} - \omega_{2,i}) + \omega_{2,i} \quad (4.7)$$

$$\rho = \frac{m}{\frac{m_1}{\rho_1} + \frac{m_2}{\rho_2}} = \frac{1}{\frac{W_1}{\rho_1} + \frac{W_2}{\rho_2}} = \frac{\rho_1 \rho_2}{W_1 (\rho_2 - \rho_1) + \rho_1}. \quad (4.8)$$

Substituting (4.7) and (4.8) into (4.1), the following relationship is obtained

$$\begin{aligned}\bar{\mu}(E) &= \frac{\rho_1\rho_2}{W_1(\rho_2 - \rho_1) + \rho_1} N_A \left[ W_1 \sum_i \left( \frac{\omega_{1,i} - \omega_{2,i}}{A_i} \bar{\sigma}_i \right) + \sum_i \left( \frac{\omega_{2,i}}{A_i} \bar{\sigma}_i \right) \right] = \\ &= \frac{\rho_1\rho_2}{W_1(\rho_2 - \rho_1) + \rho_1} N_A \left[ W_1 \left( \frac{\bar{\mu}_1}{\rho_1} - \frac{\bar{\mu}_2}{\rho_2} \right) + \frac{\bar{\mu}_2}{\rho_2} \right].\end{aligned}\quad (4.9)$$

After some algebra and using equation (4.3), it is possible to link the quantity  $W_1$  with the Hounfield number of the whole system, indicated by  $H$ , with the following equation

$$W_1 = \frac{\rho_1(H_2 - H)}{(\rho_1 H_2 - \rho_2 H_1) + (\rho_2 - \rho_1)H}.\quad (4.10)$$

To conclude, substituting (4.10) in (4.7) and (4.8), the result obtained is the following

$$\omega_1 = \frac{\rho_1(H_2 - H)}{(\rho_1 H_2 - \rho_2 H_1) + (\rho_2 - \rho_1)H} (\omega_{1,i} - \omega_{2,i}) + \omega_{2,i}\quad (4.11)$$

$$\rho = \frac{\rho_1 H_2 - \rho_2 H_1 + (\rho_2 - \rho_1)H}{H_2 - H_1}.\quad (4.12)$$

This is a good simplification only dealing with hard tissues, like the system composed by bones and marrow. It is not the same considering soft tissues because they are not composed by two components but by three components that are in general water, proteins and fat: the procedure to get a simplification becomes more complex.

### 4.3 Geant4

Geant4 is a toolkit developed by an international collaboration that includes CERN in Geneva. It allows the user to perform Monte Carlo simulations in order to simulate particle passage through the matter: in fact, the acronym *Geant* stands for *GEometry ANd Tracking*.

A group of softwares engineers developed this toolkit that has been implemented in C++ programming language which is founded on the concept of *Object Oriented* programming (O.O.): it is a particular programming technique that consists in the interaction, through information exchange, of each single object with the other

ones. It is based on *classes* and *objects*: the former allows the definition of the main characteristics of an object or of a set of objects while the latter is a class instance. Because of the use of the O.O. programming technique, Geant4 software is divided into different components that are linked one to each other.

Thanks to Geant4 it is possible to analyse a great variety of processes, like the electromagnetic and the optical ones, it is possible to study particles and materials subjected to an energy range that runs from few eV to TeV; it is used to simulate processes in different fields like the nuclear one, the medical one, the space one. During the software implementation phase, some important features have been included like geometries and materials involved in the simulations, primary and secondary particles and all the related phenomena, the physics that governs the particles diffusion and interaction and many other physical models.

### 4.3.1 Geant4 structure

The used software is characterised by a hierarchical and modular structure, each one called *domain*. Each domain can have different subdomains that are linked according to a unidirectional flow, whose scheme is represented in Figure 4.1, with no circular dependencies. Each subdomain contains different classes that can be modified according to the user needs: this is possible thanks to the O.O. programming technique previously described.

`Global` is the lowest structures; it includes the system of units, mathematical constants, numbers and their random generation.

`Geometry` structure allows the user to handle volumes and particles transmission through the model. Volume definition in Geant4 is very wide because it is made of three more different concepts that are

- *solid*: it indicates the volume with only its geometrical characteristics;
- *logical volume*: it is the solid previously defined with information concerning materials and physical properties;
- *physical volume*: it represents the logical volume defined with spatial information.

Concerning the *logical volume*, a material can be also defined *sensitive* because, once particles enter this kind of volume, the user is able to access the information linked to the passage like deposited energy, position,... Volumes structure can be described as made of different layers: the *world volume* is the one that have to be defined as first step and it will constitute the absolute system of reference and the place in which other volumes will be generated; inside the world volume all the other structures, called *mother volumes*, can be defined; each mother volume can includes subvolumes, called *daughter volumes* that are characterised by the same physical characteristics of their parent volumes thanks to the inheritance property. **Tracking** structure controls particles propagation inside matter with the use of two different classes that are *track* and *step*: the former is a sort of picture of the particle that gives information on position and physics at a certain time instant while the latter can be considered composed by more than one steps and so it contains information of tracks of different consecutive points.

**Process** structure contains instructions to simulate basic physical processes and concerning models and laws that govern the physical interaction of particles with matter. Among these, there are *Particle decay*, *Electromagnetic physics*, *Low energy processes*, *Muons* and *Hadronic physics*.

**Hits+Digits** is the class that regulates particle interactions with a sensible volume of a detector. *Hits* represent the interaction or an accumulation of interactions of a single or more than one tracks with a sensitive volume of a detector; *digits* are linked to the detector volumes outputs generated by one or more hits.

**Tracking** structure takes care of particles path that, in Geant4, are transported and they are not self moving.

**Event** collects events according to the tracks and **Run** collects events in which particles interact in the same way with the detector or events referred to the same particles beam: together, these two classes provide the event generation.

**Visualisation** category provides the representation of the simulation result in a 3D view.

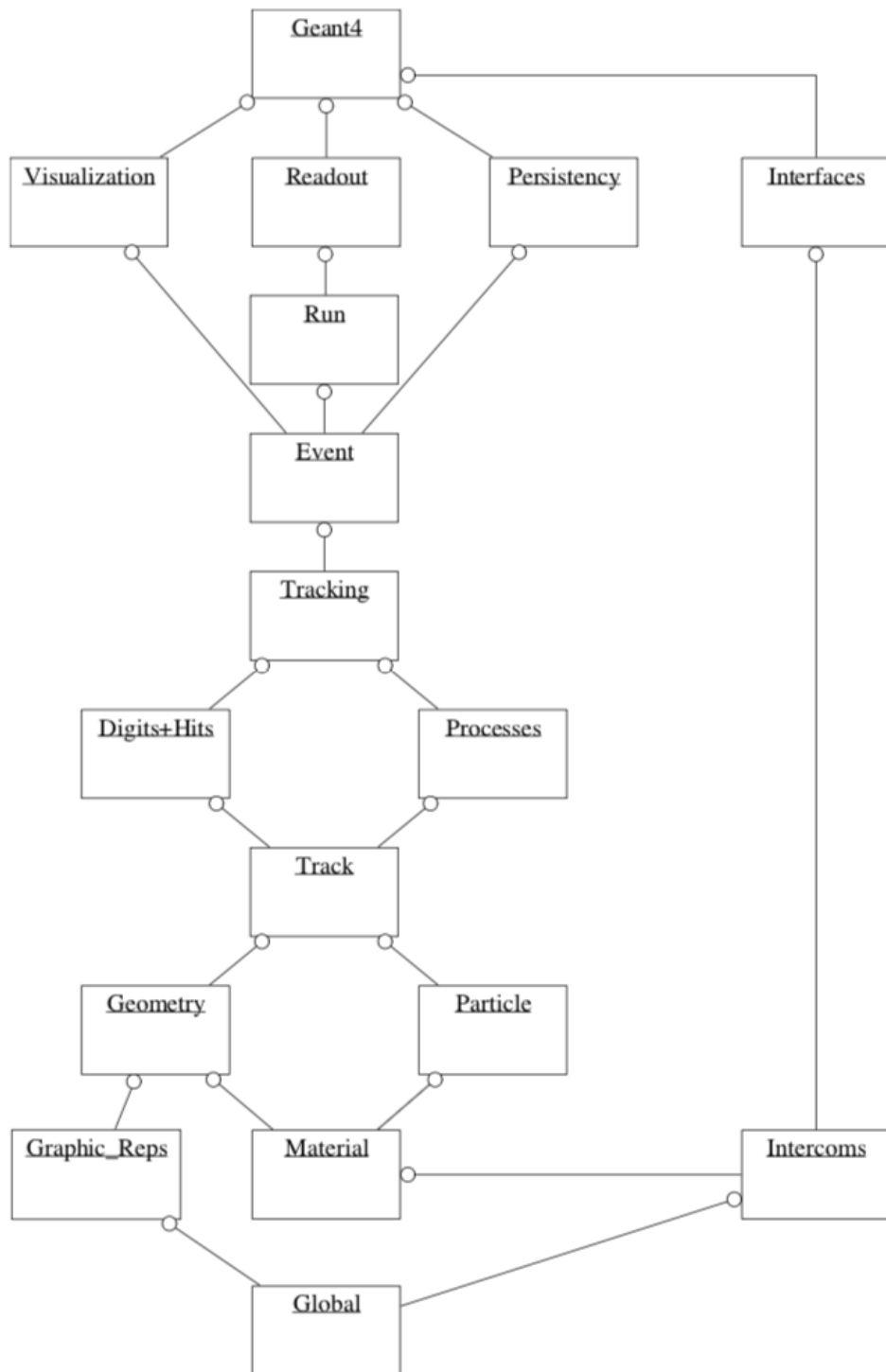


Figure 4.1: Geant4 structure flow diagram (from [1]).

# Chapter 5

## Virtual Phantom

### 5.1 General description

Anthropomorphic virtual phantoms are useful instruments used in nuclear medicine or radioprotection fields. They are 3D anthropomorphic models whose use is linked to TPSs (*Treatment Planning System*): in order to define a treatment plan, the analysis of the studied body must be given and it is an information provided by the results of a Computed Tomography. In general, CT images of real patients are characterised by different problems and for this reason it has been thought to use CT images of anthropomorphic virtual phantoms for the validation and the optimisation of TPSs. This last option has different advantages with respect to CT images of real patients:

- real CT images give the body composition that is not well represented while these ones coming from a virtual phantom are characterised by quantities that are well defined (materials, densities, chemical compositions,...);
- organs positions and limits are well delimited inside a virtual phantom but it is not true for CT scan results, where organs boundaries are not well-defined;
- real CT images quality is fixed and it is linked to the machine used to get them and so problems could arise in terms of resolution;
- real CT images use are limited by the patient privacy.

Virtual phantoms are models produced very accurately starting from patients data of different ages, sizes and physiological conditions. They are designed using CAD programs and *Boundary REPresentation* (BREP): this kind of modelling is based on three different structures that are faces, edges and vertices; each single surface is modelled using its geometrical limits and then they are covered with *textures* in order to give the final desired result. BREP representation is a very flexible technique that allows the user to design very complex geometries. Another characteristics of virtual phantoms is that organs are modelled using 3D NURBS (*Non Uniform Rational Basis-Splines*): they are particular kind of geometries used in the computer graphic field that are characterised by a great flexibility because they can be modified using control points. For these reasons, anthropomorphic virtual phantoms can be manipulated easily.

In general, the greatest advantage provided by the anatomic virtual phantom is given by the fact that they can be analysed according to a dynamic model because the user is free to change parameters of interest each time that he wants and according to the problem to be solved.

## 5.2 VPatient3D

VPatient3D is the name of the virtual phantom used in this MSs Thesis. It has been modelled by i-See s.r.l. on the basis of the MASH supine model available in the *Caldose* site. It has been projected and generated using Blender software and it is a representation of a male average human being (see Figure 5.1). VPatient3D is characterised by organs dimensions and positions that are coherent with the ICRP human-Adult Male (AM) model according to the *ICRP Report 110 (ICRP 2009)*; the information concerning material densities and compositions are not the same used for MASH, that were taken from literature, but in this case also these data are based on the ICRP recommendations.

VPatient3D has been modelled in Blender taking advantage of the possibility to work on different layers: fourteen layers have been used and each of them contains different components characterised by different materials; all organs and tissues with their own ID number are listed in Table 5.1.

Organ/Tissue	ID	Organ/Tissue	ID
Adipose abdominal	1	Linfa 04	44
Adipose breast	2	Liver	45
Adrenals	3	Lumbar spine	46
Bladder	4	Lung left	47
Bladder content	5	Lung right	48
Blood	6	Mandible	49
Blood center	7	Muscle diaphragm	50
Bones feet	8	Muscles face	51
Bones hands	9	Muscle feet	52
Brain	10	Muscle hands	53
Cartilage chest	11	Muscle legs	54
Cartilage clavicole	12	Muscle neck	55
Cartilage ear	13	Muscle thorax	56
Cartilage hands	14	Nasal cavity	57
Cartilage humerus	15	Oral cavity	58
Cartilage legs	16	Pancreas	59
Cartilage maxilla	17	Parotid gland	60
Cartilage nose	18	Patella	61
Cartilage pelvis	19	Pelvis	62
Cartilage spine 1	20	Penis	63
Cartilage spine 2	21	Pharynx	64
Cartilage thyroid	22	Prostate	65
Cervical spine	23	Ribs	66
Clavicle	24	Sacrum	67
Colon	25	Scapula	68
Colon content	26	Skin	69
Connective tissues	27	Small intestine	70
Cranium	28	Small intestine content	71
Esophagus	29	Spine	72
Eyes	30	Spleen	73
Femur	31	Sternum	74
Fibula and Tibia	32	Stomach	75
Gall bladder	32	Stomach content	76
Glandular breasts	34	Sublingual gland	77
Heart	35	Submandibular gland	78
Heart Blood	36	Teeth	79
Humerus	37	Testicles	80
Hyoid	38	Thimus	82
Kidneys	39	Thoracic spine	81
Lens	40	Thyroid	83
Linfa 01	41	Tongue	84
Linfa 02	42	Trachea	85
Linfa 03	43	Ulna and Radius	86

Table 5.1: Organs and tissues of the Virtual Phantom with their respective ID numbers.

### 5.3 Vascular system and its implementation

The object of this work is the definition of the distribution of an injected radiopharmaceutical inside the human body and the delivered dose to the surrounding biological tissues. It distributes thanks to blood circulation according to chemical and physical affinity, as it has been said in Chapter 2.1. For this reason, the vascular system has been extrapolated from VPatient3D model and it has been used to proceed with the work. It is known from Chapter 3.3.2 that the vascular system is divided into two circulations, the arterial one and the venous one. In the analysed model there is only one of them. Hypothesising that it represents the arterial system, its reference scheme is shown in Figure 5.2: as it can be seen, the arterial system represented is different from the real one because it is made of only the main vessels, without considering the smaller ones and the whole capillary network. In this way the problem is simplified but at the same time it is sufficient for the work purposes.

As it has been said, the VPatient3D model is endowed with only an half of the whole human vascular system and for this reason some modifications have been done in order to get results more similar to the reality.

The first step performed has been the connection of each single part of the original arterial system into a single component. The blender modifier "*Boolean union*" has been applied at each junction: in this way a passage for the fluid, that in this case is blood, has been created but on the other hand the phantom mesh has become thicker and thicker every time the boolean operation has been applied, resulting in a simulation time increase. Then, each single component of the initial arterial system has been duplicated in order to create the venous system that then has been connected to the arterial one: in this way, the systemic circulation has been modelled. There are differences between the real case and the modelled one:

- The intercostal veins are linked directly with the superior and inferior vena cava while in the human body they are linked with secondary veins and with the *Azygos vein* that then flows into the superior vena cava.
- The heart has not been included in the circulatory system; its entrance from

the venous circulation has been modelled making two cuts in the point where the vena cava flows into it (see Figure 5.3).

The last step consists on the modelling of the pulmonary circulation. Just like the systemic capillaries, pulmonary capillaries that surround the pulmonary alveoli have not been represented because the resulting system would have been too complicated; only the main vessels of the pulmonary circulation have been included in the model (pulmonary arteries and pulmonary veins), as it can be seen in Figure 5.4.

The final result is showed in Figure 5.5.

## 5.4 CT images generation

Virtual phantom described in Chapter 5.2 has been used to generate CT images: the result of the generation process will be the input of the software *Geant4*. Thanks to this software, the distribution of a radiopharmaceutical inside the vascular system and the deposited dose in the surrounding tissues will be evaluated.

The CT images generation is divided into two steps according to what have been previously explained: *sectioning* and *compositing*.

### 5.4.1 Sectioning

In Chapter 4.1, it has been said that the Blender modifier *Dynamic Paint* has been used to get sets of images of each organ of the virtual phantom. In order to proceed with the sectioning, after defining the analysis zone, the first thing to do is to generate a sectioning plane: on it, the modifier *Subsurf Simple* is applied five times so that its mesh becomes thicker and the obtained results are more precise; the user has also to *unwrap* the plane in the *Edit Mode* object management method so that it is possible to map a 3D object into a 2D texture.

During the animation, the sectioning plane moves along the longitudinal axis of the phantom, analysing it along its whole height (see Figure 5.6). The animation is changed into *linear* to have equidistant images along the z axis.

The distance between two consecutive images defines the resolution of the animation expressed in terms of *frames*: at each frame, the modifier generates a section of the organ under study; the more they are and the more precise is the output given

by the program but, on the other hand, the simulation time increases. In order to define the number of frames in which subdivide the simulation, some calculations are needed: considering that a mean male human being is high on average  $1.70\text{ m}$  and in Blender its height is equal to  $14.68\text{ Blender Units(B.U.)}$  (see Figure 5.7), the conversion from B.U. to real cm is given by

$$1\text{ B.U.} = 11.58\text{ cm.} \quad (5.1)$$

According to (5.1) and since the real CT images are spaced  $3\text{ mm}$  apart from each other, having set the initial sectioning plan height equal to  $+7.5\text{ B.U.}$  and the final one to  $-7.5\text{ B.U.}$ , the total number of frames is equal to 579. The resolution of the output images is set equal to the one of a standard CT image and so equal to  $512 \times 512$  voxels.

The sectioning process of the modified blood system (`blood_center.002`) has been performed differently with respect to the other objects, not only with the use of the sectioning plane: a *Boolean difference* modifier with a cube added to the scene has been applied to the modified blood system. The resulting object represents the "brush" and the sectioning plane is the "canvas" of the Dynamic Paint modifier. The whole sectioning procedure is automatised thanks to a python script that runs on the text editor integrated in Blender. The output of the process is a folder containing as many folders as the sectioned organs and tissues are; each folder contains 579 images in *.png* format that represent the CT images.

## 5.4.2 Compositing

As already introduced in Chapter 4.2, next step consists on the composition of the whole CT images and, then, on the assignment of the information concerning the Hounsfield number to each organ.

As the previous process, this one is also automatised thanks to a MATLAB script. The program uploads the images for each organ. They are converted into greyscale images and then they are read as two-dimensional matrices where the elements are different from zero if the image pixels are not black. Then, for what concerns these points, the program generates three new matrices equally sized with respect to the original ones: the first contains information on the Hounsfield number relative to

the analysed organ, the second contains the organ ID and the last one contains a number between 0 and 1 representing the grey intensity, where 0 corresponds to black and 1 to white. The definition of the Hounsfield numbers comes from the publication by Schneider et al. "*Correlation between CT numbers and tissue parameters needed for Monte Carlo simulation of clinical dose distributions.*": for air, H value has been set equal to -1000, that is the minimum value, while the one for water, and so for organic content of organs like stomach or intestine, has been set equal to zero (see Table 5.2).

Organ/Tissue	ID	H	Organ/Tissue	ID	H
Adipose abdominal	1	-98	Linfa 04	44	29
Adipose breast	2	-77	Liver	45	43
Adrenals	3	14	Lumbar spine	46	34
Bladder	4	26	Lung left	47	-741
Bladder content	5	23	Lung right	48	-741
Blood	6	56	Mandible	49	1524
Blood center	7	56	Muscle diaphragm	50	44
Bones feet	8	1524	Muscles face	51	44
Bones hands	9	1524	Muscle feet	52	44
Brain	10	40	Muscle hands	53	44
Cartilage chest	11	102	Muscle legs	54	44
Cartilage clavicole	12	102	Muscle neck	55	44
Cartilage ear	13	102	Muscle thorax	56	44
Cartilage hands	14	102	Nasal cavity	57	-1000
Cartilage humerus	15	102	Oral cavity	58	14
Cartilage legs	16	102	Pancreas	59	32
Cartilage maxilla	17	102	Parotid gland	60	14
Cartilage nose	18	102	Patella	61	1524
Cartilage pelvis	19	102	Pelvis	62	1524
Cartilage spine 1	20	102	Penis	63	36
Cartilage spine 2	21	102	Pharynx	64	54
Cartilage thyroid	22	102	Prostate	65	36
Cervical spine	23	34	Ribs	66	1524
Clavicle	24	1524	Sacrum	67	1524
Colon	25	23	Scapula	68	1524
Colon content	26	0	Skin	69	73
Connective tissues	27	40	Small intestine	70	23
Cranium	28	1524	Small intestine content	71	0
Esophagus	29	54	Spine	72	34
Eyes	30	49	Spleen	73	54
Femur	31	1524	Sternum	74	1524
Fibula and Tibia	32	1524	Stomach	75	41
Gall bladder	33	27	Stomach content	76	0
Glandular breasts	34	14	Sublingual gland	77	14
Heart	35	43	Submandibular gland	78	14
Heart Blood	36	56	Teeth	79	1524
Humerus	37	1524	Testicles	80	36
Hyoid	38	1524	Thimus	82	54
Kidneys	39	43	Thoracic spine	81	34
Lens	40	49	Thyroid	83	42
Linfa 01	41	29	Tongue	84	43
Linfa 02	42	29	Trachea	85	54
Linfa 03	43	29	Ulna and Radius	86	1524

Table 5.2: Organs and tissues of the Virtual Phantom with their respective ID numbers and Hounsfield numbers.

For each slice, organs are then sorted from the larger to the smaller one according to the sum of the non null elements of its own transversal section; in this way it is possible to generate CT images avoiding superpositions and, thanks to a *for* cycle, the final image on the transversal sectioning plane is generated. In this last procedure, the larger matrix of a particular body slice is taken and its non null elements are substituted with the non null ones of the smaller matrices. The final result consists on three different matrices containing HU, ID and greyscale data: the first two data series are then converted into binary format and they constitute the input files for the simulations in Geant4 application program. The last operation made by the code is the generation of a folder called *output* where images are stored in *.png* format; the 3D matrices containing HU and ID information are converted in binary format: these two are the real input for the next step, Geant4 simulations. Thanks to another MATLAB program, it has been possible to link each Hounsfield number to its own ID and greyscale index. The conversion Hounsfield unit to greyscale index is not unique and for this reason it has been decided to use a linear one given by the following formula:

$$I_{BW,i} = \left( \frac{HU_i + |\min(HU)|}{HU_{max} + |\min(HU)|} \right) I_{BW,max}. \quad (5.2)$$

In (5.2),  $|\min(HU)|$  is the absolute value of the minimum of the Hounsfield numbers,  $HU_{max}$  is the maximum one and  $I_{BW,max}$  is the maximum grayscale index value.

Images contained inside **output** folder of the code are not clear because it is not possible to recognise different organs: this is due to the great part of the Hounsfield numbers far from the white value. For this reason, a MATLAB code has been implemented to increase the contrast defining a new greyscale included in the range 0-0.1.

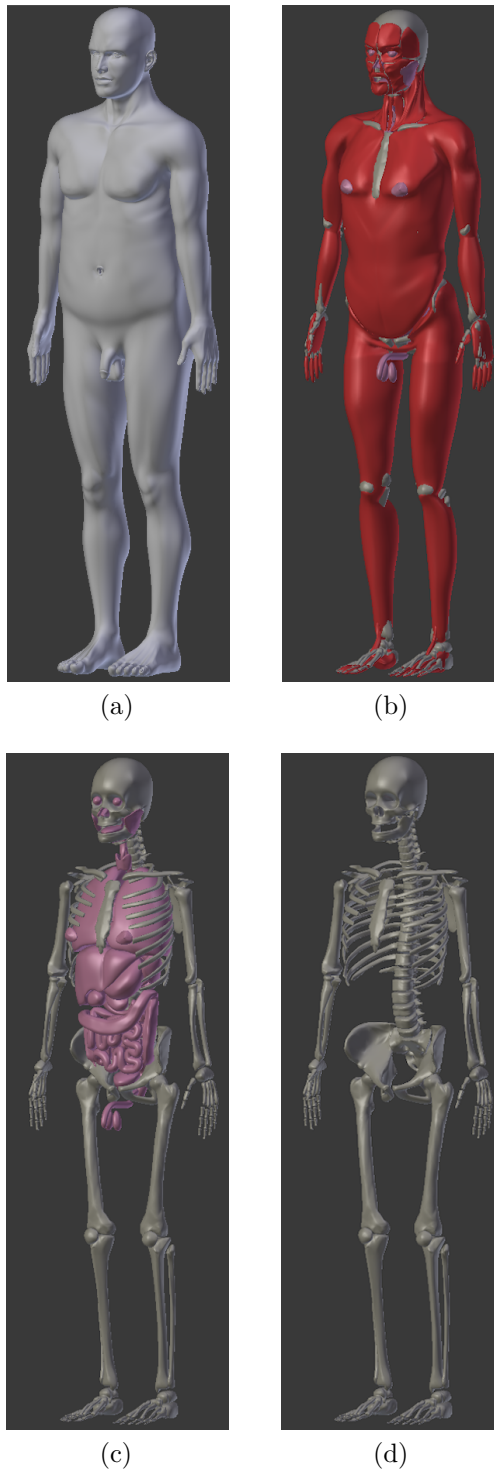


Figure 5.1: VPatient3D: (a)Body skin; (b)Muscles; (c)Skeleton and main soft tissues; (d)Skeleton.

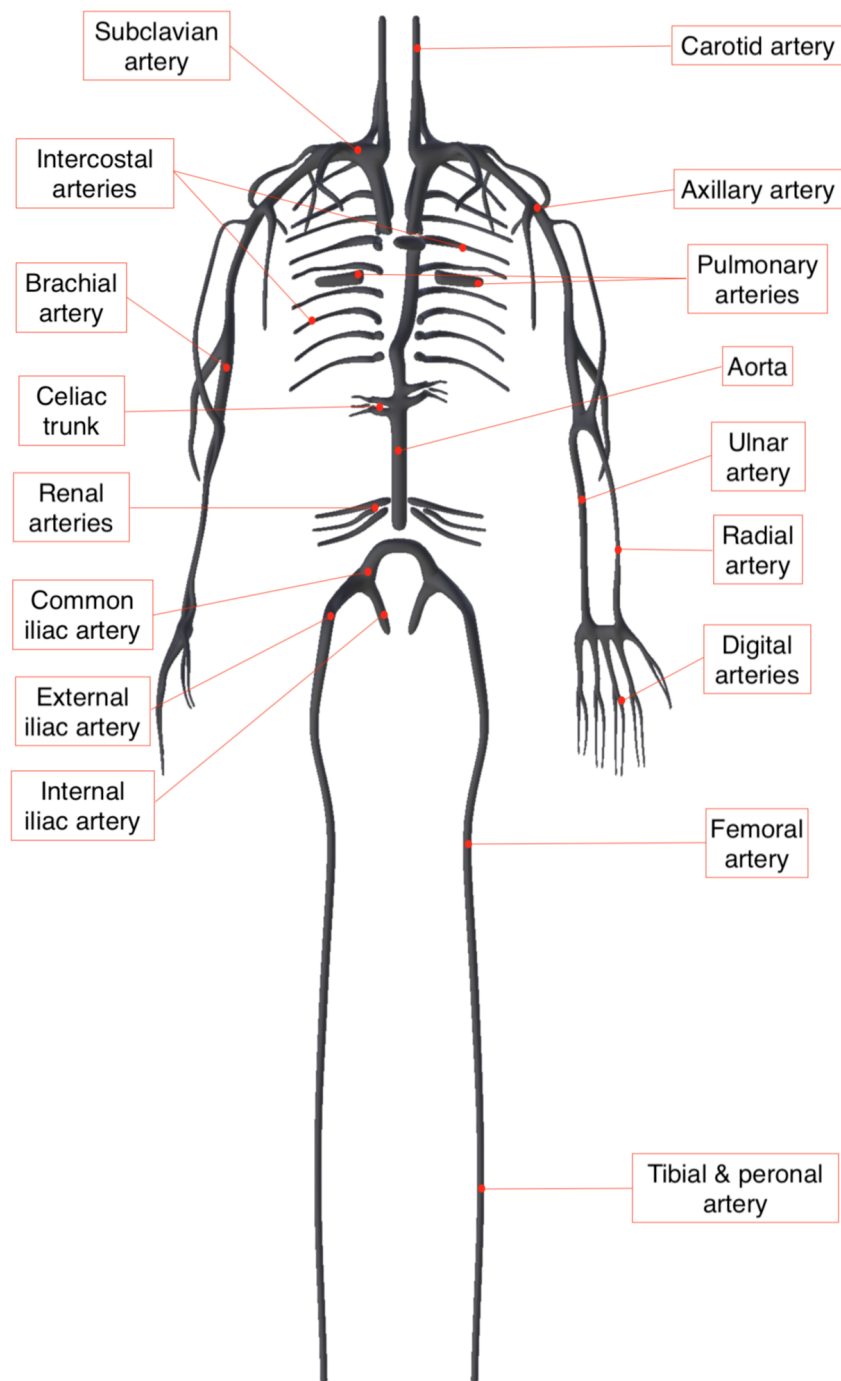


Figure 5.2: Vascular system extrapolated.

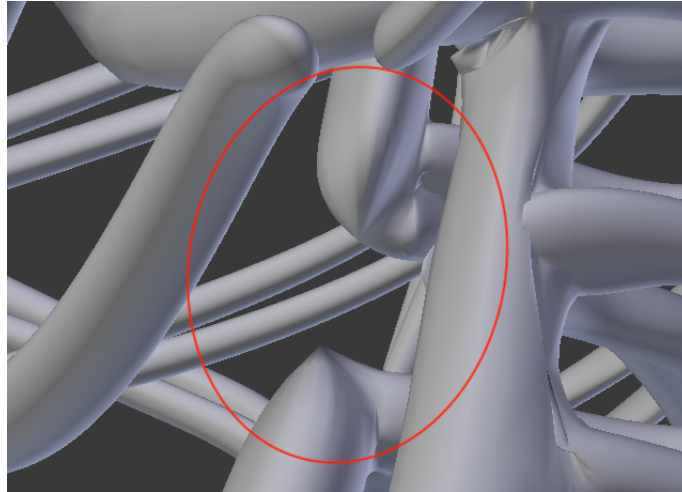


Figure 5.3: Detail of the vena cava cut: it represents the point where venous blood flows into the right atrium.

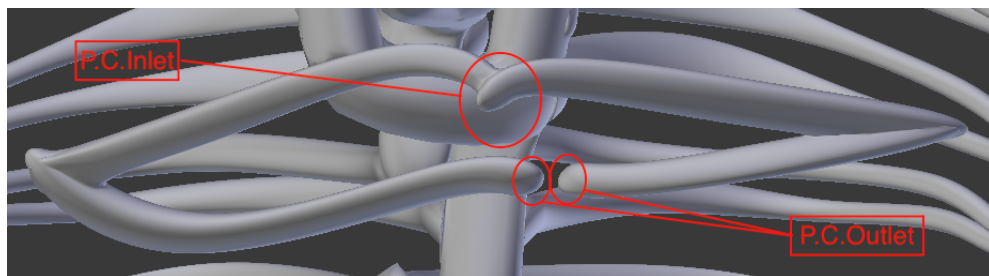


Figure 5.4: Pulmonary circulation (P.C.) modelisation.

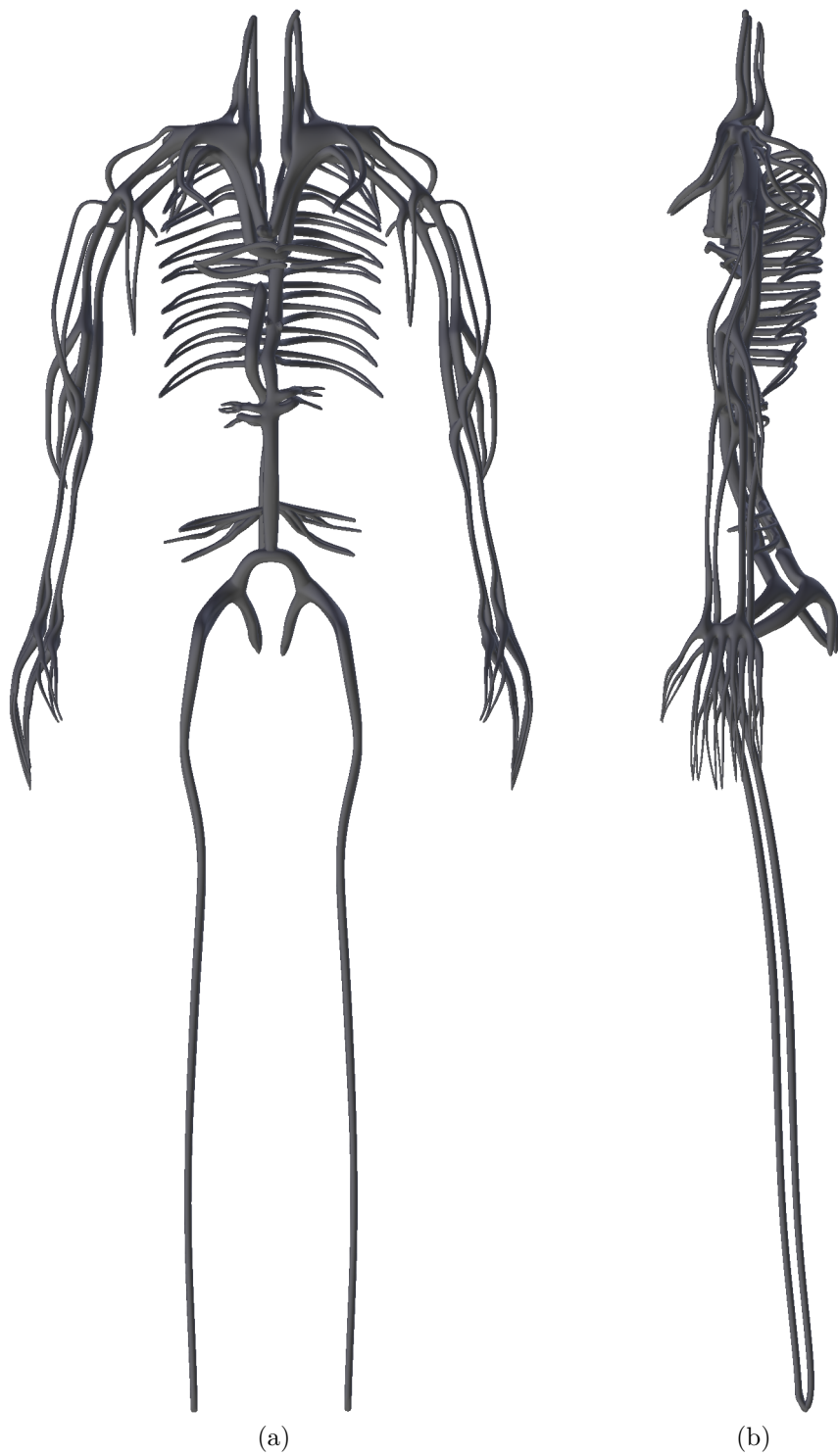


Figure 5.5: Final vascular system modelled: (a)Front view; (b)Left view.

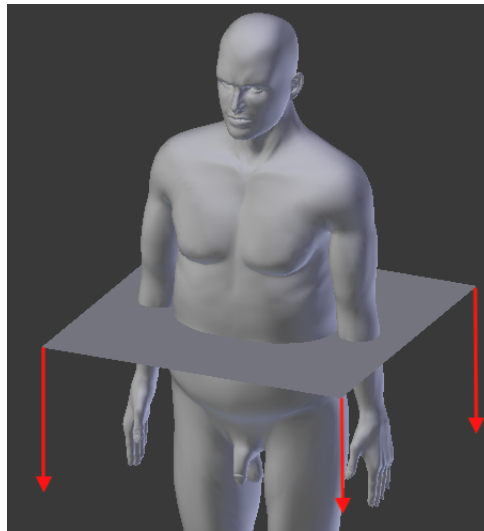


Figure 5.6: Representation of the sectioning plane.

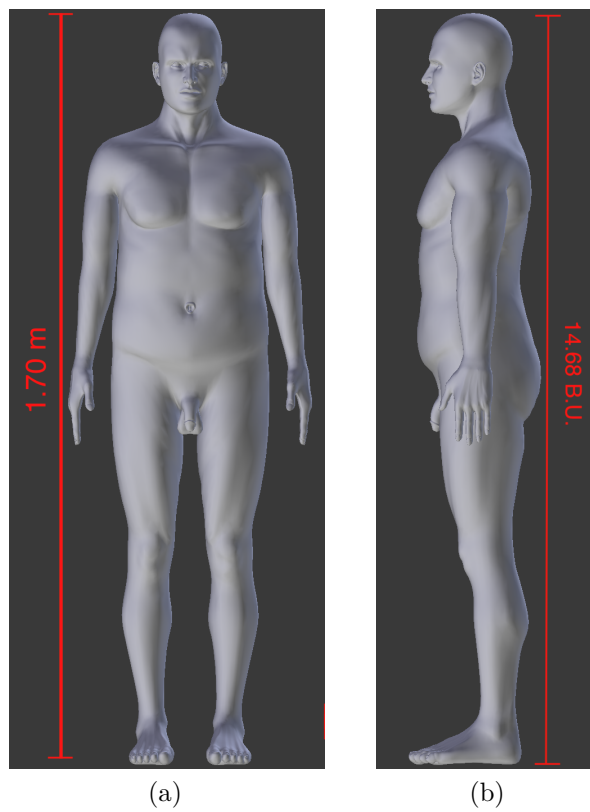


Figure 5.7: Height representation in real world and in Blender world: (a) Front view; (b) Left view.

# Chapter 6

## Simulations

### 6.1 Program description

In order to get the dose delivered by the radiopharmaceutical to the human body tissues, a pre-existing program called `OneSeePlan` has been taken as starting point. According to the *Object Oriented* programming technique explained in Chapter 4.3, the program has been written in C++ programming language using a hierarchical and modular structure. As each Geant4 application program, `OneSeePlan` is based on the use of libraries, or classes, that can be *implicit* or *explicit*: the former ones are directly defined inside Geant4 itself, while the latter ones are user-defined and so they can be build or modified directly by the user. The application program follows during the run phase a well-structured workflow that can be schematised as follow

1. *DetectorConstruction*: it is the class that handles all the geometry of the program, where volumes, sub-volumes and the whole simulation environment are created.
2. *PhysicsList*: this class contains all the physics that concerns the problem under study; it is based on wide spectra of energy, particles,...For this reason, choosing the right energy range and characteristic interactions is very crucial point.
3. *PrimaryGenerationAction*: it is the phase space in which the point source or

the source spectrum and their own characteristics are defined.

4. *SliceSD*: in this class, all the *sensitive detectors*\* are defined.
5. *SliceHit*: this class defines the exact time instant in which there has been the interaction between the sensitive detector and the particle/particles beam.
6. *RunAction*: this class provides the entire management of the files, generating and deleting them; it initialises data to be collected and how this process has to be performed.
7. *EventAction*: it is the class that is connected to all the other ones but, unlike them, it is a dynamic class; it is connected to the generated particle that is followed for its whole life.
8. *Macros*: these files are used by the user to fix simulation parameters; they can be used to overwrite information defined in classes and so they have to be called inside the reference class itself.

Some modifications have been done with respect to the starting application program that has been developed for external protontherapy:

- a script part has been added in order to upload CT scan information about HU and ID numbers coming from the previous step (see chapter 5.4.2): in this way, a region for the human phantom is created inside the Geant4 *World Volume*, where pixels spacing is  $x=1.17188$  mm,  $z=1.17188$  mm on the horizontal plane and  $y=3$  mm vertically (this last value corresponds to the distance between two consecutive CT scan slices);
- while in protontherapy case the source was located outside the phantom, using radiopharmaceuticals the source have to be placed inside the human body and for this reason it has been moved inside the phantom region;
- the *defaultPrimaryParticle* has been set equal to *gamma*;

---

\*Sensitive detectors are those logical volumes from which the user wants to collect information: these last one can be physical or concerning the interactions with particles.

- the physics of the model has been modified by changing the Geant4 implicit library `G4EmStandardPhysics` from `option3` to `option4` that results to be more suitable for internal radiotherapy case because it is characterised by better precision for low energy models and it presents modifications with respect to the previous one like a new model for energies larger than 200 MeV, for Compton Scattering and changes to the *Penelope* model for what concerns the conversion of gamma rays below 1 GeV;
- the script has been furthermore modified including the part in which the deposited dose is calculated and the one of the generation of the output file containing the deposited dose values in each pixel of each slice analysed.

Four different analysis have been performed, each one constituted by five different simulation runs: the first and the second analysis are general testing analysis performed to get the first results and to control if the code works properly, the third and the fourth ones analyse the dose deposited by a radiopharmaceutical in the most radiosensitive organs that are heart and eyes. `OneSeePlan`, and more in general all the Geant4 application programmes, simulates radiation passage through the use of Monte Carlo methods and so a very wide statistic and a great number of events simulated are needed in order to get acceptable results: for this reason, each analysed case include five different simulation runs each one composed by a hundred millions events. There is a very important quantity in Geant4 application programmes called *seed*. It is a number that can be either chosen by the user or that varies according to the simulation launching time; according to its value, it calls a certain random numbers library rather than another one. Simulations results in the same analysed case are all different one by each other because in each simulation run the seed depends on the simulation launching time.

## 6.2 Test simulations

As it has been said in the previous section, the first two analysis have been performed as tests.

In both cases, the body region under study is the same and it includes the lower part of the head, starting about at the nose level, till the upper part of the trunk

including the shoulders. This body region includes a range of fifty slices spaced of  $3\text{ mm}$  one to each other. The two simulations differ because of some changes in the Geant4 class `G4GeneralParticleSource` (GPS): it is the class where there are all the characteristics of the primary source particles, including energy spectrum and angular and spatial distributions. In order to modify these quantities, some changes have been made in a *macro* file, called `singlebeam.mac`.

The first analysis provides the use of a source that emits *gamma rays* of type "Beam"<sup>†</sup>. In order to be as close as possible to the reality, the source has been defined isotropic with a constant spectrum of energy equal to 500 keV, that represents the order of magnitude of the energy used in brachytherapy field. The information included in the macro file of this analysis are summarised in the following list:

- `/gps/particle gamma`
- `/gps/pos/type Beam`
- `/gps/ang/type iso`
- `/gps/pos/sigma_r 0. mm`
- `/gps/energy 500. keV`

The second analysis is similar to the first one but some modifications have been made in order to study the real case of radiopharmaceuticals inside the human body. Gamma source used in the previous case has been turned into a "Point source" constituted by a radionuclide that could be used during studies of these kinds of problems: it has been chosen to use  $^{64}\text{Cu}$  as radiation source, whose characteristics have been previously described (see Chapter 2.1). For each radioactive element or molecule, all the information concerning the decay modes with their occurrence percentage and the energy spectrum are stored inside Geant4 libraries and so the user has only to choose which radionuclide or radiomolecule to use. Information different with respect to the first analysis case and included in the current macro file of this analysis are the following:

---

<sup>†</sup> *Beam* type of source lets the user to generate radiation with a Gaussian distribution along a certain direction.

- `/gps/particle ion`
- `/gps/ion 29 64 29 0`

The last point of the previous list has four different parameters: the first two represent respectively the atomic and mass numbers, the third one is the ion charge per unit energy and the last one is the excitation energy expressed in keV.

In both analysis, the source is located in the centre of the part of the phantom analysed, and so in the centre of the 25<sup>th</sup> slice and its position is represented in Figure 6.1.

Considering both first and second analysis, the region of the maximum deposited dose values coincides with the position where the source is located, as it can be seen in Figure 6.2 and in Figure 6.3. The first two analysis have been performed only under a qualitative point of view and for this reason values in colorbars represent the ratio between the actual deposited dose in that particular pixel and the maximum value in the analysed case and so the colorbar range runs from a minimum equal to zero to a maximum equal to one. Although that, the maximum deposited dose value concerning the second analysis is about 1 Gy while the first analysis one is about 0.01 Gy. There is a difference between the two cases of two orders of magnitude and it is due to the source nature. In fact, gamma rays of the first analysis source are characterised by an infinite range of penetration inside matter and, according to Equation 1.34, the energy loss rate, and so the energy deposition rate, is slow; looking at Table 2.4, the second analysis source decays emitting light charged particles that are characterised by a finite penetration range in matter and, interacting with the external electronic shell, they suffer large energy exchanges according to Equation 1.28: these kinds of particles deposit almost instantaneously their energy and this is the reason that explains the difference between the two cases.

Regions that absorb radiation dose represented in Figure 6.2b and Figure 6.3b have both the same dimensions: isolines can be approximated with a circle and the diameter of the outermost ones is equal to 3 pixels that correspond to about 3.5 mm, according to previous data concerning pixels spacing. Looking at the isolines colours and referring to the colorbar scale, the external isoline, in the first analysis case, denotes a deposited dose value that falls to the 10% of the maximum while,

in the second analysis case, it drops to 1% of the corresponding maximum. The value of the deposited dose decreases if points further and further away from the source are analysed. This behaviour can be seen in Figure 6.4 and in Figure 6.5 that represent the dose deposited in the two different analysis on a plane situated, according to the previous definition of pixels spacing, 3 mm below the plane in where the source is located. The inner isoline indicates, for the first analysis, a reduction of the deposited dose value to 10% of the maximum one, while, for the second analysis, the reduction is about to 1% of its own maximum. Analysing the dose distribution behaviour moving far from the source, the isolines distribute according to the shape of the organs of the phantom itself. Figure 6.6 and in Figure 6.7 show this behaviour at a distance equal to 3.6 cm from the source position. If the distance continue increasing, the scattering phenomenon for photons becomes dominant and, for this reason the results very far from the source for what concerns the first analysis are more dispersed (see Figure 6.8) than the second analysis ones(see Figure 6.9).

It has been hypothesised that the whole dose of the two test analysis has been released after five half-life, when the concentration of the radionuclide is about one-thirty-second of the starting concentration and the delivered dose can be neglected. Another thing that must be kept in mind is that the two test analysis have been performed in a static case: in the real world, the radiation source is carried by the blood flow so its dose is not released in a single point and for this reason the evaluation of the blood speed in that particular vessel and the transit time of the radionuclide in the analysed voxel must be considered.

Dose limits have been determined by the ICRP (International Commission on Radiological Protection) on the basis of data coming from past experience on patients treated with radiotherapy treatments and on the survivors of the WWII atomic bombs. Many of these exposure limits data have to be changed in last years: in particular, some of them have to be reduced because of the development of new techniques to treat radioinduced effects while others have been increased because it has been noticed the insurgence of latent effects after years from radiation exposure. In ICRP *Recommendations of 2007*, two critical organs have been identified as critical organs/tissues that are eyes and the cardiovascular system, and so the heart.

The following two analysis are concerned with these two radiosensitive targets and they are performed taking into account the fact that the radiation source is dynamic.

### 6.3 Eyes simulation

The main effect of radiation exposure of the eyes is the generation of cataract. In general, its generation process is not known but it could be due to the modification of the genetic heritage that affects crystalline cells that could generate regions with different transparency if their damage is not repaired: there are some hypotheses that assert that the damaged cell, if not destroyed or inhibited, could divide and differentiate thus generating a group of mutagenic cells. There are other theories, although without proofs, according to which the damage to a single cell could generate cataract (zero-threshold phenomenon). Today this topic is one of the main research subjects of the field.

The studies taken as references by the ICRP have shown that all the exposed people for both treatment and working and professional reasons are subjected to high risk of radioinduced cataract generation if the dose value is equal to 1 Gy. These studies have also shown that the effects on patient treated with protons or with conventional radiotherapy are the same. The studies results are summarised in Table 6.1.

The region under study in this analysis has been sectioned using 20 planes that analyse the whole eyes zone of the head. The radiation source has been located in the right temporal artery, that is one of the most important and larger vessels in human head: there are a great number of vessels and capillaries here but none of them has been considered because they have a very small diameter and so the radiopharmaceutical quantity that could flow inside them would be negligible. The position of the source used in this analysis is shown in Figure 6.10.

In order to take into account the dynamic behaviour of the source, blood flow and residence time of the source inside the volume under study must be considered. Hypothesising that Geant4 application programmes evaluate the deposited dose during the whole radionuclide life and that it is the same that it would have deposited it in the whole body, in a single position, the radiopharmaceutical will

Table 6.1: Estimation of the limit dose with an incidence of pathological effects equal to 1% (Data from [8]).

<b>Effect</b>	Cataract with obstacle to vision
<b>Organ/Tissue</b>	Eye
<b>Time interval needed for symptoms offset</b>	>20 years
<b>Acute exposure (Gy)</b>	~ 0.5
<b>Highly fractioned exposures (2 Gy)</b>	~ 0.5
<b>Annual dose rate for many years (<math>\frac{Gy}{year}</math>)</b>	~ 0.5 divided by the treatment duration

deposit only a part of the total energy: the resulting deposited dose is proportional to the total value that comes out from the simulations by means of a constant that depends on the residence time of the radiopharmaceutical itself in the whole body and on volume under study. If the constant is called with letter  $p$ , it results

$$p = \frac{V_{vessel}}{V_{blood}} * (1 - e^{-\lambda T_{res}}) \quad (6.1)$$

In equation (6.1),  $V_{vessel}$  is the volume of the chamber where the source is located,  $V_{blood}$  is the blood volume that in an average human being is equal to 5l,  $T_{res}$  is the residential time of the radiopharmaceutical inside the human body that, according to [5], can be approximated as four days after that radioactivity becomes negligible and  $\lambda$  is the *decay constant* expressed in  $\frac{1}{s}$  that is equal to

$$\lambda = \frac{\log 2}{T_{\frac{1}{2}}}, \quad (6.2)$$

where  $T_{\frac{1}{2}}$  is taken from Chapter 2.1. For what concerns the eyes analysis, considering that the diameter of the temporal artery is approximately equal to 3 mm and the length of the vessel stretch where the source is located is equal to 3 mm (this is true hypothesising a complete vertical vessel),  $V_{vessel} = 2,121 \times 10^{-5} mm^2$ . Substituting

all data inside (6.1), it results that

$$p = 3,968 \times 10^{-6} \quad (6.3)$$

As the first two analysis, the maximum deposited dose value can be found in the point where the source is located (see Figure 6.11) and it is equal to  $2,0949 \times 10^{-6}$  Gy: it is a value very far away compared to both acute and fractioned exposure limits of Table 6.1 and so it guarantees a good safety margin. The area subjected to radiation exposure can be treated as a circle whose diameter is equal to 3 pixels and so, considering that pixels spacing is the same as the previous two analysis, to about 3.5 mm. The deposited dose falls to about the 1.33 % of the maximum value after about 1.8 mm (see Figure 6.11b). Moving far from the source, deposited energy decreases as in the first and the second analysis. This can be noticed analysing the slice below the source, represented in Figure 6.12, that is 3 mm far from it: the inner isodose indicates a deposited value equal to  $2,454 \times 10^{-9}$  Gy that correspond to a reduction to the 0.12 % of the maximum value. Referring to Slice#13 (Figure 6.13), situated 0.6 cm below the source, and to Slice#19 (Figure 6.14), situated 2.4 cm below the source, the deposited dose values continue decreasing: analysing the inner isodose values, the deposited dose in the first case is equal to  $1,665 \times 10^{-10}$  Gy with a reduction of four order of magnitude with respect to the maximum, while, in the second case, it is equal to  $8,472 \times 10^{-12}$  Gy with a reduction of almost six orders of magnitude; moreover, in Figure 6.14, it can be seen as, the further you are from the source and the more spread is the signal due to the photon scattering effect that becomes dominant. Considering the last results, it can be said that the dose deposited is very low and it becomes almost negligible if the distance from the source is about 6 mm. It can be noticed that the radiation does not affect the eye if it is located in that position. Temporal artery is positioned between the skin and the cranium: bones are the denser tissues of the human body and they have the largest HU value because the attenuation coefficient is directly proportional to density (in Table 5.2, bones HU number is equal to 1524). Due to this characteristic, cranium provides a good shielding from radiation, although bones in general could experience embrittlement and subsequent fracture for fractioned exposition for a time period larger than one year to dose values larger than 50 Gy for adults (data

from [8]).

Eyes and all the brain region are characterised by capillaries whose diameter is of the order of 5-10  $\mu\text{m}$  and so the radiopharmaceutical quantity that flows through them is very small: it has been seen in this analysis that the dose due to a radiopharmaceutical flow in a medium-small artery is very low and so in capillaries it would be even more.

## 6.4 Heart Simulation

Deposited dose limits on cardiovascular system have been added with [8] because in the previous documents they were not treated: this is due to the fact that all heart diseases symptoms have been detected after years from the last exposure of the patients under study (survived to the atomic bombs, patient whose heart has been irradiated during radiotherapy for breast cancer or for Hodgking's). Another problem for cardiovascular system diseases is linked to the fact that each of them has a very high death rate that is around 30%-50% and it is very difficult to distinguish if their onset is linked to radiation exposure or to some other causes, like inheritance, unhealthy lifestyle,...Like in the eyes case, there is a very high uncertainty on the available data and difficulties on the definition of a limit dose: concerning partial exposure, it is not yet clear what is the most sensitive cells of heart or of the cerebrovascular system and for this reason all dose limits are referred to a mean value. Damages to the cardiovascular system are of inflammatory nature if the human subject is exposed to low dose values but, on the other hand, if the exposure level increases, the whole system becomes compromised: starting from capillaries destruction (ischemia), effects could bring to heart damage, heart function reduction, heart failure and, finally, death. There are not yet treatments for radioinduced cardiovascular diseases but there is something under study like the use of stamina-based products or stamina transplants. In Table 6.2 there are data concerning dose/volume/effect due to total organ irradiation, while in Table 6.3 there are data referring to different kinds of exposure.

The heart region has been analysed by means of 51 sectioning planes spaced of 3 mm one to each other and the source has been positioned inside the right atrium (see Figure 6.15). In order to take into account the dynamic behaviour of the blood

Table 6.2: Dose/volume/effect data for organ irradiation (values are referred to the whole organ if not differently indicated) with conventional fractioning (1.8-2 Gy/fraction). In the table,  $D_{mean}$  represents the mean value of the dose to the organ,  $V_x$  indicates the organ percentage exposed to x dose. (Data from [8])

Organ	Effect	Dose (Gy) or dose parameters	Percentage (%)
Heart	Pericarditis	$D_{mean} < 26$	$< 5$
	Long-term mortality	$V_{30} < 46\%$	$< 15$
		$V_{25} < 10\%$	$< 1$

Table 6.3: Estimation of the limit dose with an incidence of pathological effects equal to 1% (Data from [8])

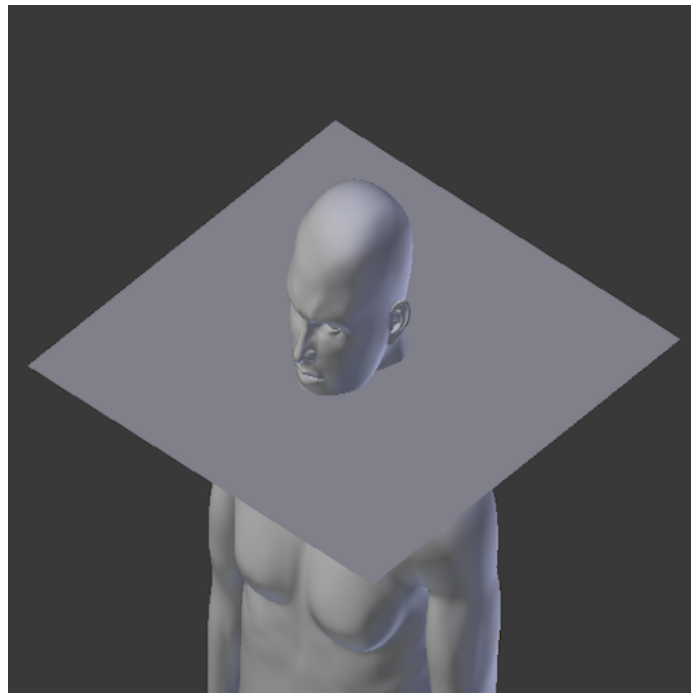
<b>Effect</b>	Cerebrovascular diseases
<b>Organ/Tissue</b>	Carotid artery
<b>Time interval needed for symptoms offset</b>	$> 10$ years
<b>Acute exposure (Gy)</b>	$\sim 0.5$
<b>Highly fractioned exposures (2 Gy)</b>	$\sim 0.5$
<b>Annual dose rate for many years (<math>\frac{Gy}{year}</math>)</b>	$\sim 0.5$ divided by the treatment duration

like in the eyes analysis, it is used also in this case the corrective factor of (6.1), where  $V_{vessel}$  is the volume of the right atrium chamber that is equal, considering an average value between the systolic and diastolic one, approximatively to 30 ml. The corrective factor results

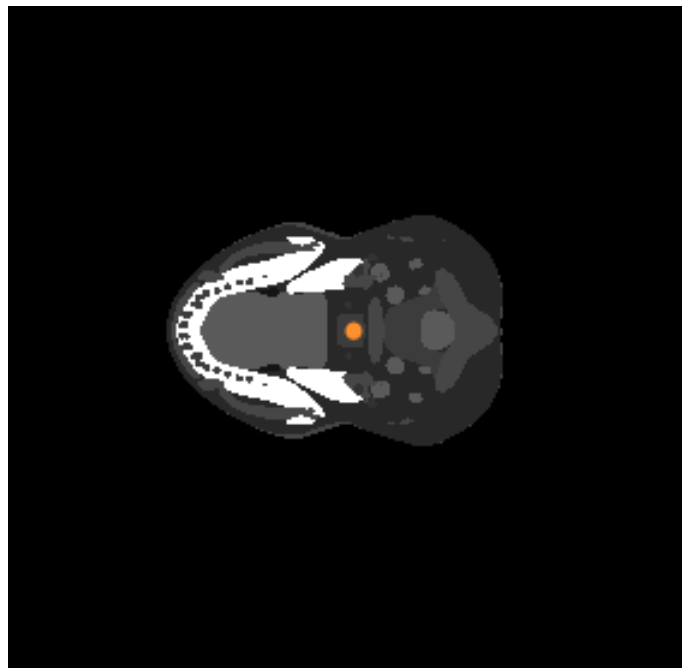
$$p = 5,382 \times 10^{-3} \quad (6.4)$$

The maximum value of the deposited dose coincide with the source position and it is equal to 0.0016 Gy (see Figure 6.16). The areas affected by radiation can be approximated as a circle: the diameter of the outermost isoline is equal to 3 pixels (about 3.5 mm), in which the deposited dose falls to a value that correspond to

the 1.38% of the maximum one, as it can be seen in Figure 6.16b. Analysing what happens moving from the source plane to another one, it can be seen that in the slice situated 3 mm below the source one, the inner isoline indicates a deposited dose value equal to  $2,443 \times 10^{-5}$  Gy that is the 1.53% of the maximum one (see Figure 6.17). In Slice #24, shown in Figure 6.18, that is 0.6 cm far from the source, in the internal isoline the deposited dose reduces of four orders of magnitude to a value equal to  $2 \times 10^{-7}$  Gy that corresponds to 0,0128% of the maximum: like the previous analysis concerning eyes, doses becomes negligible at a distance equal to 0.6 mm. In Slices #40 (Figure 6.19) and #50 (Figure (6.20)), it can be seen that the decreasing behaviour continue. In fact, in the both cases the higher dose value is of the order of  $10^{-9}$ Gy for either a distance equal to 6.4 cm and equal to 8.4 cm; in these conditions, an exact dose value can not be determined because of the signal dispersion linked to photons scattering. The time in which the radiopharmaceutical remains inside the atrium chamber is characterised by a high uncertainty because there could be cases in which a part of the blood portion containing the substance remains there and so also the transit time increases with a consequent deposited dose increase: this is a crucial point that will need in future more attention in the study. Moreover, it can be noticed that if a radiopharmaceutical flows through heart, the maximum distance at which a reasonable dose value could arrive is about 5 or 6 mm and for this reason surrounding organs are not affected: in order to analyse the effect on these organs, radiation source should be placed in blood vessels that pass through or next to them.

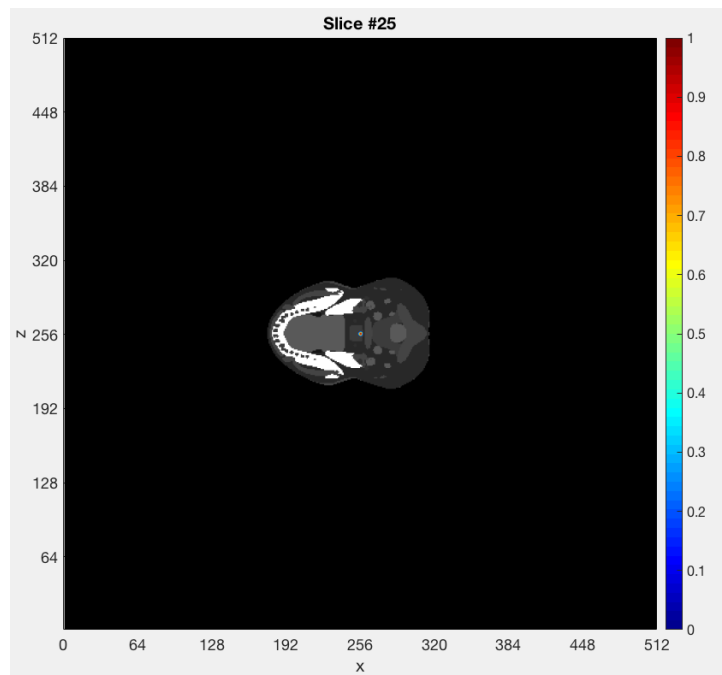


(a)

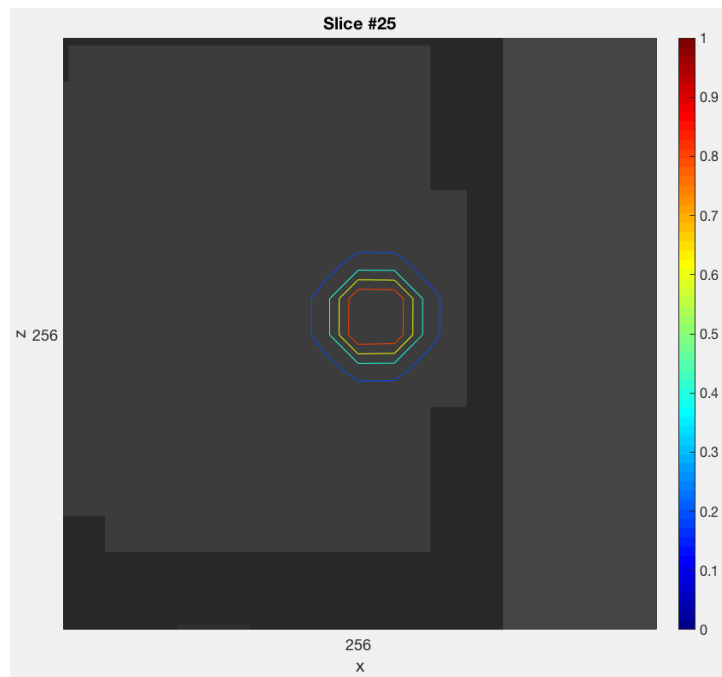


(b)

Figure 6.1: Cutting plane and source position for test analysis during simulations: (a) Position of the sectioning plane where the source is located; (b) Source position inside the human phantom.

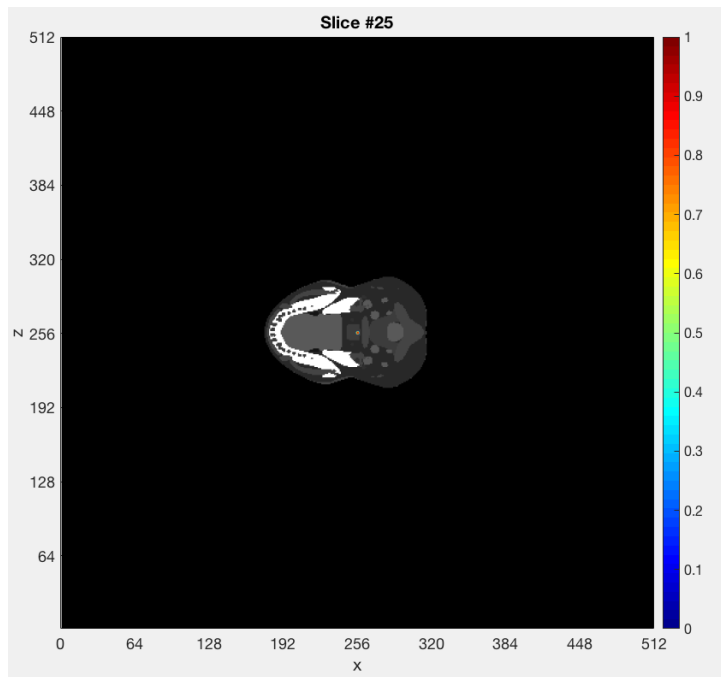


(a)

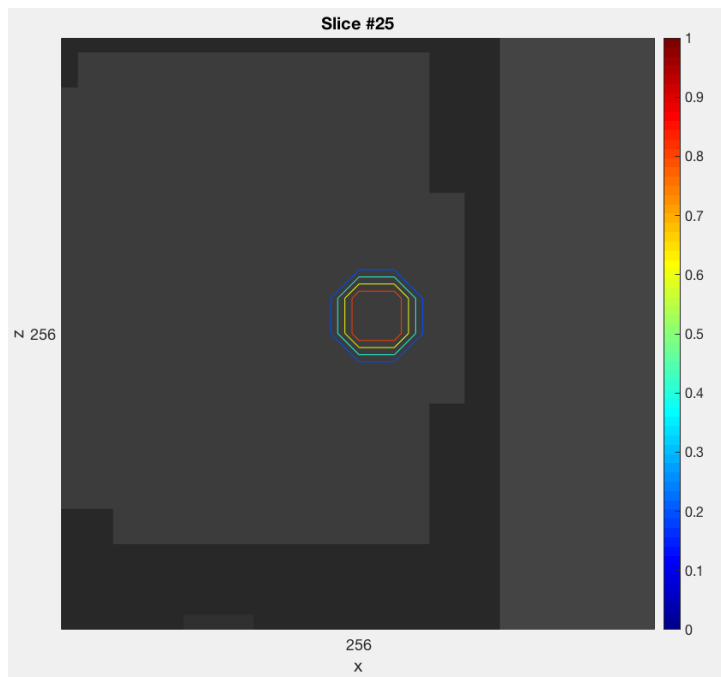


(b)

Figure 6.2: Slice that corresponds to the centre of the analysed phantom part for the first analysis: (a) Slice 25 with source located in the centre; (b) Detail of slice 25.

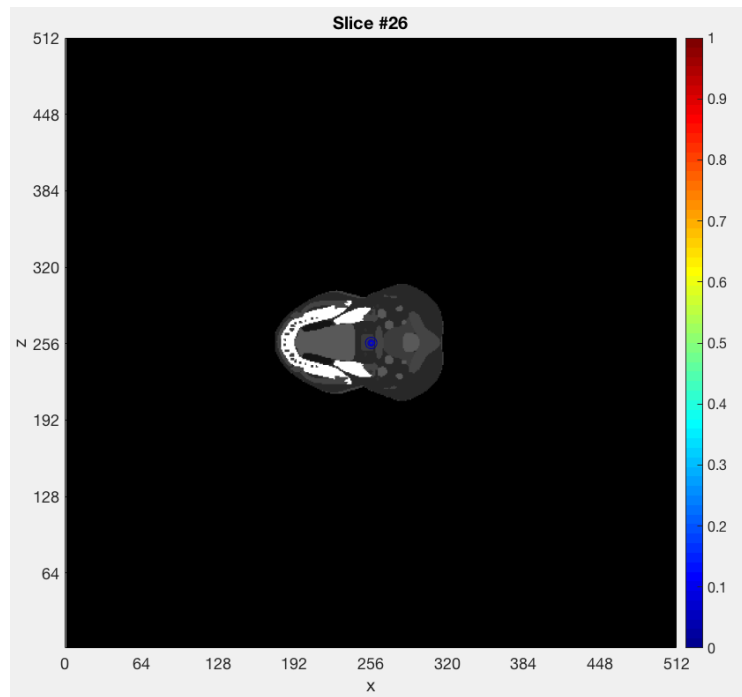


(a)

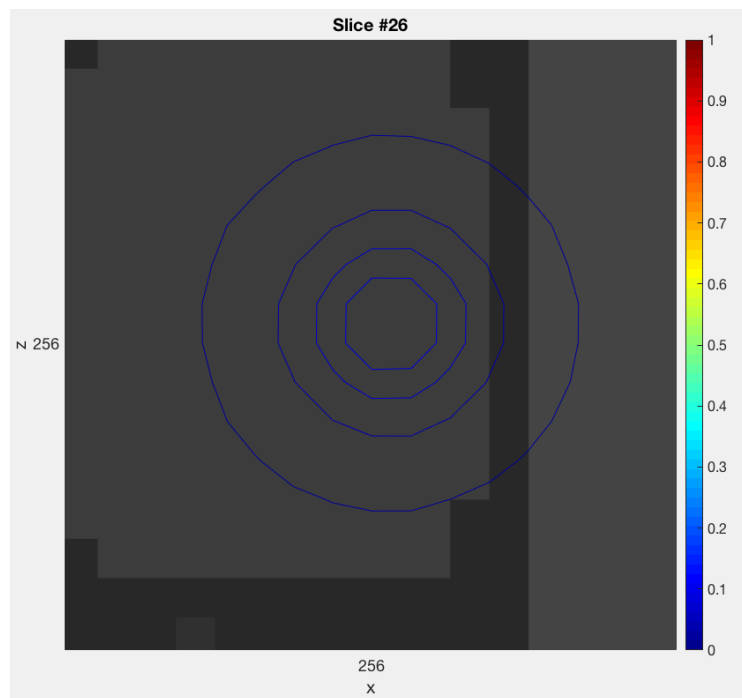


(b)

Figure 6.3: Slice that corresponds to the centre of the analysed phantom part for the second analysis: (a) Slice 25 with source located in the centre; (b) Detail of slice 25.

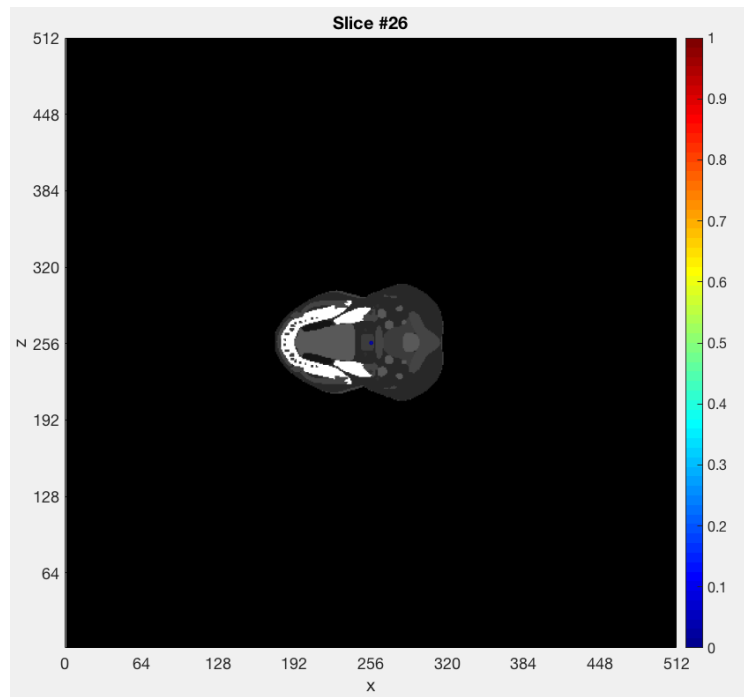


(a)

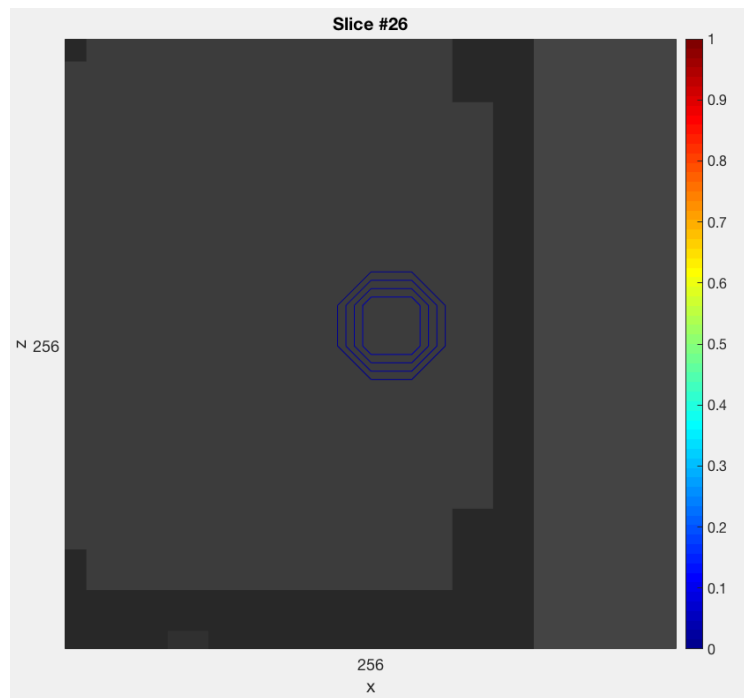


(b)

Figure 6.4: Representation of the slice located below the central slice in the first analysis: (a) Slice 26; (b) Detail of slice 26.



(a)



(b)

Figure 6.5: Representation of the slice located below the central slice in the second analysis: (a) Slice 26; (b) Detail of slice 26.

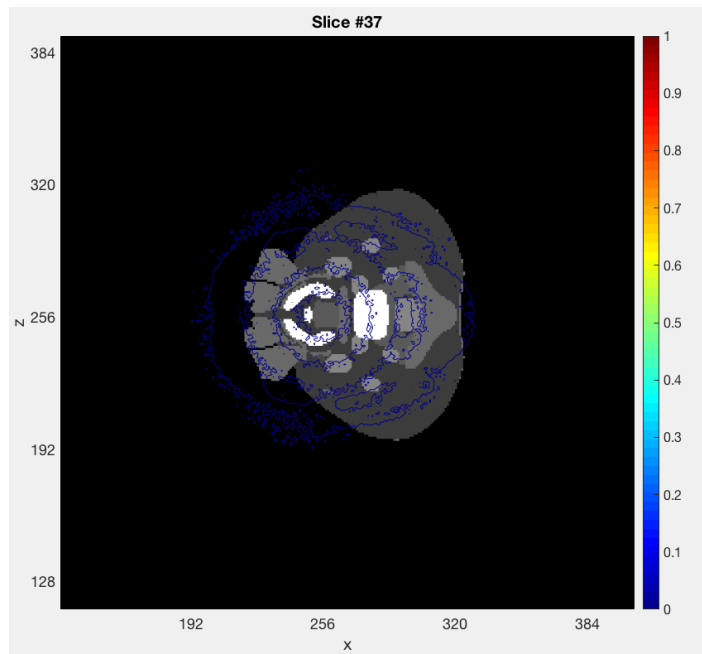


Figure 6.6: Representation of the slice located 3.6 cm below the central slice in the first analysis.

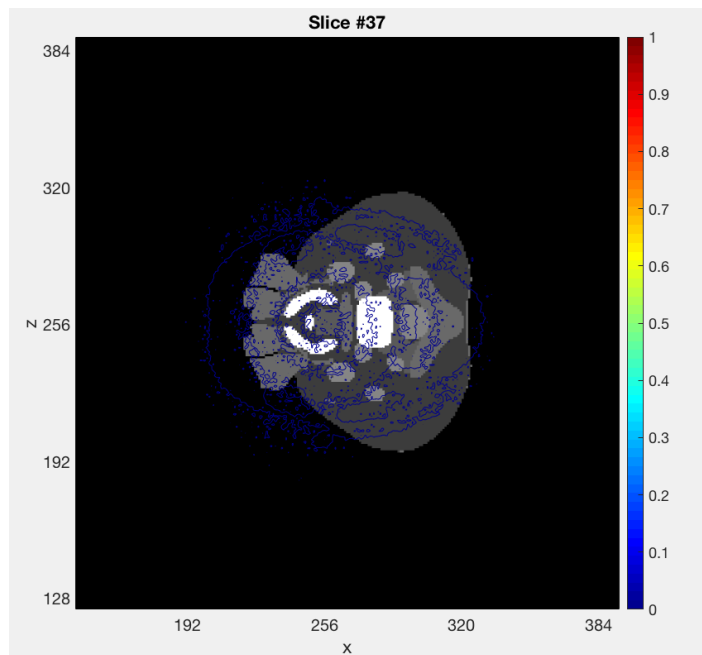


Figure 6.7: Representation of the slice located 3.6 cm below the central slice in the second analysis.

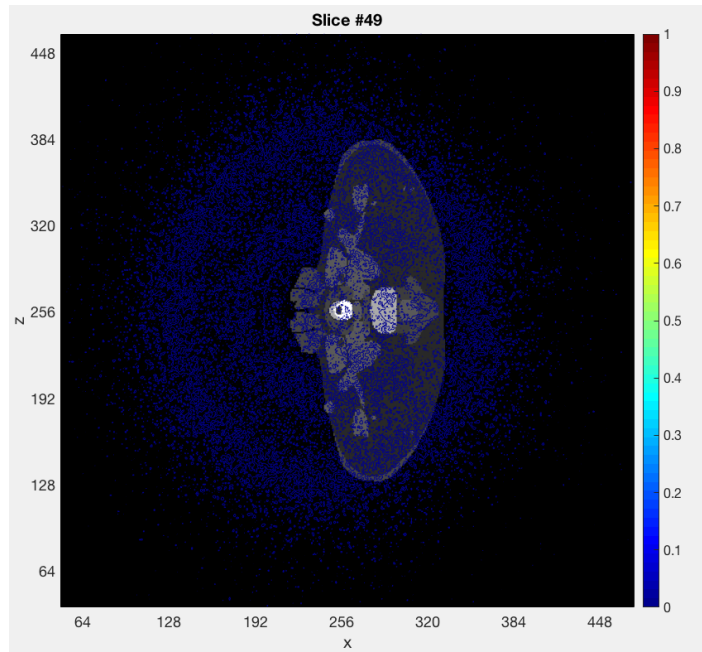


Figure 6.8: Representation of the slice located 7.2 cm below the central slice in the first analysis.

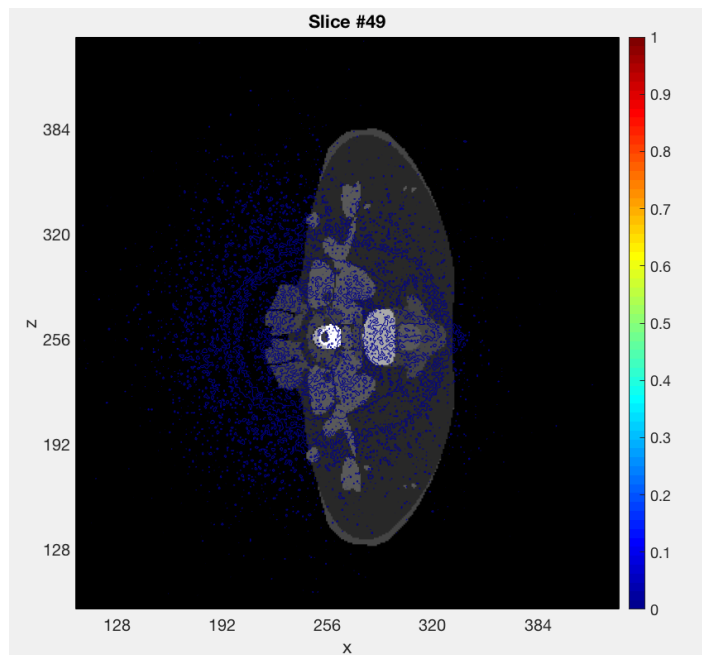
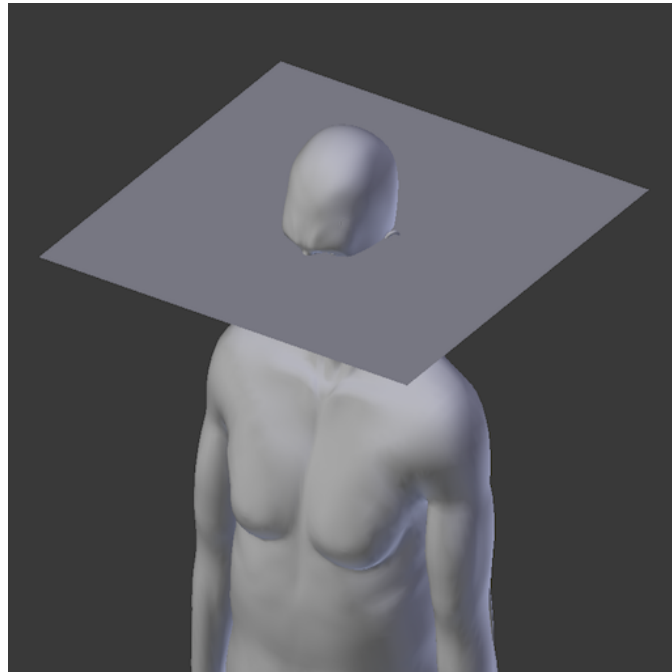
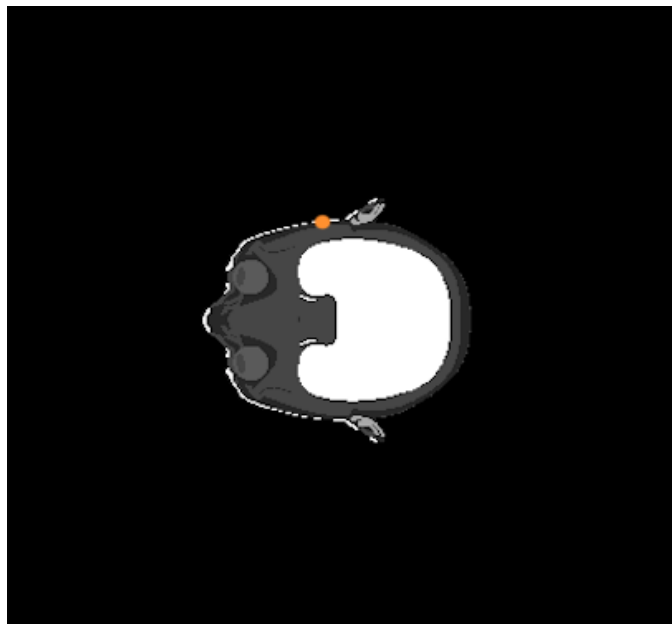


Figure 6.9: Representation of the slice located 7.2 cm below the central slice in the second analysis.

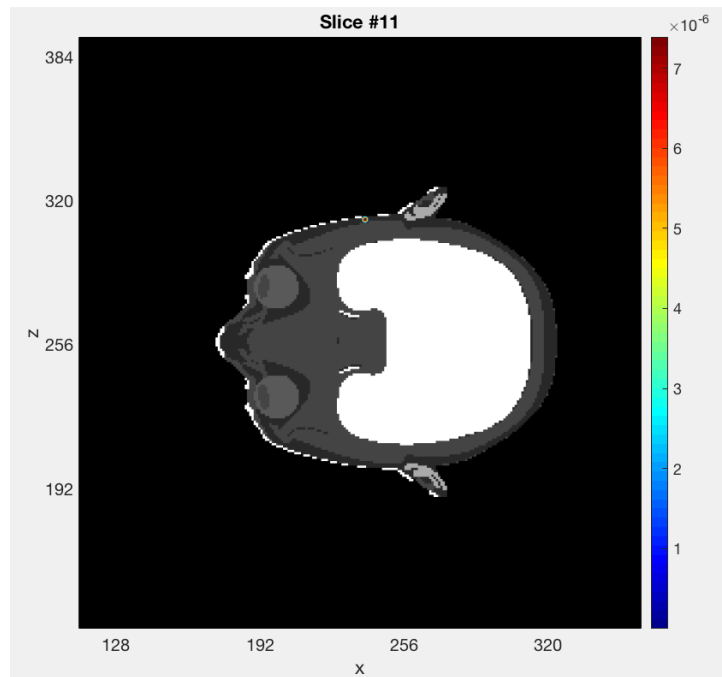


(a)

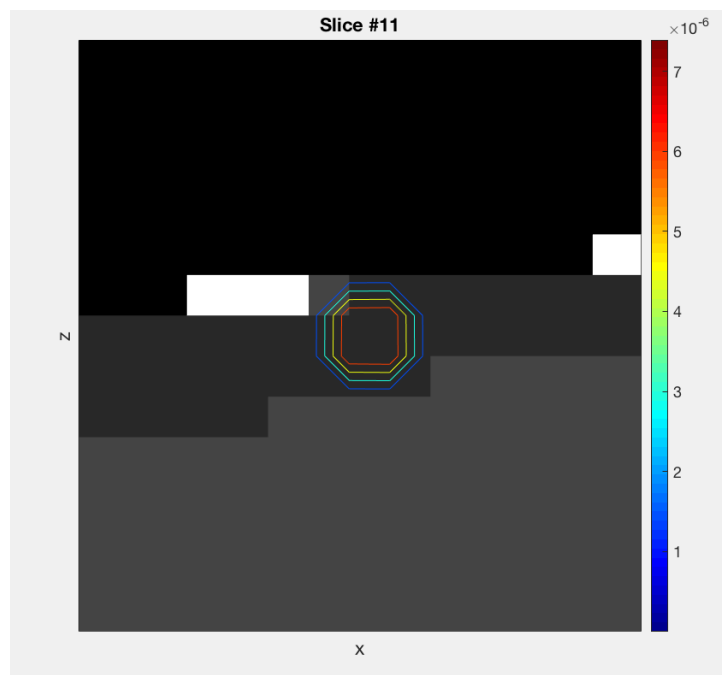


(b)

Figure 6.10: Cutting plane and source position for eyes analysis during simulations: (a) Position of the sectioning plane where the source is located; (b) Source position inside the human phantom head.

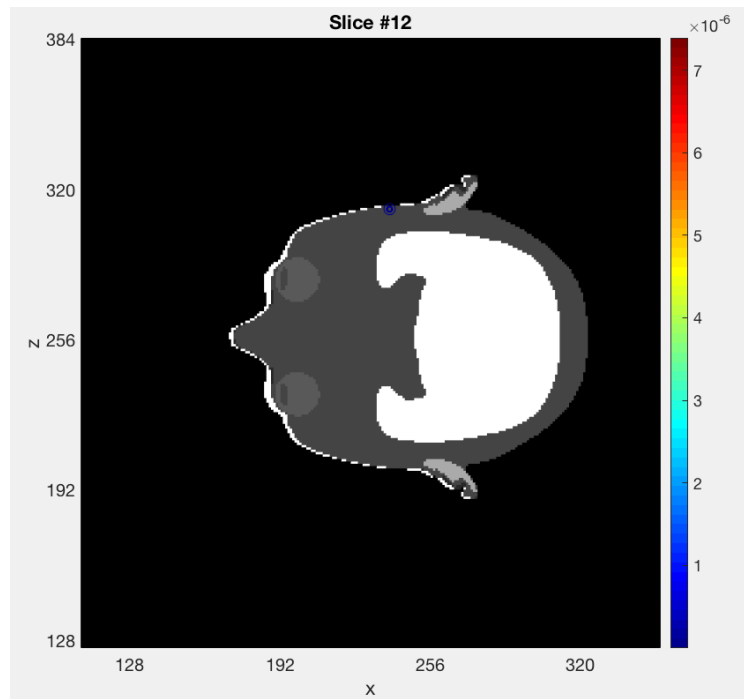


(a)

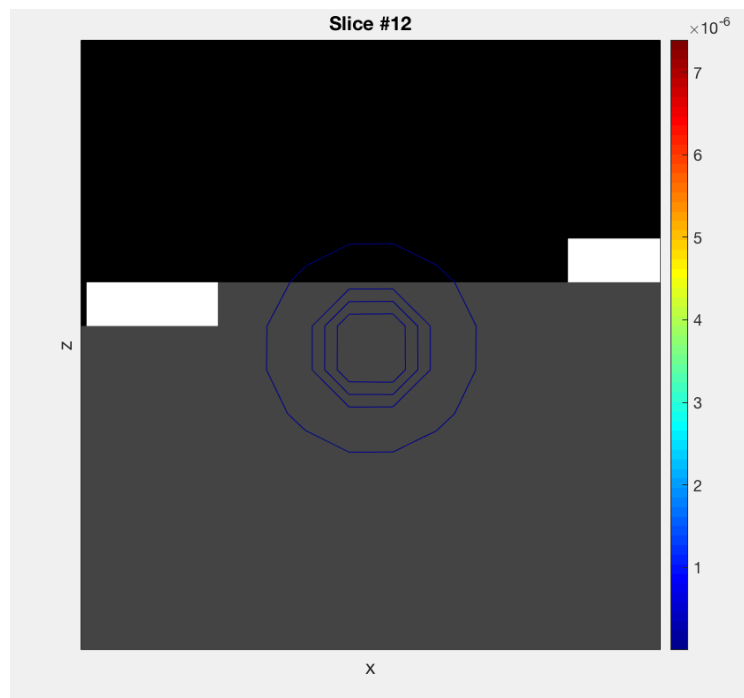


(b)

Figure 6.11: Slice that corresponds to the centre of the analysed phantom part for the eyes analysis: (a) Slice 11 with source located in temporal zone; (b) Detail of slice 11.



(a)



(b)

Figure 6.12: Representation of the slice located below the central slice in the eyes analysis: (a) Slice 12; (b) Detail of slice 12.

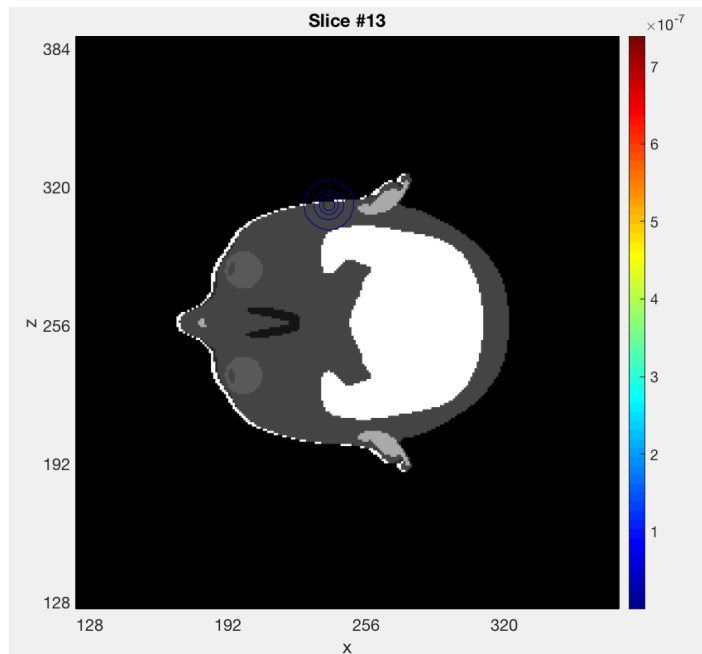


Figure 6.13: Representation of the slice located 0.6 cm below the central slice in the eyes analysis.

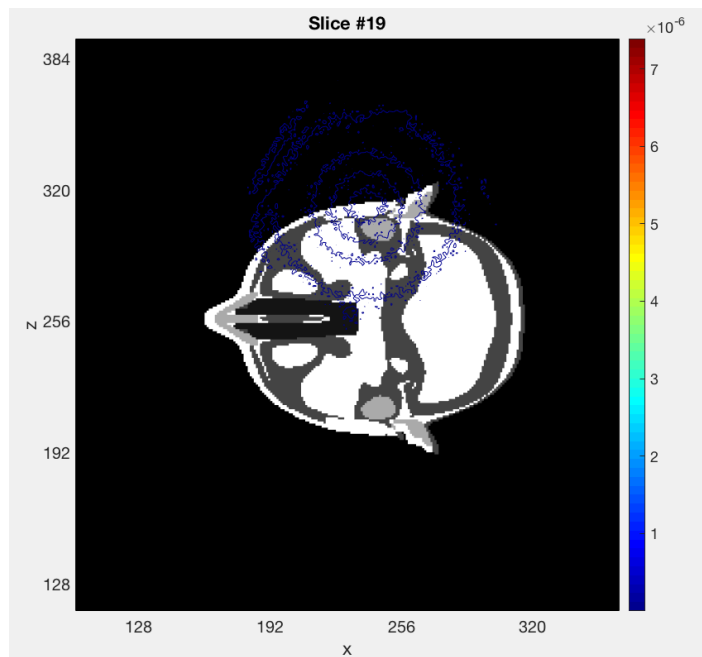
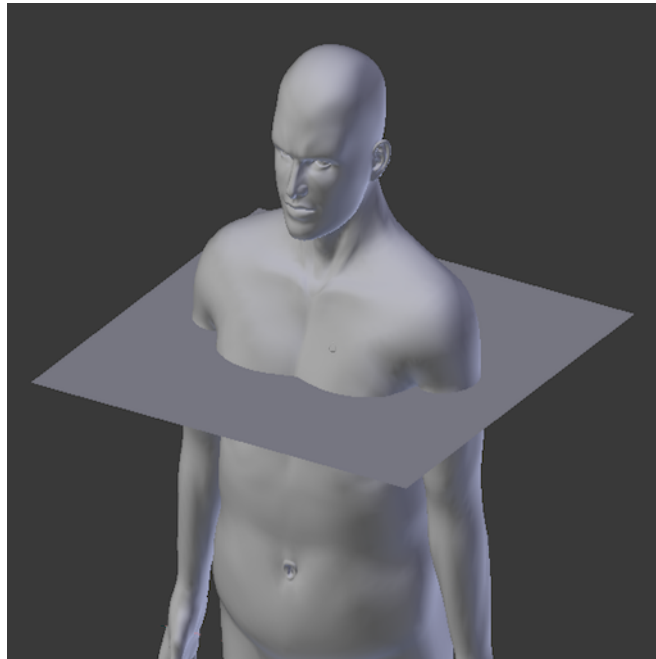
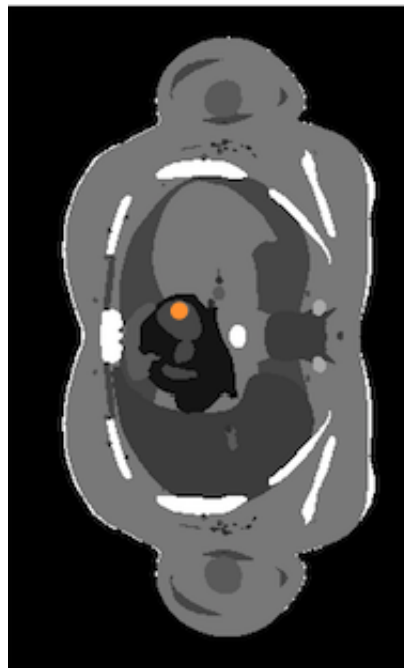


Figure 6.14: Representation of the slice located 2.4 cm below the central slice in the eyes analysis.

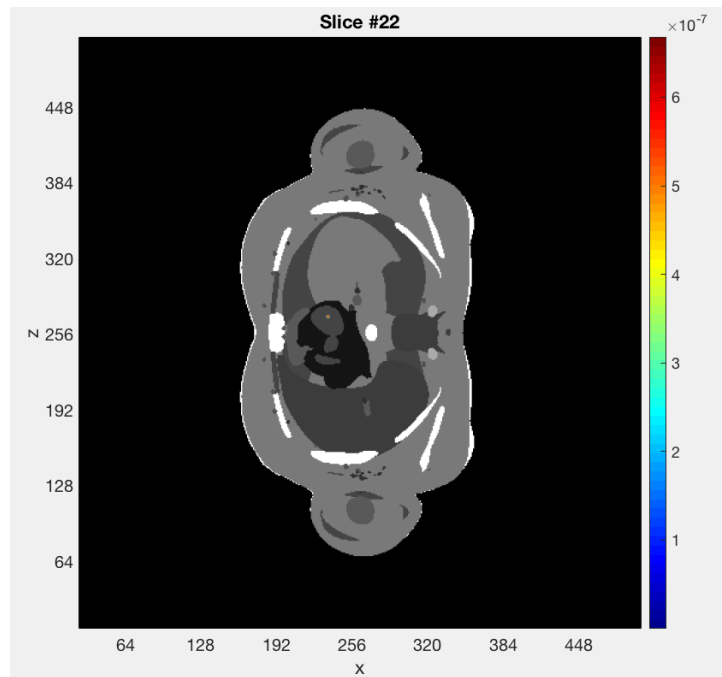


(a)

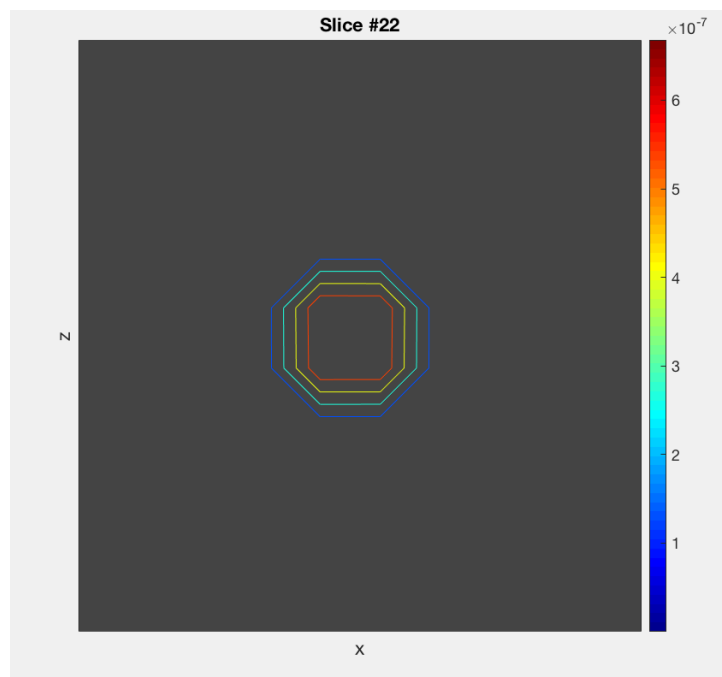


(b)

Figure 6.15: Cutting plane and source position for analysis during heart simulation: (a) Position of the sectioning plane where the source is located; (b) Source position inside the human phantom heart.

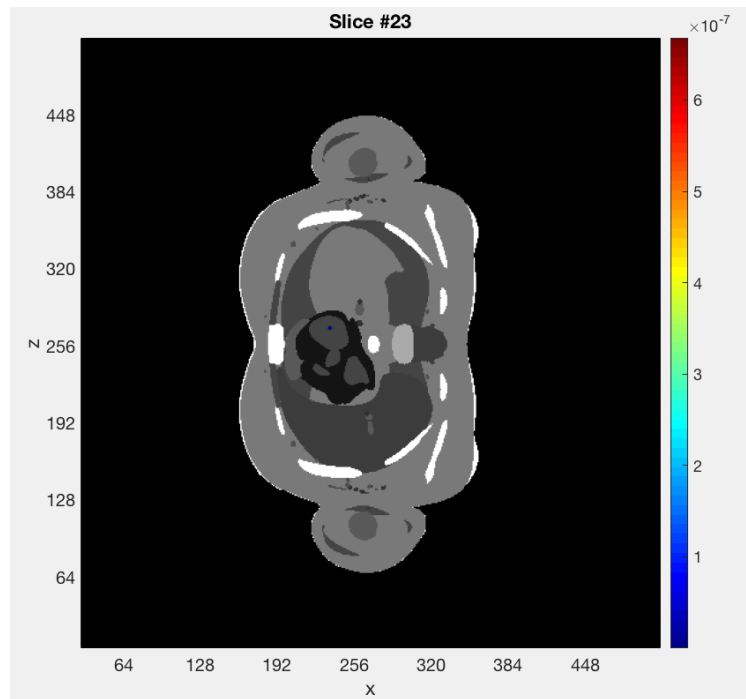


(a)

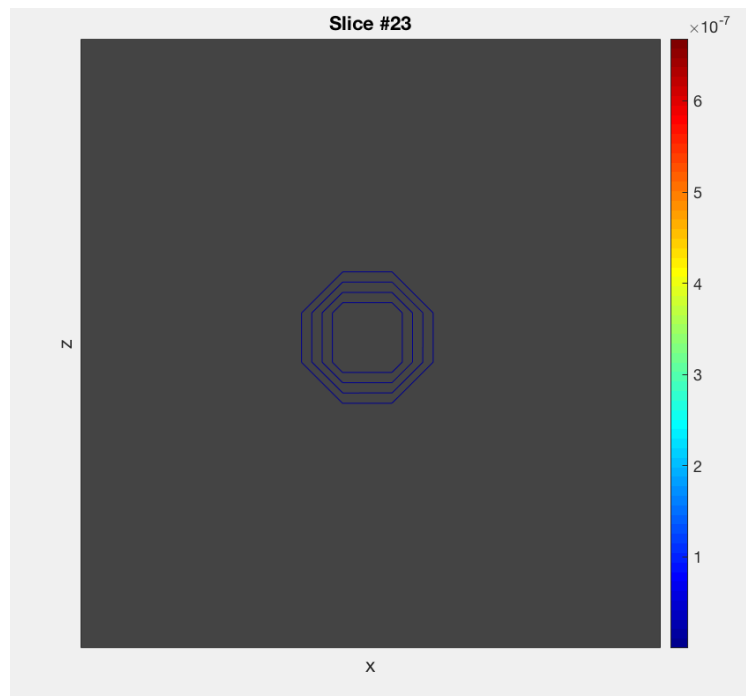


(b)

Figure 6.16: Slice that corresponds to the centre of the analysed phantom part for the heart analysis: (a) Slice 22 with source located in the centre; (b) Particular of slice 22.



(a)



(b)

Figure 6.17: Representation of the slice located below the central slice in the heart analysis: (a) Slice 23; (b) Particular of slice 23.

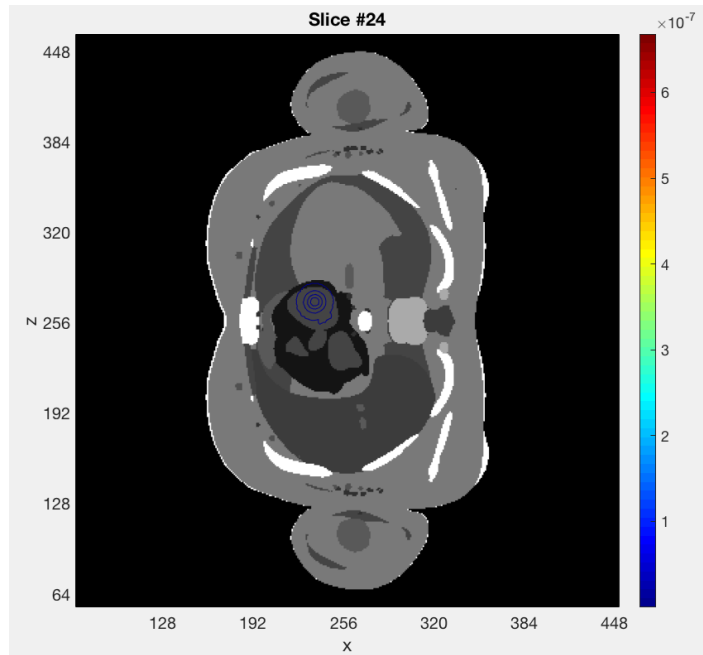


Figure 6.18: Representation of the slice located 0.6 cm below the central slice in the heart analysis.

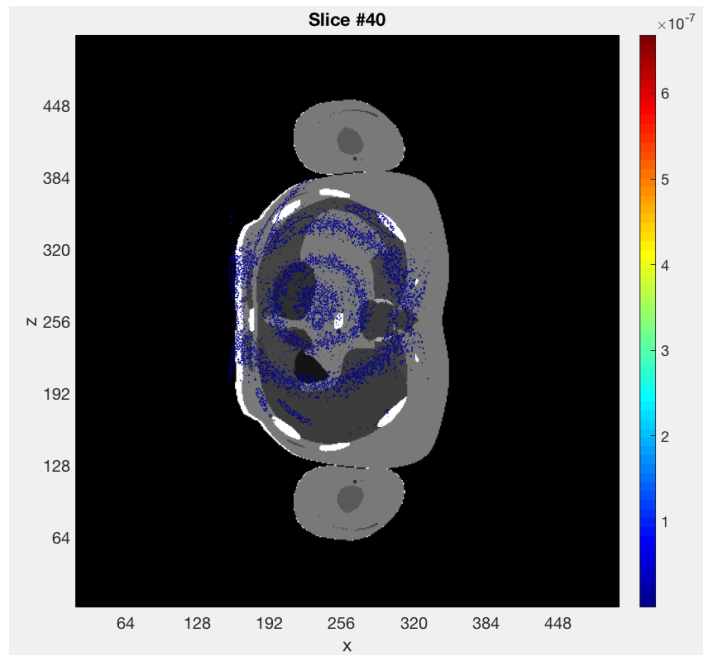


Figure 6.19: Representation of the slice located 5.4 cm below the central slice in the heart analysis.

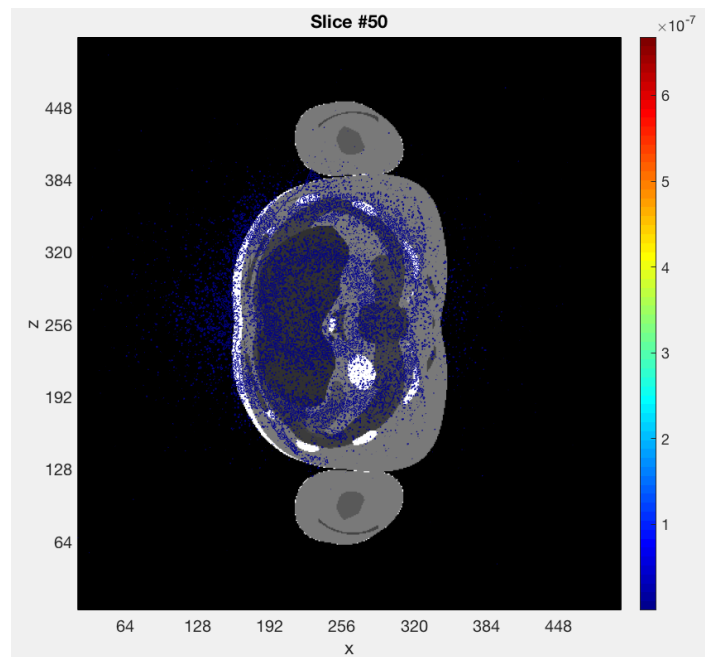


Figure 6.20: Representation of the slice located 8.4 cm below the central slice in the heart analysis.

# Chapter 7

## Conclusions

This work constitutes the basis of a wider project. Future studies objective is to implement a model that will focus on some aspects that have been approximated. The first point to be analysed is the cardiovascular system scheme. In real world, in an average human being it is more than 100000 km with vessels diameters that run from 2-3 cm to few  $\mu\text{m}$ : both arterial and venous system should be modelled without superposition with other organs and analysing vessels even smaller than the ones treated in this work so that the dose deposited by an hypothetic radiopharmaceutical that flows through circulatory system is the most accurate as possible.

Hemodynamic plays a crucial role in these kinds of studies, especially combined with the use of virtual human phantoms because knowing the blood kinetic in blood vessels would let to evaluate the radiopharmaceutical transit time in each voxel and so the deposited dose value. In addition, a general radiopharmaceutical do not distributed uniformly inside the human body, as it has been hypothesised in the work in order to get a primary evaluation of the deposited dose. As a matter of fact, it distributes according to physical and chemical properties of the radionuclide itself or of the labelling molecule and, for this reason, reached the heart, the radiopharmaceutical will be pumped towards the target organ and only a limited fraction will distributed in other body parts. In this way, the only affected organs are the ones located along the path from the injection point to the target position.

<sup>64</sup>Cu-Copper Chloride (Cuprymina) is a substance that is used for labelling other

medicines and it can not be injected directly into the patient. Its behaviour inside the human body and its side effects depend on the labelled substance: for this reason, considering that no  $^{64}\text{Cu}$ -labelled molecule has reached clinical phase III although Cuprymina obtained marketing permission in 2012, it would be interesting to take advantage of the virtual human phantom technology to reduce as much as possible tests on human beings in a way to reduce risks and ensuring a high level of accuracy at the same time. If all problems concerning  $^{64}\text{Cu}$  manufacturing will be solved, it could become a great improvement in medical physics field. In fact it could be used for both imaging and therapeutic purposes: in the first case, it has been seen  $^{64}\text{Cu}$  guarantees a better image quality than  $^{18}\text{F}$ , that is the the most used labelling radionuclide today; for what concerns therapy, copper is used by the organism to generate DNA filaments and so it would release its radioactivity near the chain, thus increasing the probability to destroy the cell itself thanks to the emission of light charged particles.

In general, *in silico* experiments on such a realistic virtual patient could be a great help and a complementary study for a better investigation of the effects of radiopharmaceuticals on patients.

# Bibliography

- [1] S. Agostinelli et al. “Geant4—a simulation toolkit”. In: *Nuclear Instruments and Methods in Physics Research Section A: Accelerators, Spectrometers, Detectors and Associated Equipment* 506.3 (July 2003), pp. 250–303. DOI: [https://doi.org/10.1016/S0168-9002\(03\)01368-8](https://doi.org/10.1016/S0168-9002(03)01368-8).
- [2] Hans-Jürgen Biersack and Leonard M. Freeman. *Clinical nuclear medicine*. Ed. by Hans-Jürgen Biersack and Leonard M. Freeman. Springer Berlin Heidelberg, 2007. DOI: <https://doi.org/10.1007/978-3-540-28026-2>.
- [3] F. Bourhaleb et al. “250 IN SILICO DOSIMETRY, MONTE CARLO WEB APPLICATIONS FOR SIMULATIONS IN ADVANCED RADIATION THERAPY, RADIATION BIOLOGY AND RADIATION PROTECTION FIELDS.” In: *Radiotherapy and Oncology* 102 (Mar. 2012), S129. DOI: [https://doi.org/10.1016/S0167-8140\(12\)70217-7](https://doi.org/10.1016/S0167-8140(12)70217-7).
- [4] P. Coan, A. Bravin, and G. Tromba. “Phase-contrast x-ray imaging of the breast: recent developments towards clinics”. In: *Journal of Physics D: Applied Physics* 46.49 (Nov. 2013), p. 494007. DOI: [10.1088/0022-3727/46/49/494007](https://doi.org/10.1088/0022-3727/46/49/494007).
- [5] *Cuprymina: EPAR - Product Informations*. Tech. rep. European Commission, 2012. URL: [https://www.ema.europa.eu/en/documents/product-information/cuprymina-epar-product-information\\_en.pdf](https://www.ema.europa.eu/en/documents/product-information/cuprymina-epar-product-information_en.pdf).
- [6] Silverthorn Dee Unglaub. *Human physiology - an integrated approach*. Fifth. Benjamin Cummings, 2009. ISBN: 978-0-321-55980-7.

- [7] Alberto Del Guerra et al. *Fondamenti di medicina nucleare*. Ed. by Duccio Volterrani, Giuliano Mariani, and Paola Anna Erba. Springer Milan, 2010. DOI: <https://doi.org/10.1007/978-88-470-1685-9>.
- [8] *Dichiarazione ICRP sulle reazioni tissutali ed effetti immediati e tardivi delle radiazioni nei tessuti e negli organi normali - Dosi soglia per le reazioni tissutali nell'ambito della radioprotezione*. 41/1-2. Traduzione della Pubblicazione ICRP 118. ICRP. Dec. 2015. ISBN: 978-88-88648-43-9.
- [9] Peter B. Farmer and John M. Walker, eds. *The molecular basis of cancer*. Springer US, 1985. DOI: 10.1007/978-1-4684-7313-1.
- [10] M. A. Flower. *Webb's physics of medical imaging*. Second. Taylor & Francis, 2012. ISBN: 0750305738.
- [11] Paul-Emmanuel Goethals and Richard Zimmermann. "Radionuclides - Copper64". In: *Nuclear Medicine World Market Report & Directory* (July 2017), pp. 148–150.
- [12] Henry Gray et al. *The anatomical basis of clinical practice*. Thirtyninth. Grey's anatomy. Elsevier Churchill Livingstone, 2004. ISBN: 978-0443071683.
- [13] J. Jadvar H. & Anthony Parker. *Clinical PET and PET/CT*. First. Springer Verlag, May 2005. ISBN: 1852338385.
- [14] B. Jagielski. "Elements of wave-particle duality of light". Cand. thesis. University of Oslo, May 2009.
- [15] Glenn F. Knoll. *Radiation Detection and Measurement*. Ed. by John Wiley & Sons Inc. Fourth. Sept. 2010. ISBN: 9780470131480.
- [16] Kenneth S. Krane. *Introductory nuclear physics*. John Wiley & Sons, Inc., 1988. ISBN: 0-471-85914-1.
- [17] J. R. Lamarsh. *Introduction to nuclear reactor theory*. Ed. by American Nuclear Society. Addison-Wesley Publishing Company, Sept. 2002. ISBN: 978-0894480409.
- [18] J. Magill, R. Dreher, and Z. Soti. *Karlsruhe Nuclide Chart*. Tenth. 2018. URL: <https://www.nucleonica.com/wiki/index.php?title=Category:KNC>.

- [19] J. Magill and J. Galy. *Radioactivity radionuclides radiation*. Ed. by Springer. Vol. 32. 5. Springer Nature, Apr. 2005, pp. 628–628. ISBN: 3-540-21116-0. DOI: 10.1007/s00259-005-1805-0.
- [20] J. Martin Brown. “The Hypoxic Cell A Target for Selective Cancer Therapy—Eighteenth Bruce F. Cain Memorial Award Lecture”. In: *Cancer research* 59 (Jan. 2000), pp. 5863–70.
- [21] M. Mezzano. “Studio e applicazione del fantoccio antropomorfo virtuale nel campo dell’adroterapia”. Cand. thesis. Politecnico di Torino, Mar. 2015.
- [22] Renata Mikolajczak and Piotr Garnuszek. “Radiopharmaceuticals in cardiology”. In: *Nuclear medicine review. Central & Eastern Europe* 15 (Apr. 2012), pp. 39–45.
- [23] Bruce R. Munson et al. *Fundamentals of fluid mechanics*. Sixth. Wiley, Oct. 2010. ISBN: 0470926538.
- [24] Tatiana de Oliveira Sato, Gert-Åke Hansson, and Helenice Jane Cote Gil Coury. “Goniometer crosstalk compensation for knee joint applications”. In: *Sensors* 10.11 (Nov. 2010), pp. 9994–10005. DOI: 10.3390/s101109994.
- [25] Anwar R. Padhani et al. “Imaging oxygenation of human tumours”. In: *European Radiology* 17.4 (Oct. 2006), pp. 861–872. DOI: 10.1007/s00330-006-0431-y.
- [26] E. B. Podgorsak. *Radiation oncology physics: a handbook for teachers and students*. Intl Atomic Energy Agency, Sept. 2005. ISBN: 9201073046.
- [27] “Preface, executive summary and glossary”. In: *Annals of the ICRP* 37.2-4 (Apr. 2007), pp. 9–34. DOI: 10.1016/j.icrp.2007.10.003.
- [28] J. Saphiro. *Radiation protection: a guide for scientists, regulators, and physicians*. Fourth. Harvard University Press. 2002. ISBN: 0-674-00740-9.
- [29] Wilfried Schneider, Thomas Bortfeld, and Wolfgang Schlegel. “Correlation between CT numbers and tissue parameters needed for Monte Carlo simulations of clinical dose distributions”. In: *Physics in Medicine and Biology* 45.2 (Jan. 2000), pp. 459–478. DOI: <http://dx.doi.org/10.1088/0031-9155/45/2/314>.

## BIBLIOGRAPHY

---

- [30] Michael G. Stabin. *Radiation protection and dosimetry*. Springer New York, 2003. ISBN: 978-0-387-49982-6. DOI: 10.1007/978-0-387-49983-3.
- [31] Howard D. Thames. “An ‘incomplete-repair’ model for survival after fractionated and continuous irradiations”. In: *International journal of radiation biology and related studies in physics, chemistry and medicine* 47.3 (Jan. 1985), pp. 319–339. DOI: <https://doi.org/10.1080/09553008514550461>.
- [32] N. Tsoulfanidis. *Measurements and detection of radiation*. Ed. by Williams and Edwards. Second. Taylor & Francis, 1995. ISBN: 1-56032-317-5.